Taxonomy and evolutionary history of peradectids (Metatheria): New data from the early Eocene of France

Killian Gernelle, Guillaume Billet, Emmanuel Gheerbrant, Marc Godinot, Bernard Marandat, Sandrine Ladevèze, Rodolphe Tabuce

▶ **To cite this version:**

Killian Gernelle, Guillaume Billet, Emmanuel Gheerbrant, Marc Godinot, Bernard Marandat, et al.. Taxonomy and evolutionary history of peradectids (Metatheria): New data from the early Eocene of France. Journal of Mammalian Evolution, 2024, 31 (3), pp.31. 10.1007/s10914-024-09724-5 . hal-04663420

HAL Id: hal-04663420
https://hal.science/hal-04663420v1

Submitted on 27 Jul 2024

HAL is a multi-disciplinary open access archive for the deposit and dissemination of scientific research documents, whether they are published or not. The documents may come from teaching and research institutions in France or abroad, or from public or private research centers.

L'archive ouverte pluridisciplinaire **HAL**, est destinée au dépôt et à la diffusion de documents scientifiques de niveau recherche, publiés ou non, émanant des établissements d'enseignement et de recherche français ou étrangers, des laboratoires publics ou privés.

Distributed under a Creative Commons Attribution 4.0 International License

Journal of Mammalian Evolution, 2024, **31**. With 17 figures (DOI: https://doi.org/10.1007/s10914-024-09724-5)

Taxonomy and evolutionary history of peradectids (Metatheria): new data from the early Eocene of France

Killian Gernelle[1,*], Guillaume Billet[2], Emmanuel Gheerbrant[2], Marc Godinot[3], Bernard Marandat[1], Sandrine Ladevèze[2,†] and Rodolphe Tabuce[1,†]

[1] Institut des Sciences de l'Évolution de Montpellier (ISEM, UMR 5554), Univ Montpellier, CNRS, IRD, cc64, Place Eugène Bataillon, F-34095 Montpellier Cedex 05, France

[2] Centre de Recherche en Paléontologie - Paris (CR2P, UMR 7207), Sorbonne Université, Muséum National d'Histoire Naturelle, CNRS, 8 rue Buffon, F-75005, Paris, France

[3] Ecole Pratique des Hautes Etudes, PSL, UMR 7207, CR2P, 8 rue Buffon, F75005, Paris, France

[†] Co-senior authors

*** Corresponding author:**

Killian Gernelle

Email address: killian.gernelle@umontpellier.fr

ORCID identifiers: Killian Gernelle: https://orcid.org/0000-0001-9698-0223

Guillaume Billet: https://orcid.org/0000-0002-3200-1548

Emmanuel Gheerbrant: https://orcid.org/0000-0003-3355-458X

Sandrine Ladevèze: https://orcid.org/0000-0001-6009-4107

Rodolphe Tabuce: https://orcid.org/0000-0002-4713-3981

Abstract Peradectidae are Paleogene 'opossum-like' stem-metatherians, largely Laurasian, whose evolutionary history remains unclear. Based on new remains (mainly dental) discovered in several French localities, we carry out a comprehensive systematic revision of all early Eocene peradectids from Europe (~MP7 reference level to MP10-11 interval). We describe well-preserved specimens from Palette (Southern France, MP7-MP8+9 interval) documenting the earliest European peradectid, *Peradectes crocheti* sp. nov. This new species exhibits an interesting mosaic of characters, including plesiomorphic traits found in the North American type species, *Peradectes elegans* Matthew and Granger, 1921. Molars allocated to the strikingly ubiquitous *Peradectes crocheti* sp. nov. are found in eight additional localities from northwestern and southwestern Europe, all limited to the time interval MP7-MP8+9. Moreover, the study of unpublished material of the MP8+9 and ~MP8+9 peradectids allows us to recognize two younger coeval species (*Peradectes louisi* Crochet, 1979, and *Peradectes russelli* Crochet, 1979). Our taxonomic conclusions are supported a posteriori by the first quantitative assessment of the variation in height of metatherian stylar cusps. The holotype of *Peradectes louisi* is reinterpreted, and *Peradectes 'mutigniensis'* Crochet, 1979 appears to be a junior synonym of *Peradectes russelli*. In addition to size, the otherwise similar *Peradectes louisi* and *Peradectes russelli* can be distinguished based on subtle yet consistent differences, such as lower molar proportions. Phylogenetic analyses using a novel matrix of dental characters shed new light on the relationships among Eocene peradectids, confirming the paraphyly of *Peradectes* with respect to *Armintodelphys* and *Mimoperadectes*. Our results suggest a single dispersal from North America to Europe in the evolutionary history of peradectids, which likely occurred immediately after the Paleocene-Eocene Thermal Maximum, *Peradectes crocheti* sp. nov. being recovered as the earliest offshoot of the European clade. Scarce lower molars from the MP10 reference locality and ~MP10 localities analyzed within this constrained phylogenetic

framework reveal a trend towards shrinking of the entoconid in the European lineage throughout the early Eocene.

Keywords dentition, Europe, paleobiogeography, Paleogene, Peradectidae, systematics

This article is registered in ZooBank under urn:lsid:zoobank.org:pub:CCD67F33-98A5-40DC-B1C1-C1D1F549FA96

Introduction

Peradectidae are an assemblage of extinct and small Cenozoic stem-metatherians with a superficially 'opossum-like' unspecialized tribosphenic dentition (e.g., Ladevèze et al. 2020). They have long been distinguished based on plesiomorphic dental features within Metatheria (but see Williamson et al. 2012, 2014), and were likely arboreally adapted (e.g., Szalay 1994; Kurz 2005; Rose 2012; Rose et al. 2012). Most of their occurrences are from North America (earliest Paleocene to early Oligocene; e.g., Korth 2008, 2018) and Europe (early to possibly earliest middle Eocene; Crochet 1979, 1980b; Kurz 2007). Putative peradectid isolated molars have also been identified in South America (early Paleocene to early Eocene; Sigé 1971, 1972; Marshall and Muizon 1988; Muizon 1991; Tejedor et al. 2009), Asia (early Oligocene to Early Miocene; Ducrocq et al. 1992; Mein and Ginsburg 1997; Storch and Qiu 2002; Ni et al. 2007) and Africa (early Eocene; Crochet 1986; Crespo and Goin 2021; but see Hooker 1998: p. 443; Gunnell 2010). Although Peradectidae is a key metatherian taxon for paleobiogeographic reconstructions, controversies remain about its monophyly and phylogenetic affinities (e.g., Horovitz et al. 2009; Williamson et al. 2012; Maga and Beck 2017; Ladevèze et al. 2020; Beck 2023). This is particularly true due to the apparent uniformity of their dental morphology, and because early Eocene European peradectids, last studied in detail by Crochet (1977a, 1977b,

1979, 1980a, 1980b), have not been revised in light of new material nor included in phylogenetic analyses.

Two genera first defined in North America are hitherto recognized in Europe, namely *Peradectes*, with at least three species, mostly known from French localities (Crochet 1980b), and possibly *Armintodelphys*, with one species from Belgium (Smith and Smith 2013). *Peradectes* is a genus of uncertain monophyly spanning the whole of the Paleocene and Eocene epochs (e.g., Krishtalka and Stucky 1983b; Williamson et al. 2012). The earliest reports of European *Peradectes* were made by Crochet (1977a, 1979, 1980b), who recognized up to four species from early to late early Eocene localities of France, mainly represented by isolated molars. Crochet (1979) also coined the tribe Peradectini, later elevated to a familial rank (Reig et al. 1985, 1987). Contrary to the fossil record of North America, peradectids and metatherians as a whole are absent from the Paleocene of Europe (Gheerbrant 1991). Peradectids first appeared in Europe in various localities following the Paleocene-Eocene Thermal Maximum (PETM), which are somewhat younger than the reference level MP7 (earliest Eocene; BiochroM'97 1997) but older than MP8+9 and ~MP8+9 (i.e., MP7–MP8+9 interval) (Crochet 1980b; Godinot 1981; Russell et al. 1988; Marandat 1991; Louis 1996; Hooker 2010, 2020; Smith et al. 2011). Consequently, the dispersal of peradectids from North America to Europe after the PETM was formally proposed by Hooker (1998: p. 434, 2015: fig. 8), but is still blurred by the lack of identified morphological intermediate(s) between representatives of the two continents.

In this study, we report fossils of a new early European peradectid species, *Peradectes crocheti*, collected after recent excavations (2017-2019) in Palette (Provence, southern France), a locality within the MP7-MP8+9 interval (Cojan et al. 2000; Marandat et al. 2012; Yans et al. 2014), although initially considered close to MP7 (Godinot et al. 1987). These new specimens represent the most comprehensive assemblage attributed to *Peradectes* since the definition of

its type species (Matthew and Granger 1921; Simpson 1928, 1935). We identified *Peradectes crocheti* sp. nov. in all MP7-MP8+9 interval localities that have yielded rare peradectid specimens (e.g., Fordones and Meudon). Moreover, the characterization of the morphology of the earliest European peradectids allowed us to carry out a revision of the species from the middle early Eocene (MP8+9 and ~MP8+9) of the Paris Basin, first described by Crochet (1979). This includes the referral of numerous unpublished dental specimens from the MP8+9 reference locality (Avenay) and various ~MP8+9 localities (Mutigny, Condé-en-Brie, Sables de Brasles, Sézanne-Broyes and Saint-Agnan). The greater abundance of remains of these later occurring species enabled us to account for intraspecific variation, and to refine their diagnostic characters and taxonomic status. In order to provide a more complete revised picture for the early Eocene, we also discuss the taxonomic status of the rare MP10 and ~MP10 peradectids. The phylogenetic position of the European taxa within Peradectidae was finally assessed via a phylogenetic analysis including most late Paleocene – middle Eocene Peradectidae sensu stricto, to provide formal insights on the origin of its European representatives, and on the Laurasian evolution of peradectids.

Material and methods

Provenance of the specimens

Most of the material from the fossiliferous locality of Palette (MHN.AIX.PV.), including the dental rows assigned to *Peradectes crocheti* sp. nov., was found after the field expeditions conducted between 2017 and 2019 by some of us (GB, EG and RT). The material was isolated after processing the sampled sediment by careful acid etching, use of screen-washing, and sorting methods. This is the first occurrence of a peradectid metatherian in the Palette fauna, which adds to the 16 previously listed mammalian species in this locality (Table 1), most of

Table 1 Updated list of mammals from Palette (Provence; MP7-MP8+9 interval, ~55 Ma). Attributions up to family rank are from Godinot et al. (1987), Russell and Godinot (1988), Marandat (1991), Rose et al. (1994), López-Martínez et al. (2006), Hooker and Russell (2012), Marandat et al. (2012), Hand and Sigé (2017), Boivin et al. (2018), Solé et al. (2018, 2023), Vautrin et al. (2020), Vianey-Liaud and Marivaux (2021), and this study.

- **Metatheria**
  - Peradectidae
    - *Peradectes crocheti* sp. nov.
  - Herpetotheriidae
    - *Peratherium constans*
- **Eulipotyphla**
  - Nyctitheriidae
    - *Saturninia* sp. or *Leptacodon* sp.
- **Order *incertae sedis***
  - Adapisoricidae
    - gen. and sp. indet.
- **Chiroptera**
  - ?Archaeonycteridae
    - gen. and sp. indet.
- **Pantolesta**
  - Paroxyclaenidae
    - *Merialus martinae*
- **Plesiadapiformes**
  - Paromomyidae
    - *Arcius rougieri*
- **Primates**
  - Notharctidae
    - *Donrussellia magna*
- **Rodentia**
  - Ischyromyiformes, family *incertae sedis*
    - *Corbarimys cezannei*
    - gen. and sp. indet.
- **‘Condylarthra’**
  - Hyopsodontidae
    - *Lessnessina praecipuus*
  - Louisinidae
    - *Paschatherium plaziati*
- **Mesonychia**
  - Mesonychidae
    - *Hyaenodictis rougierae*
- **Hyaenodonta**
  - Hyaenodontidae
    - *Parvagula palulae*
- **Artiodactyla**
  - Diacodexeidae
    - *Diacodexis* cf. *gigasei*
- **Perissodactyla**
  - Lophiodontidae
    - *Lophiaspis maurettei*
  - Equoidea, family *incertae sedis*
    - *Cymbalophus hookeri*

which correspond to eutherian taxa that have been extensively studied (Godinot 1984, 1992; Godinot et al. 1987; Russell and Godinot 1988; Marandat 1991: 110; Ramdarshan et al. 2015;

Solé et al. 2015, 2018, 2023; Boivin et al. 2018; Orliac et al. 2018; Vautrin et al. 2020; Vianey-Liaud and Marivaux 2021). *Peradectes crocheti* sp. nov. represents the first addition to the alpha diversity of the mammalian fauna of Palette (excepting an unidentified rodent species; Marandat et al. 2012: p. 427) since the establishment of the first and single faunal list of Godinot et al. (1987) for mammals, althought the taxonomic status or classification of some taxa have changed (Table 1).

The new peradectid specimens from Palette are permanently stored at the Muséum d'Histoire Naturelle of Aix-en-Provence (France). Other studied specimens are also the result of past or recent long and fruitful field research. The specimens from Meudon, Rians, Soissons, Avenay, Condé-en-Brie, Mutigny, Sables de Brasles, Sézanne-Broyes, Saint-Agnan, Cuis and Grauves (MNHN.F.) are housed in the paleontological collections of the Muséum National d'Histoire Naturelle (Paris, France). Specimens from Fordones, Fournes, one specimen from Palette, one specimen from Coulondres, two specimens from Mas de Gimel, and one specimen from Vielase, are housed at the University of Montpellier (France). The two specimens from Sotteville-sur-Mer are housed at the Royal Belgian Institute of Natural Sciences (Brussels, Belgium). The single specimens from Croydon and Abbey Wood are housed at the Natural History Museum, London (England), and were studied via photographs available in the literature. Casts of North American peradectids (AMNH, UCMP, UM, USNM) were used for comparisons with European peradectids. We accounted for intraspecific variation in the descriptions of dental material based on comparisons with the variation ranges of morphological characters known in other marsupialiforms, such as *Pucadelphys* (Ladevèze et al. 2011) and *Peratherium* (Ladevèze et al. 2012).

Ages of the localities

The nine studied fossil-bearing localities of the MP7-MP8+9 interval are younger than the PETM (MP7). Four of them are located in southern France (Palette and Rians, in Provence; Fordones, in Corbières; Fournes, in Minervois), the five others being in northern France (Meudon, Île-de-France; Soissons, Aisne; Sotteville-sur-Mer, Normandie) and England (Abbey Wood and Croydon, London) (Fig. 1a). Palette and Fordones, correlated in age with Le Clot locality (Corbières) based on evolutionary stages of mammalian lineages (Marandat et al. 2012), are considered by chemostratigraphic analysis approximately 1 myr younger than the MP7 reference locality of Dormaal (Belgium; ~56 Ma), and hence close to 55 Ma (Yans et al. 2014). Fournes (Minervois) is positioned by marine correlation and chemostratigraphic analysis just after the ETM2 (~54 Ma), closer to the MP8+9 than to the MP7 reference level (Noiret et al. 2016: fig. 2), and is probably coeval with the Wasatchian Wa-5 mammal fauna (Noiret et al. 2016: p. 477). Rians (Provence) is a locality possibly similar in age to Fournes, based on mammalian biostratigraphy (Marandat et. 2012; Noiret et al. 2016; Philip et al. 2017: p. 328). Fournes and Rians are the youngest faunas of the MP7-MP8+9 interval here studied. The age retained for Abbey Wood (London; biozone PE III of Hooker 1996) is 55.12 Ma (Hooker 2010), and therefore older than Fournes and Rians. Sotteville-sur-Mer is probably the oldest of all the MP7-MP8+9 localities studied. It is probably older than Soissons and Meudon (both in biozone PE II; Hooker 1996) according to Smith et al. (2011), and was thus assigned to biozone PE II (Hooker 2015). These two northern localities are considered pene-contemporaneous with the southern localities of Palette and Fordones (Marandat et al. 2012). Altogether, except Fournes and Rians, the MP7-MP8+9 interval localities are bracketed between the PETM and the Eocene Thermal Maximum 2 (ETM2), and are closer to MP7 than to MP8+9 given the approximate age of Mutigny, the oldest ~MP8+9 locality (see below).

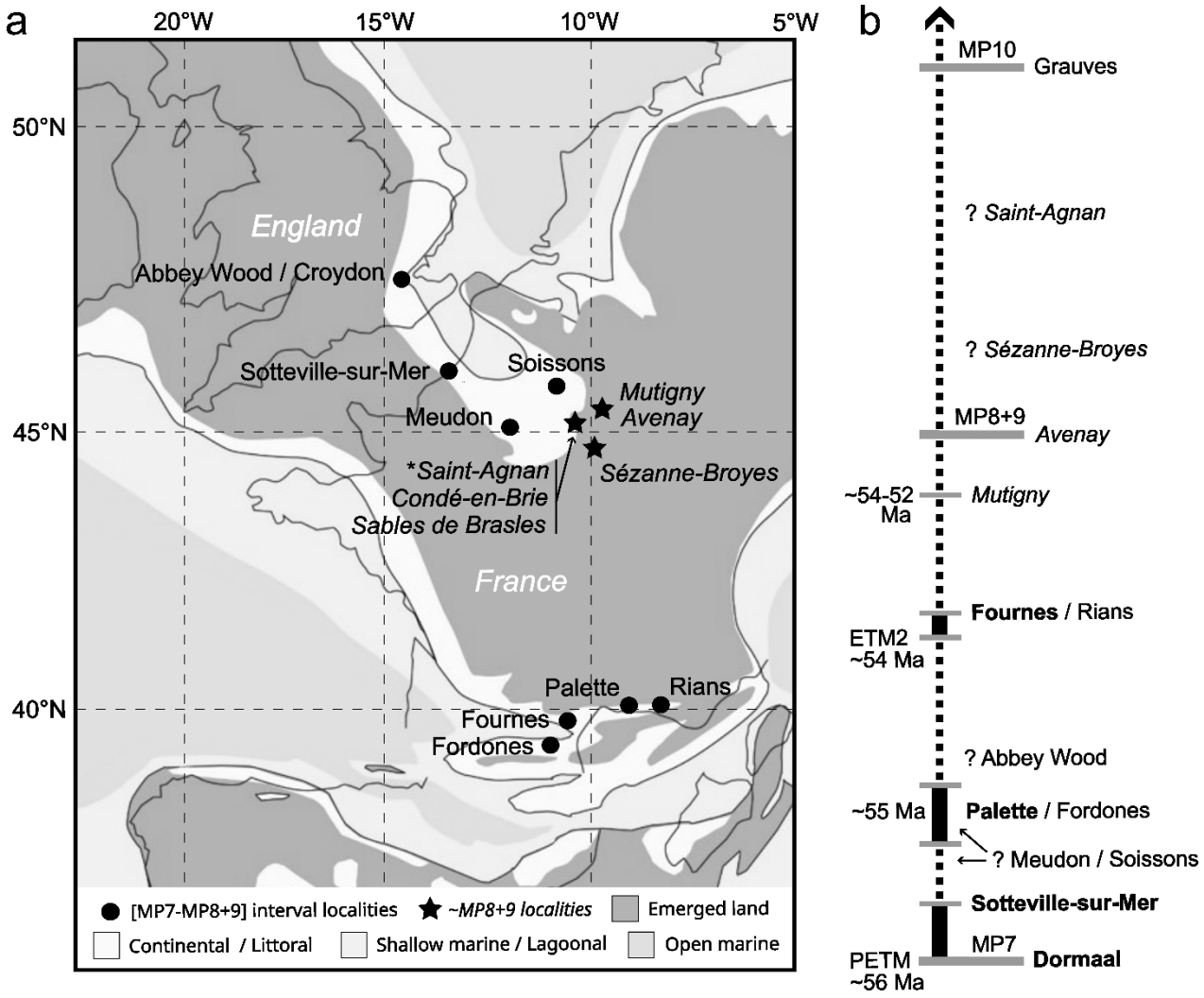

Fig. 1 Geographical and temporal positions of the studied MP7-MP8+9 interval and ~MP8+9 faunas (including that of Avenay, the MP8+9 reference locality) that yielded peradectid remains. **a**. paleogeographic map of France and England during the early Eocene (modified from Marandat et al. 2012) with the position of studied localities. *, the Saint-Agnan locality is more likely in the MP8+9-MP10 interval rather than MP8+9 or MP10. **b**. schematic relative temporal positionning of MP7-MP10 reference levels, PETM and ETM2, and selected MP7-MP10 localities mentioned in the main text. The dashed parts of the temporal extension indicate uncertain temporal gaps. The age of localites in bold have been discussed via chemostratigraphic data (Cojan et al. 2000; Steurbaut et al. 2003; Noiret et al. 2016).

Five localities MP8+9 or ~MP8+9 in age from the Paris Basin (northwestern Europe) are here studied, namely Mutigny (Marne), Avenay (MP8+9 reference level, Marne), Condé-en-Brie (Aisne), Sables de Brasles (='Gland', Aisne) and Sézanne-Broyes (Marne) (Fig. 1a). Mutigny

(biozone PE IV) is the oldest ~MP8+9 locality considered (slightly older than MP8+9), with an approximate age of 54 to 52 Ma (Neal 1996; Duprat 1997). Avenay, Condé-en-Brie and Sables de Brasles (biozone PE V) must be slightly younger than Mutigny according to the study of metatherian and rodent lineages (Schmidt-Kittler et al. 1987; Escarguel 1999), and slightly older than Sézanne-Broyes (also in PE V; Hooker 1996) (Louis 1970; Louis and Laurain 1983). Saint-Agnan (Aisne), of which the attribution of the single peradectid specimen is here revised, has been alternatively placed in the MP8+9 and MP10 reference level, depending on authors (e.g., Bronnert and Métais 2023 vs BiochroM'97 1997: table 1). The Saint-Agnan fauna is probably younger than MP8+9, and might be positioned in the MP8+9-MP10 interval according to most authors (Louis and Laurain 1983; Lecomte 1994; Escarguel 1999; Solé et al. 2018). Finally, rare localities from the late early Eocene have yielded peradectids (see Discussion), notably Grauves and Cuis (MP10, Paris Basin, BiochroM'97 1997), Mas de Gimel (~MP10; Vianey-Liaud et al. 2024) and Vielase (?MP10-11, Quercy, Legendre et al. 1992). The localities of Grauves and Cuis have long been considered distinct (Stehlin 1940: p. 293; Rat 1965: p. 251), but the two names may designate the same locality (e.g., Escarguel 1999).

Dental nomenclature

For upper molars, the nomenclatures and homologies of Williamson et al. (2014: fig. 3), Goin et al. (2016: fig. 1.2) and Muizon and Ladevèze (2022: fig. 1) are mostly followed. Following these studies, the internal edge of all teeth (upper and lower), including premolars and canines, is designated as lingual, and the external edge as labial. The anterior and the posterior edges are designated as mesial and distal, respectively (Fig. 2b, 2c). An updated nomenclature for upper molars (Fig. 2b) includes the following structures. The paraconular cristae are termed pre- and postparaconular crista and the metaconular cristae are termed pre- and postmetaconular crista, as in Muizon and Ladevèze (2022). The postparaconular and the premetaconular cristae are the

internal conular cristae. The term ‘talon’ designates the part of the crown which is lingual to the bases of the paracone and metacone (e.g., Marshall and Muizon 1995: fig. 5; Oliveira and Goin 2011: fig. 2); it includes the protocone, paraconule, metaconule, the conular cristae, the trigon basin (= protofossa of Crochet 1980b: fig. 2, or Gheerbrant 1992: fig. 1B), and the lingual part of the paracingulum. In occlusal view, a concave distal margin between the talon and stylar shelf is called a ‘distal emargination’ of the molariform tooth outline. The ‘stylar cusp E’ (not figured) corresponds to the labial termination of the postmetacrista, which is similar to a stylar cusp in labial view. The metastylar wing (e.g., Rothecker and Storer 1996; = ‘metastylar lobe’, e.g., Williamson and Taylor 2011; and ‘metastylar area’, e.g., Muizon and Ladevèze 2022) is the distolabial corner of the stylar shelf of molariform teeth, distal to the ectoflexus. It encompasses the stylar cusp D and the postmetacrista. The parastylar wing is the mesiolabial corner of the stylar shelf, mesial to the ectoflexus. It encompasses the stylar cusp A and the labial part of the paracingulum.

We propose a terminology of lower molars accounting for the dental peculiarities of European peradectids (Fig. 2c). We use the term ‘protocristid’ (= protolophid) as in Muizon and Ladevèze (2022), which encompasses the distolingual cristid of the protoconid (= postprotocristid) and the labial cristid of the metaconid; the latter was often considered as a ‘postmetacristid’ in metatherians (e.g., Goin et al. 2016). The metaconid of peradectids and other marsupialiforms, such as *Glasbius* (Williamson et al. 2014: fig. 3) and herpetotheriids (Wessels et al. 2024: fig. 1), also bears a sharp distal cristid in addition to this ‘postmetacristid’ (Fig. 2c). In the dental terminology of Williamson et al. (2014: fig. 3), the ‘postmetacristid’ of Goin et al. (2016) has thus been interpreted as the premetacristid and the distal cristid of the metaconid as the postmetacristid. However, some deltatheroidans (such as *Oklatheridium*) and early marsupialiforms (such as *Arcantiodelphys*) can have a mesial cristid of the metaconid (Averianov 2015: fig. 5), termed the ‘premetacristid’ (Vullo et al. 2009: p. 19912, fig. 2A).

Thus, the cristids described as the premetacristid and postmetacristid in Vullo et al. (2009) and Williamson et al. (2014) are not homologous. In order to avoid confusion and to maintain structural homology among therians, the labial cristid of the metaconid is here named the 'protocristid lingual segment', a term derived from the terminology of primitive tribosphenic molars (e.g., Van Valen 1966: fig. 1; Crochet 1980b; Gheerbrant 1992). The distal cristid of the metaconid is named the 'postmetacristid' due to its position (a cristid which is itself possibly not homologous with the 'distal metacristid' of some stem therians, see Martin et al. 2023). In the same way, the paracristid is subdivided into the preprotocristid, on the mesiolingual edge of the protoconid, and the 'paracristid lingual segment' on the labial edge of the paraconid. The 'paracristid lingual segment' is not a widely-used name in studies of metatherian molars. The labial cristid of the paraconid has been alternatively named the 'postparacristid' (e.g., Abello 2013: fig. 2D; Goin et al. 2016), or the 'preparacristid' (e.g., Ladevèze et al. 2012: p. 259; Muizon et al. 2018), by various authors. As before, in some deltatheroidans and stem marsupialiforms, a distal cristid of the paraconid (= postparacristid) lingually closes the trigonid basin, together with the premetacristid (Vullo et al. 2009: p. 19912, fig. 2A; Averianov 2015: fig. 5). Moreover, some peradectid molars studied here have a small cristid on the paraconid keel, mesial to the paraconid, which is the preparacristid. In lingual view, the lingual opening of the trigonid basin (= prefossid in Crochet 1980b and Gheerbrant 1992) refers to the opening between the paraconid and metaconid, and the lingual opening of the talonid basin (= postfossid) refers to the opening between the metaconid and the entoconid. The lingual opening between the entoconid and the hypoconulid is referred to as the entoconid – hypoconulid notch. The entocristid of Crochet (1980b), Gheerbrant (1992), and Muizon and Ladevèze (2022) is named the pre-entocristid, as in Goin et al. (2016), because a small postentocristid often occurs in the entoconid – hypoconulid notch of peradectids (Fig. 2c). When present, the postentocristid is a true cristid; it differs from the 'hypoconulid-entoconid talonid fold' present in some

herpetotheriid and didelphid species (Hooker et al. 2008: p. 644, pl. 1, figs. 1-2) in being observable even on unworn lower molars. The distolingual cristid of the hypoconid is designated as the postcristid following Crochet (1980b) and Gheerbrant (1992), instead of the posthypocristid, because it generally implicitly includes the posthypocristid and also the unnamed labial cristid of the hypoconulid, which occurs in some peradectid specimens (Fig. 2c). In occlusal view, a concave labial margin between trigonid and talonid is called a labial emargination of the molar outline (not illustrated in Fig. 2c).

Orientation of molariform teeth for descriptions and measurements

Clemens (1966: p. 4) was the first author to stress the need for an orientation method of metatherian molariform teeth ensuring consistent descriptions and measurements. The repeatability of measurements and descriptions of the upper molars and deciduous premolar has been achieved using the paracone – metacone axis for orientation. This method was efficiently used by several authors working on upper molars of metatherians since the work of Clemens (1966) (see Rose 2010: p. 561).

Regarding metatherian lower molars, the orientation used for descriptions and/or measurements differ between authors and was often unspecified. The methodology of Crochet (1980b) and Korth (1994) to measure lower molars is not detailed, although their drawings (e.g., Crochet 1980b: figs. 3, 10; Korth 1994: fig. 1) suggest the chosen orientation of lower molars allowed their maximum length to be measured. This protocol has been used by other workers for measurements of small mammal teeth in general, and is still employed for metatherian lower molars in recent studies (e.g., Muizon and Ladevèze 2022). However, it does not allow to locate structures properly on the occlusal surface of lower molars and to define characters consisting in precise relative position of structures, because the chosen orientation may vary between

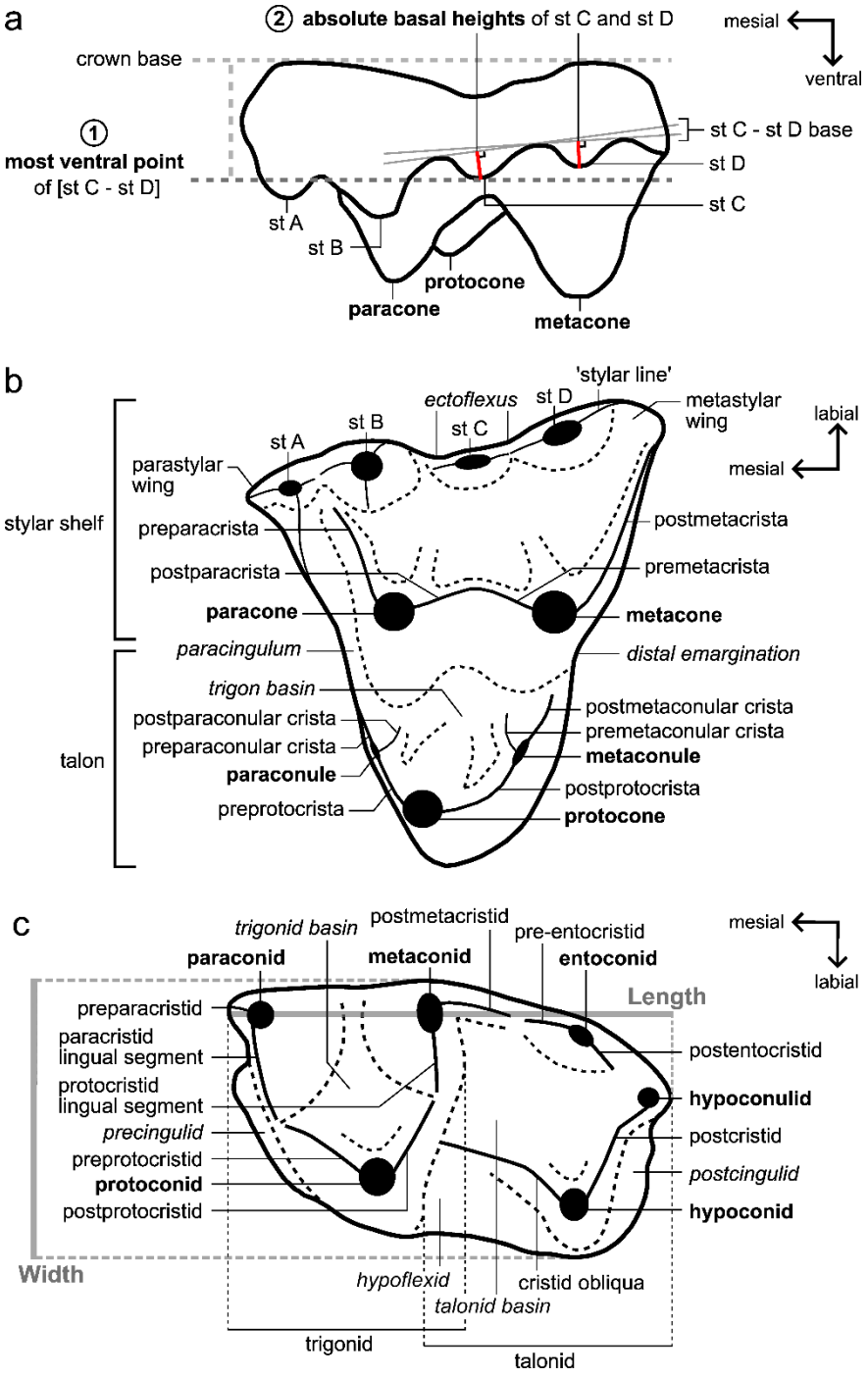

Fig. 2 Molar nomenclature and measurement methods used in this study, based on schematic drawings of peradectid molars. **a**. upper molar in labial view, with the two methods employed for estimations of the heights of stylar cusps C and D: (1) position of the most ventral point of the [stylar cusp C – stylar cusp D] mesiodistal extension parallel to the crown base, and (2) absolute basal height of stylar cusps C and D, with a ratio calculated from the two values. **b**. upper molar in occlusal view. **c**. lower molar in occlusal view. The measurement methods for length and width of lower molars are illustrated in grey. The dashed lines concern depressions on the occlusal surface (**b** and **c**). Cusps (except stylar cusps) / cuspids and conules are indicated

in bold text, crests / cristids are in full text, and cingula / cingulids, emarginations of the crown and basins are in italics. The molar nomenclature is mainly derived from Crochet (1980b), Gheerbrant (1992), Williamson et al. (2014), Goin et al. (2016), and Muizon and Ladevèze (2022). Abbreviations: **st A**, stylar cusp A; **st B**, stylar cusp B; **st C**, stylar cusp C; **st D**, stylar cusp D. Schematic drawings are not to scale

specimens and dental loci. Lower molars have tentatively been precisely oriented using the paraconid - entoconid apices axis (Clemens 1966: p. 4) or the metaconid – entoconid apices axis (Lillegraven 1969: p. 16, fig. 5; Gheerbrant 1992: p. 80). On the lower molars of most metatherians, including herpetotheriids and the earliest *Peradectes* species *Peradectes minor* Clemens, 2006 (see also Williamson et al. 2012), and *Peradectes coprexeches* Williamson & Taylor, 2011, the paraconid, the metaconid, and the entoconid are aligned. As a consequence, the orientation of the lower molars for most Cenozoic metatherians varies little, no matter which lingual cuspid axis is chosen as reference. We noted that the relative configuration between the trigonid and talonid cuspids is different in most peradectids, such as the type species *Peradectes elegans* Matthew & Granger, 1921 (Gazin 1956: pl. 2, fig. 6; Krishtalka and Stucky 1983b: fig. 3), *Peradectes protinnominatus* McKenna, 1960 (see also Bown 1979: fig. 40b, Rose 1981: fig. 8A, Gingerich and Smith 2006: fig. 26b), all European peradectid species (this study), and the genus *Armintodelphys* (Krishtalka and Stucky 1983a: fig. 5; Krishtalka and Stucky 1984: fig. 4A), where the entoconid, pre-entocristid and postentocristid are oblique with respect the the mesiodistal axis. Such a ‘curved talonid lingual edge’ was first noted in a description of some peradectid lower molars by Smith and Smith (2013: p. 305), but it is not exclusive to the species included in *Armintodelphys* by these authors. A curved talonid implies that the paraconid, metaconid and entoconid are often not aligned on the lower molars of the concerned taxa. The entoconid apex is either more labial than the paraconid and metaconid apices if these two trigonid cuspids are chosen to form the reference axis for orientation, or the metaconid apex is

lingually deflected if the paraconid and entoconid apices are chosen as reference. The entoconid has been highlighted as one of the most variable structures of lower molars of extant and extinct metatherians, especially for the last lower molar (e.g., Martin 2005: fig. 4; Ladevèze et al. 2012: p. 256). We consequently regard the use of the paraconid-metaconid apices axis as a reference as the best way to produce reliable measurements (Fig. 2c) and dental descriptions (including the coding of dental characters) of tribosphenic metatherian material, and we thus use it in this study for both purposes.

Maximum values were retained for the mesiodistal length, parallel to the paraconid – metaconid apices axis, and the labiolingual width, perpendicular to the paraconid - metaconid apices axis. All measurements are given with an accuracy of 0.01 millimetres. Measurement values for molars are presented in Online Resource 1: Tables S1-S3. Unbiased coefficients of variation (CV) were calculated to compare variability between dental measurements. Statistical treatment of the data was carried out using the R software environment (R Core Team 2020; v.4.0.2). In order to statistically compare mean molar proportions between *Peradectes louisi* Crochet, 1979, and *Peradectes russelli* Crochet, 1979 (at a 5% alpha risk), Welch's unequal variances *t*-test were performed (as recommended in Ruxton 2006). The measurement method for premolars is the one of Clemens (1966: p. 4). Mandibular heights were taken on the lingual aspect of the mandible, from its ventral edge to the adjacent dorsal molar alveolus. All measurements were made on screenshots of volume rendering or surface models of the scanned specimens (see below), using Avizo® 9.3 (Thermo Fisher Scientific-FEI) measurement tools, and/or via photographs of specimens taken with an optical stereomicroscope (Leica M 205C) connected to a camera (Leica DFC 420C), using tools of the Leica Application Suite v. 4.13. Body mass estimates were calculated using the predictive equation for M3 length (the most accurate predictor, as indicated by R^2 values) from the 'pooled Didelphidae and Dasyuridae' (i.e., dentally conservative marsupials) dataset of Gordon (2003: fig. 7).

Evaluation of the heights of stylar cusps

In studies directly addressing stylar shelf intraspecific variation among extant and extinct metatherian taxa, no clear pattern of variation of the relative sizes of the stylar cusps C and D for a given molar locus of a given species was noted, although the stylar cusps C and D are known to vary in absolute size (confounded with height by most authors), morphology, and position within a comprehensive series of metatherian teeth (e.g., Storer 1991: table 6; Johanson 1994: fig. 2; Eberle and Storer 1995: p. 791; Hershkovitz 1997: fig. 19; Flores and Abdala 2001: p. 105; Hayes 2005: fig. 4; Korth 2018; but see Kihm and Schumaker 2015: p. 105). Few authors formally used the sizes of stylar cusps to distinguish metatherian species or genera (e.g., Crochet 1979, 1980b; Marshall et al. 1990: tables 1-2; Korth 1994: table 2; Muizon and Lange-Badré 1997: table 1), and in particular peradectid species (Williamson and Taylor 2011). Although the vast majority of the fossil record of metatherians is composed of molars, there has not been a procedure to objectively decide which one of two given stylar cusps on one specimen is higher, nor an attempt to quantify the size of these stylar cusps.

For this purpose, we here propose two methods to evaluate the relative height of the stylar cusps, examplified by the stylar cusps C and D, based on labial views of the upper molars (Fig. 2a). One can first find the most ventral point of the [st. C – st. D] mesiodistal extension parallel to the base of the crown (Fig. 2a [1]). In previous works, the relative height of the stylar cusps was probably implicitly estimated in this way. This method is used in the Systematic Paleontology section of this study (in differencial diagnoses of species and comparative descriptions).

Second, the absolute basal height of a stylar cusp corresponds to a measurement performed (in mm, also in labial view) perpendicular to a baseline drawn between the most mesial and distal

points of this stylar cusp, that are the most dorsal (i.e the closest to the crown base). The measurement is taken between the baseline of the stylar cusp and its most ventral point (i.e., the stylar cusp tip) (Fig. 2a [2]). The measurements of the absolute basal heights of the stylar cusps C and D were here conducted on stylar shelves with limited and homogeneous wear, of upper molars of the three European peradectids *Peradectes crocheti* sp. nov., *Peradectes louisi* and *Peradectes russelli*. For each available specimen, a ratio of the absolute basal height of the stylar cusp C to the absolute basal height of the sylar cusp D was calculated for comparative purposes, because one out of the three species studied (*Peradectes russelli*) is larger than the others. This second method allows to precisely quantify the variation in height of the stylar cusps. It is used in the Results section of this study, a posteriori of taxonomic attributions. Measurements of stylar cusp heights and ratio values are available in Online Resource 1: Table S4. Non-parametric Wilcoxon-Mann-Whitney tests were performed with the R software environment on species pairs (the normality assumption was not met for the st. C / st. D heights ratio values of *Peradectes crocheti* sp. nov. [Shapiro-Wilk normality test; W = 0.892, P = 0.042]), in order to define between which species the sum rank of the ratio values of the absolute basal height of st. C / st. D differ significantly (at a 5% alpha risk). Parametric Welch's *t*-test were alternatively performed on the same species pairs. The R package *ggplot2* (Wickham 2016) was employed to produce boxplots of absolute basal stylar cusp heights ratio values, as well as bivariate diagrams of length x width of molars.

High-resolution x-ray microtomography

Illustrated specimens were scanned using a µ-CT-scanning station EasyTom 150 / Rx Solutions (Montpellier RIO Imaging, ISE-M, Montpellier, France). Images of these specimens were achieved using the 'snapshot' tool of Avizo® 9.3. The segmentation of the cheek teeth and

dentary of MHN.AIX.PV.2017.6.8 (scanned with a resolution of 6.5 µm) was performed with the Avizo® 9.3 'blow' tool, in order to clarify the morphology and positioning of peradectid premolars on the dentary. The segmentation of the holotype of *Peradectes crocheti* sp. nov., MHN.AIX.PV.2018.26.14 (scanned with a resolution of 5.3 µm), required the 'threshold' tool. An attempt was made to position the segmented fragments of the maxilla MHN.AIX.PV.2018.26.14 in anatomical position, using the MorphoDig® software (Lebrun 2018), with comparison to the complete maxilla of '*Peradectes*' from Messel (Kurz and Habersetzer 2004: figs. 2-3) and accounting for the typical crushing of fossil bones from Palette, which may have suffered from synsedimentary compression (e.g., Vautrin et al. 2020: figs. 3-4). The 'threshold' tool was also used for segmenting the isolated M3 MHN.AIX.PV.2017.6.7 and MNHN.F.SN18, as a way to numerically assemble the lingual and labial halves of the former, and extract sediment from the trigon basin of the latter.

Intrafamilial phylogenetic analysis

The aim of the phylogenetic analysis was to unravel relationships within part of Peradectidae sensu stricto, with a focus on European representatives. Fourteen metatherian taxa were coded for this purpose. The outgroup is composed of two stem-metatherian species, the deltatheroidan (= non-marsupialiform metatherian) *Deltatheridium pretrituberculare* Gregory & Simpson, 1928, and the stem-marsupialiform *Asiatherium reshetovi* Trofimov & Szalay, 1994 (taxon data used for coding are in Online Resource 2). Among marsupialiforms, *As. reshetovi* is usually found to be more basal than Peradectidae (e.g., Williamson et al. 2014; Ladevèze et al. 2020; Muizon and Ladevèze 2022; but see Maga and Beck 2017: fig. 38 vs fig. 39). All late Paleocene – middle Eocene species of Laurasian Peradectidae sensu stricto were included in the ingroup (12 taxa), with the exception of *Mimoperadectes houdei* Horovitz, Martin, Bloch, Ladevèze,

Kurz & Sánchez-Villagra, 2009, and *M. sowasheensis* Beard & Dawson, 2009, because we mainly aimed to resolve phylogenetic relationships of *Peradectes* and *Armintodelphys* species (both genera having been recognized in Europe and North America before this study), and because *M. sowasheensis* is known by a single isolated upper molar (Beard and Dawson 2009). *Mimoperadectes* is thus only represented in this analysis by its type species, *Mimoperadectes labrus* Bown & Rose, 1979. The 11 remaining taxa of the ingroup belong to *Peradectes* and *Armintodelphys*. *Peradectes pauli* Gazin, 1956, was here not considered as a valid species, following Kurz (2007: p. 44) and Williamson et al. (2012); it is probably a junior synonym of the type species *Peradectes elegans* (Williamson et al. 2012: p. 631). Consequently, dental material previously ascribed to *Peradectes pauli* (Gazin 1956; Krishtalka and Stucky 1983b) was used here for the coding of *Peradectes elegans*, following Williamson et al. (2012: supplemental material, appendix 1). The ingroup taxa, along with their precise temporal extension (all occurring in the Eocene) and the nature of data used for their coding, are listed in Online Resource 2.

The fossil record of peradectids comprising predominantly isolated cheek teeth and incomplete dental rows, our dataset is composed of 37 characters which concern only the postcanine dentition. Among them, three are related to the morphology of lower premolars (characters 1 to 3), 18 to lower molars (characters 4 to 21) and 16 to upper molars (characters 22 to 37). The characters of these three subpartitions relate to the occlusal, lingual and labial morphology of cheek teeth. Approximately half of the characters (18) were either directly taken (8), or modified in their spelling or character states (10), from characters of the data matrices of Williamson et al. (2014) and Muizon and Ladevèze (2022). The others (19 characters) are here newly defined to reflect substantial differences observed among the dentition of peradectid taxa. The only two multistate characters (3 and 34) were unordered because we did not hypothesize a hierarchical transformation for them (i.e., getting from state 0 to state 2, or vice versa, does

not necessarily involve an intermediate state 1). All characters were unweighted. Ranges of measurements were coded onto four new discrete characters (4, 5, 14 and 22) by gap coding. The characters implying comparisons of length and/or width between molar loci (4, 6, 22) were coded using available means of dental measurements if these loci are known only by isolated molars for the concerned taxon. Frequencies of observation of character states in our sample were employed in four new characters (11, 31, 36 and 37). We paid attention to avoid cases of similar characters being repeatedly scored at successive molar loci since these may highly covary (serial homologs, see Billet and Bardin 2019). Thus, although 32 out of 37 characters are restricted in their application to given molar loci because of their spelling, only two characters (10 and 11) may represent serial homologs at successive molar loci (however, their coding differs greatly). The illustration of most of the new characters is available in Online Resource 3: Figs. S1-S12. The numbers in superscript used after a character number in the main text and figures denote the character state.

The new character-taxon matrix (Online Resource 4) was edited with Mesquite v. 3.61 (Maddison and Maddison 2019). The parsimony analysis was performed with PAUP* v. 4.0a169 (Swofford 2002), through the Heuristic search method, with a random step-wise addition (1000 replications with randomized input order of taxa) and tree-bisection-reconnection (TBR) branch swapping options. Intraspecific variation was accounted as polymorphic states in PAUP* (noted 'x&y' in Mesquite and '(xy)' in PAUP*). Non-applicable states have been coded '-' in Mesquite. The robustness of each clade was evaluated with Bremer indices (BI, Bremer 1994), going up to five additional steps. A second analysis, with the same parameters, was run with a new scoring of characters requiring frequencies of observation to be scored (characters 11, 31 and 36). The frequencies were replaced by polymorphism when needed. Character 37 was additionally scored as such in a third analysis. The changes in the spelling of characters and scoring, and the result of the second and third analysis are presented

in Online Resource 5. A fourth analysis with the same scoring as the previous one (i.e., polymorphism included in the scoring of the characters 11, 31, 36 and 37) was performed, but with implied weighting instead of unweighted characters, with the Goloboff constant (k) value = 3 (as recommended by Goloboff 1993) in order to downweight homoplasic characters. Finally, the multistate characters (3 and 34) were ordered in a fifth analysis, which is otherwise identical to the first one.

Abbreviations

Institutions and localities: AMNH, American Museum of Natural History, New York; **MHN.AIX.PV.**, Muséum d'Histoire Naturelle d'Aix en Provence, collection from Palette; **MNHN.F.**, Muséum National d'Histoire Naturelle, Paris, fossil collections; **MNHN.F.Av**, Avenay; **MNHN.F.CB**, Condé-en-Brie; **MNHN.F.GL**; Sables de Brasles (= 'Gland'); **MNHN.F.Gr**, Grauves; **MNHN.F.Me**, Meudon; **MNHN.F.Mu**, Mutigny; **MNHN.F.Ri**, Rians; **MNHN.F.SN**, Soissons; **MNHN.F.STA**, Saint-Agnan; **MNHN.F.SZ**, Sézanne-Broyes; **NHMUK.PV.M**, Natural History Museum, London, UK, palaeontological vertebrate collections; **UCMP**, University of California Museum of Paleontology, Berkeley; **UM**, University of Michigan Museum of Paleontology; **UM-AV-SK**, Avenay, Université de Montpellier (France), Schmidt-Kittler collection; **UM-BRT**, Le Bretou, Université de Montpellier; **UM-CLR**, Coulondres, Université de Montpellier; **UM-FDN**, Fordones, Université de Montpellier; **UM-FNR2**, Fournes 2, Université de Montpellier; **UM-MGL**, Mas de Gimel, Université de Montpellier; **UM-PAT**, Palette, Université de Montpellier; **UM-VIE**, Vielase, Université de Montpellier; **USNM**, United States National Museum.

Other abbreviations: L, maximal mesiodistal length; **st.**, stylar cusp; **W**, maximal labiolingual width.

Reference levels and biozones: MP, Mammal Paleogene reference level (BiochroM'97 1997); ~MP is used when the designated locality/localities is/are similar in age to the reference locality (i.e., possibly slightly older or younger); PE, Paleocene-Eocene biozone (Hooker 1996).

Dental loci: C, upper canine; c, lower canine; dPX, upper deciduous premolar; dpX, lower deciduous premolar; MX, Xth upper molar; mX, Xth lower molar; PX, Xth upper premolar; pX, Xth lower premolar.

Systematic Paleontology

Mammalia Linnaeus, 1758

Metatheria Huxley, 1880

Marsupialiformes Vullo, Gheerbrant, Muizon & Néraudeau, 2009

Peradectidae Crochet, 1979

Peradectes Matthew & Granger, 1921

Type species: *Peradectes elegans* (see Krishtalka and Stucky 1983b; Fox 1983), early Tiffanian (middle Paleocene) to early Wasatchian (early Eocene).

Peradectes crocheti sp. nov.

LSID urn:lsid:zoobank.org:act:DDB4D655-E26D-46AA-96BA-192DB23B61D4

Figures 3, 4, 5, 6, 7, 8

1980b *Peradectes louisi* Crochet; Crochet: p. 39-42 (in part).

1981 *Peradectes louisi* Crochet; Godinot: p. 51-52, pl. 1, fig. 1 (no fig. 4a; pl. 1, fig. 2) (in part).

1987 *Peratherium constans* Teilhard de Chardin; Godinot et al.: p. 283 (in part).

1988 *Peradectes* sp.; Russell et al.: p. 431.

1991 *Peradectes* sp. indet. (cf. *Peradectes* sp. indet. in Crochet 1980); Marandat: p. 66-68, pl. 1, figs. 1-2, 18 (in part).

1991 *Peratherium constans* Teilhard de Chardin; Marandat: p. 68-69 (in part).

1991 *Amphiperatherium* cf. *brabantense* Crochet; Marandat: p. 71-72 (no pl. 1, fig. 4) (in part).

1996 *Peradectes louisi* Crochet; Louis: p. 94, pl. 2, fig. 7.

2010 *Peradectes* sp.; Hooker: p. 17, fig. 8a-b.

2011 *Peradectes* sp. 2; Smith et al.: p. 18, fig. 5.18.

2020 *Peradectes louisi* Crochet; Hooker: p. 461, fig. 3F-G.

Holotype: MHN.AIX.PV.2018.26.14 (Fig. 3a-c), fragmentary left maxilla with C-P1, anterior root of P2, and M1-M3, housed at the Natural History Museum of Aix-en-Provence. A 3D surface model of this specimen is available on MorphoMuseuM (Lebrun and Orliac 2016).

Etymology: Dedicated to Jean-Yves Crochet, who was the first to describe peradectids from Europe (Crochet 1977a), and who erected the tribe Peradectini (Crochet 1979), later elevated to familial rank (Reig et al. 1985, 1987).

Nomenclatural remark: This new species must be referred to as *Peradectes crocheti* Gernelle, 2024, following the article 50.1 and the recommendation 50A concerning multiple authors of the International Code of Zoological Nomenclature (ICZN 1999: p. 52).

Remark on abbreviations: We use the abbreviation '*Pd.*' for the genus *Peradectes* in order to avoid confusion with species of the genus *Peratherium*, which is abbreviated '*Pt.*'. In fact, the type species of these genera, mentioned for comparative purposes in this study, have the same species name: *Peradectes elegans* and *Peratherium elegans* (Aymard, 1846).

Type locality: Palette, in Provence, France; early Eocene, MP7-MP8+9 interval, ~55 Ma.

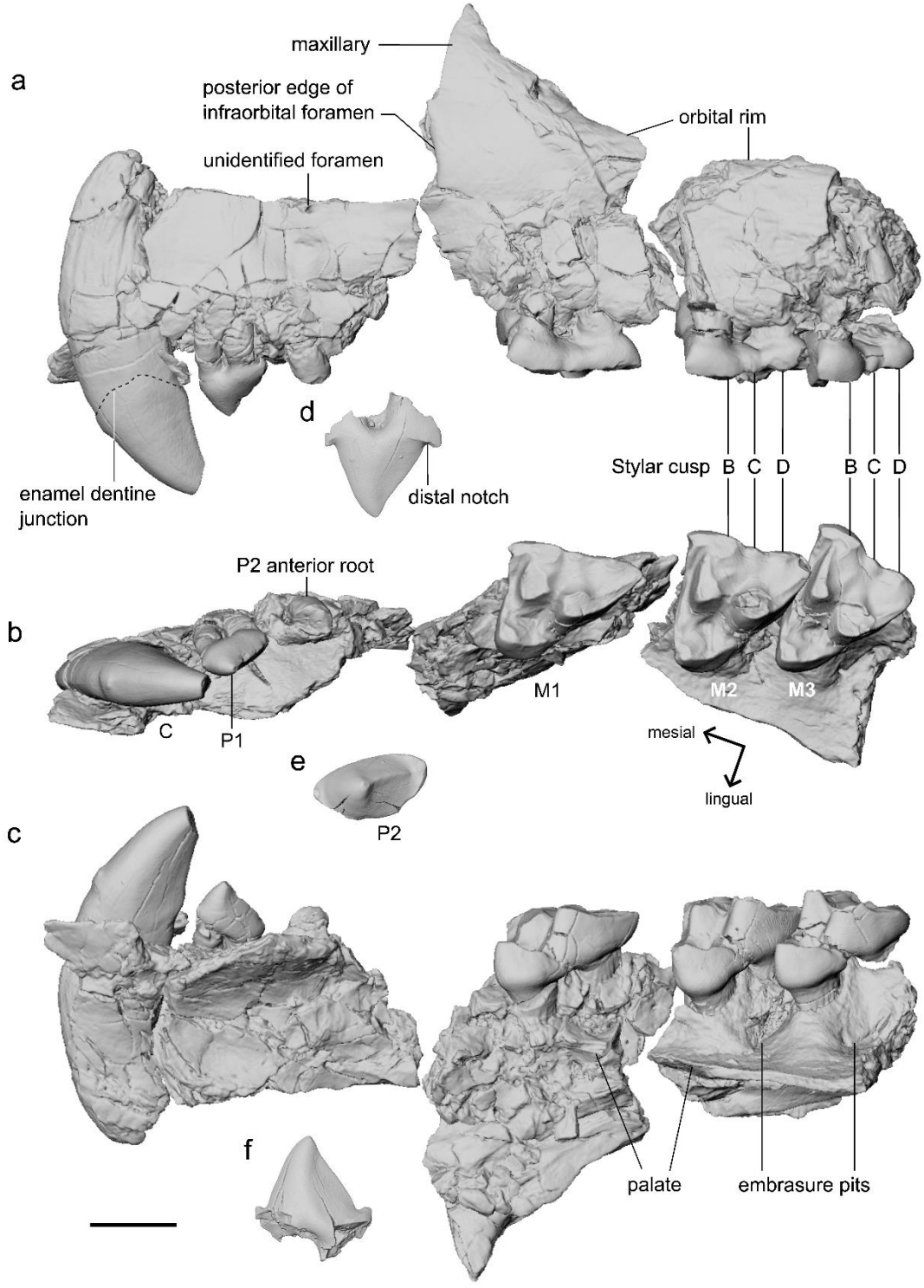

Fig. 3 Composite upper dental row of *Peradectes crocheti* sp. nov. from Palette (Provence; MP7-MP8+9 interval). **a-c**. MHN.AIX.PV.2018.26.14, holotype, fragmentary left maxilla with C-P1, anterior root of P2, and M1-M3 (surface model); **a**. labial (lateral) view; **b**. occlusal (ventral) view; **c**. lingual (medial) view. **d-f**. MHN.AIX.PV.2017.6.6, left P2; **d**. labial view; **e**. occlusal view; **f**. lingual view. The arrows indicating mesial and lingual directions apply to the occlusal view of M1 and M2 (**b**). Scale bar equals 1 mm.

Other localities: Fordones, Fournes and Rians in southern France; Meudon, Soissons and Sotteville-sur-Mer in northern France; Abbey Wood and Croydon in England.

Age: Early Ypresian, known from localities younger than the reference level MP7 and older than MP8+9 (~ mammalian biozones PE II and PE III).

Material: Additional material from Palette: left P2 (MHN.AIX.PV.2017.6.6), mesiolabial fragment of left M1 (MHN.AIX.PV.2017.6.11), right M1 (MHN.AIX.PV.2018.26.20), left M3 (MHN.AIX.PV.2017.6.7), talon of left M3 (MHN.AIX.PV.2017.6.13), lingual fragment of left M4 (MHN.AIX.PV.2017.6.12), fragment of right dentary with alveoli of p1, and p2–m3 (MHN.AIX.PV.2017.6.8), left m1–m4 with fragments of dentary (MHN.AIX.PV.2017.6.9), left worn m3 lacking enamel (MHN.AIX.PV.2017.6.10), right worn m3 (UM-PAT-103), right astragalus (MHN.AIX.PV.2017.6.14). 3D surface models of the specimens MHN.AIX.PV.2017.6.6, MHN.AIX.PV.2017.6.7, MHN.AIX.PV.2017.6.8, MHN.AIX.PV.2017.6.9 and MHN.AIX.PV.2017.6.14 are available on MorphoMuseuM.

Material from Fordones: right M1 (UM-FDN-1, Marandat 1991: pl. 1, fig. 1), fragmentary right M1 (UM-FDN-2), right partial maxillary with fragmentary M2-M3 (UM-FDN-21), labial fragment of right M2 (UM-FDN-285), distal fragment of right M2 (UM-FDN-287), worn fragment of left M2 (UM-FDN-288), labial fragment of right M3 (UM-FDN-23, Marandat 1991: pl. 1, fig. 2), labial fragment of right M4 (UM-FDN-286), worn fragment of left M4 (UM-FDN-289).

Material from Soissons: left M1 (MNHN.F.SN76), left M3 (MNHN.F.SN18), fragment of left M3 (MNHN.F.SN78), right m1 (MNHN.F.SN121), right m3 (MNHN.F.SN2508; Louis 1996: pl. 2, fig. 7).

Material from Meudon: right worn M1 (MNHN.F.Me16079), labial fragment of right M2 (MNHN.F.Me15975), left M4 (MNHN.F.Me16084), left m2 (MNHN.F.Me16101), left trigonid (MNHN.F.Me16167).

Material from Sotteville-sur-Mer: right M3 (Smith et al. 2011: fig. 5.18).

Material from Croydon: right M2 (NHMUK.PV.M66046; Hooker 2020: fig. 3F-G).

Material from Abbey Wood: labial fragment of left M2 (NHMUK.PV.M44991; Hooker 2010: fig. 8a-b).

Material from Fournes: left M1 (UM-FNR2-1), fragment of left M2 (UM-FNR2-2). The acronym FNR2 is relative to a recent sampling of the fossiliferous level, lateral to the classic FNR locality (Marandat 1991).

Material from Rians: right m1 (MNHN.F.Ri516), left m2 (MNHN.F.Ri221; Godinot 1981: pl. 1, fig. 1).

Differential diagnosis: Differs from all other European peradectids (*Pd. russelli*, *Pd. louisi* and '*Armintodelphys*' *dufraingi* Smith & Smith, 2013) in having lower molars with: (i) a weaker, sometimes absent, labial emargination of the crown; (ii) trigonid as labiolingually wide as talonid on m3; (iii) relatively higher entoconid and hypoconulid separated by a deeper notch; and (iv) distinct postcingulid on m4. Further differs from *Pd. louisi* and *Pd. russelli* in having stylar cusp C apex as or more ventral than stylar cusp D apex on M3 (upper molars of '*Arm.*' *dufraingi* are unknown). Further differs from *Pd. louisi* and '*Arm.*' *dufraingi* in: (i) its relatively wider lower molars; and (ii) always curved instead of at least most often rectilinear postcristid. Further differs from *Pd. louisi* in having: (i) stylar cusp D labial instead of distolabial to metacone apex on M3; and (ii) stylar cusp C apex as or more ventral than stylar cusp D apex also on M1 and M2. Further differs from *Pd. russelli* in its smaller size. Further differs from

'*Arm.*' *dufraingi* notably by: (i) entoconid higher than hypoconulid on m2 and as high as hypoconulid on m3; and (ii) larger postcingulid on m2 and m3.

Peradectes crocheti sp. nov. differs from the North American species *Pd. elegans* (type species) and *Pd. protinnominatus* (Fig. 4) in having: (i) p3 higher than m1; (ii) stylar cusp D distolabial instead of labial to metacone apex on M1; (iii) stylar cusp B labial instead of mesiolabial to paracone apex on M3; (iv) asymmetric ectoflexus on M3; and (v) less disparity between length to width ratio of M2 and M3. Further differs from *Pd. elegans* in having: (i) m1 slightly shorter than m2; (ii) m4 shorter than m3; (iii) postcingulid that attenuates labially to the hypoconulid; (iv) stylar cusp B much larger than stylar cusp A on M3; (v) postmetaconular crista that ends lingually to the base of the metacone; (vi) less mesiodistally long talon on upper molars; and (vii) protocone strictly lingual to the paracone apex on M1 and M2.

Comparative description

Remarks: Due to its status as the oldest known European peradectid, and the relative completeness of allocated fossils, *Peradectes crocheti* sp. nov. is compared to Paleocene – Eocene North American peradectids (e.g., Fig. 4), in addition to other European species.

Maxillary region: The holotype MHN.AIX.PV.2018.26.14 is composed of three fragments of maxillary. The fragment bearing the canine, P1, the anterior root of P2 and part of the palate is crushed transversally (Fig. 3a-c). On the fragment bearing M1, the wide distal opening of the infraorbital foramen, with a vertical and straight distal edge, was positioned dorsally to P3 (Fig. 3a). This is congruent with the position of the infraorbital foramen in the other few peradectids in which the maxillary is known, namely *Pd. gulottai* Rose, 2010, *M. houdei* (Horovitz et al. 2009: fig. 2B), and a possible unnamed peradectid from Messel (Kurz and Habersetzer 2004: fig. 2). A small foramen is present dorsally to the anterior root of P2. Compared to the position

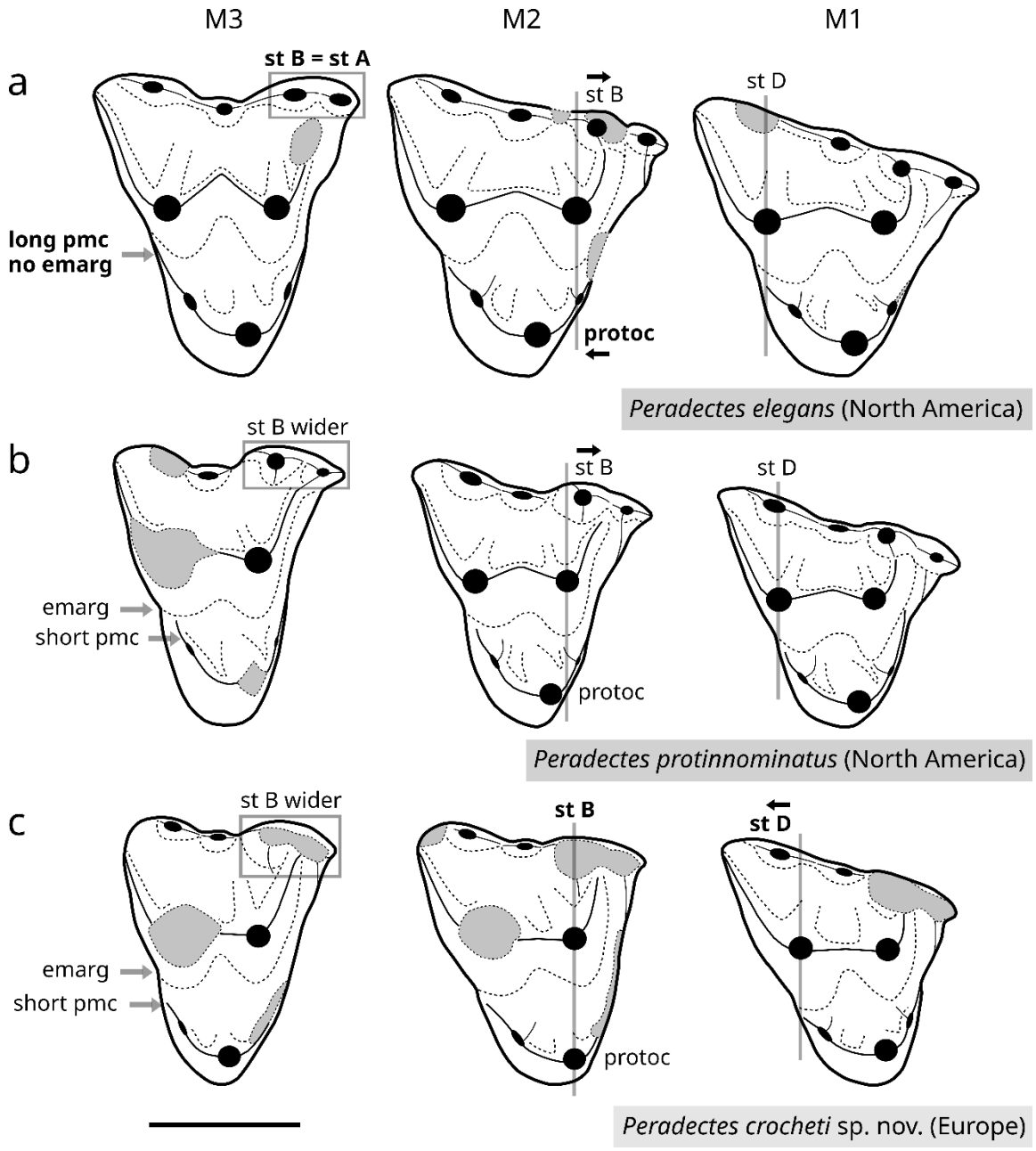

Fig. 4 Interpretative drawings of the occlusal morphology of upper molar rows (M1-M3) of *Peradectes elegans*, *Pd. protinnominatus* and *Pd. crocheti* sp. nov. **a**. *Peradectes elegans*, based on a cast of AMNH 17383 (attribution from Simpson 1935). Grey coloured areas are either broken or lacking on the available cast. **b**. *Peradectes protinnominatus*, based on casts of the holotype, UCMP 44077. The metacone is broken (here in grey coloured area) on the M3 of the original specimen (McKenna 1960). **c**. *Peradectes crocheti* sp. nov., based on the original specimen MHN.AIX.PV.2018.26.14 (reversed view). Note the progressive loss of metastylar wing preservation from M1 to M3 on this specimen. The grey coloured areas are either broken (metacone) or worn (stylar cusps A and B, and mesial edge of the talon). The dashed lines concern depressions on the occlusal surface on all drawings. Main morphological differences

between the three dental rows are figured on drawings. Abbreviations: **emarg**, distal emargination; **pmc**, postmetaconular crista; **protoc**, protocone; **st A**, stylar cusp A; **st B**, stylar cusp B; **st D**, stylar cusp D. Black arrows indicate the offset position of a cusp or stylar cusp compared to the axis perpendicular to the paracone – metacone axis. Scale bar equals 1 mm.

that would be expected for an incisivomaxillary foramen (just mesial to the infraorbital foramen; e.g., Rose 2010), it is more ventral and probably more mesially positioned. The fragment bearing the M1 extends more dorsally than the two others. It potentially preserved the most external part of the lacrimal on its dorsoposterior crushed region. The maxillary-jugal suture is not visible, as in *Pt. cuvieri* (Fisher, 1829) (Selva and Ladevèze 2017: p. 5). However, the rostrum fragment with the M2 and the M3 probably includes part of the jugal in addition to the maxillary, because the orbital rim is preserved on the most dorsal points between M1 and M3 (Fig. 3a). The most ventral point of the orbital rim is distal to the infraorbital foramen. The orbital rim ascends dorsally on the maxillary distally to the infraorbital foramen, and dorsally to the posterior root of the M1. These observations are also congruent with the position and morphology of the orbital rim in other peradectids. The palate region of the maxillary is preserved without apparent deformation distolingually to M1, and lingually and around M2 and M3 (Fig. 3b-c). M1-M4 alveoli are separated by deep embrasure pits (Fig. 3c).

Upper canine: MHN.AIX.PV.2018.26.14 documents the most complete upper canine of *Peradectes*. Only the apex of the crown is not preserved. The whole tooth is sharp and distally curved. The base of the crown is transversally compressed, less than twice as long as wide (Table 2). The crown is relatively low compared to the root, the latter being dorsoventrally longer (Fig. 3a). The crown is also less than twice as high as the one of P2. In *Mimoperadectes*, the crown of the upper canine is on the contrary much higher than its root and more than twice as high as P2 (Horovitz et al. 2009: fig. 2B). Compared to the upper premolars, the upper canine has an oval-shaped cross-section with equally convex lingual and labial edges. This tooth is

particularly short in cross-section, being mesiodistally longer than P1 (MHN.AIX.PV.2018.26.14), but shorter than P2 (MHN.AIX.PV.2017.6.6). Such a mesiodistally relatively short upper canine is known in *Pd. elegans*, for which the section of a partial right canine is documented (Simpson 1935: fig. 3), but not in *Mimoperadectes*, in which the single specimen preserving this tooth has a upper canine longer than the P2 (Horovitz et al. 2009: fig. 2B). The relative height and length of the upper canine of MHN.AIX.PV.2018.26.14 are similar to those of specimens interpreted as females of *Pucadelphys* by Ladevèze et al. (2011) (Muizon and Ladevèze 2022: p. 616-617), and to some herpetotheriids (Crochet 1980b: figs. 165-167; Sánchez-Villagra et al. 2007: fig. 1c). The crescentiform distal edge of the crown is labiolingually pinched, unlike the convex mesial edge. Mesial and distal edges are both flanked by a small bulge positioned at the base of the crown. The upper canine is separated from the premolars by a small space, which could be the result of fragmentation (see the lingual view, Fig. 3c). Furthermore, no diastema is present between the upper canine and the P1 of *Pd. elegans* (Simpson 1935: fig. 3), *Mimoperadectes houdei* (Horovitz et al. 2009: figs. 1A, 2B), or the most complete possible peradectid specimen from Messel (Kurz and Habersetzer 2004: fig. 3B).

Table 2 Measurements (in mm) of selected teeth of *Peradectes crocheti* sp. nov. from Palette (MHN.AIX.PV.).

Locus	Length (mm) x Width (mm) [Length / Width]			
	MHN.AIX.PV.2018.26.14 (upper)	2017.6.6 (upper)	2017.6.8 (lower)	2017.6.9 (lower)
C	1.23 x 0.69 [1.78]	-	-	-
P1	0.93 x 0.44 [2.11]	-	-	-
P2 or p2	-	1.35 x 0.64 [2.11]	? x 0.71	-
p3	-	-	1.20 x 0.68 [1.76]	-
M1 or m1	1.55 x 1.59 [0.97]	-	-	1.57 x 0.93 [1.69]
M2 or m2	1.50 x 1.70 [0.88]	-	1.65 x 1.04 [1.59]	1.64 x 1.03 [1.59]
M3 or m3	1.40 x 1.77 [0.79][a]	-	1.66 x 1.04 [1.60]	1.68 x 1.06 [1.58]
m4	-	-	-	1.55 x 0.92 [1.68]

[a] Metastylar wing worn; length value possibly slightly underestimated

Upper premolars: The upper premolars are two-rooted. The mesial root of P2 has a much larger diameter and is higher than the roots of P1 (MHN AIX.PV.2018.26.14, Fig. 3a-b); thus, P2 was considerably larger than P1. The mesial root of P2 is aligned with the roots of P1. The crown of P1 is asymmetric, with the apex of the main cusp mesially placed, ventral to the posterior margin of its anterior root. The convex anterior edge of the crown is slightly triangular in shape in lateral view. The most mesial point of the crown is closer to the base than to the apex of the crown. The lingual and labial edges of P1 are equally convex. The main cusp of P1 bears a relatively long and worn distal crista. In lateral view, this distal crista is not strictly rectilinear, but more vertically inclined near the apex. There are no basal accessory cusps nor cingula on P1. P1 and P2 are separated by a small diastema, slightly longer than the space between C and P1. P1 and P2 are also separated by a diastema in *Mimoperadectes houdei* and in the most complete peradectid-like specimen from Messel, but not in *Pd. elegans*. No crown of P2 or P3 is preserved on the holotype, but an isolated premolar crown from Palette is interpreted as a left P2 (MHN.AIX.PV.2017.6.6, Fig. 3d-f), based on its similarity with that premolar locus in other peradectids, as detailed below. It is longer and wider than the crown of P1, and approximately twice as high as P1, as for *Pd. elegans* (Simpson 1935: fig. 3), whereas it is much higher in *Mimoperadectes* (Horovitz et al. 2009). P1 and P2 of *Pd. crocheti* sp. nov. have the same value for their length to width ratio (Table 2). Similarly to *Pd. elegans* and *Mimoperadectes*, the P2 MHN.AIX.PV.2017.6.6 is relatively less mesiodistally elongated than that of *Pd. gulottai*. P2 is less asymmetric than P1, the apex of the former being positioned more distally relatively to the ventral inter-alveolar septum. In occlusal view, the labial edge of the crown is almost rectilinear, whereas the lingual edge is convex. The main cusp is surrounded by one mesial and one distal basal accessory cusp. The mesial accessory cusp is placed slightly labially to the mesiodistal axis of P2. Each accessory cusp is connected to a lingual and a labial cingulum. Both accessory cusps of P2 are the same height, but the distal one is longer, wider,

and has stronger cingula. In *Pd. elegans* and *Pd. gulottai*, for which both P2 and P3 are documented, the mesial accessory cusp of P3 has more distally extended cingula than the one of P2 in occlusal and lingual views. The whole labial edge of P3 in *Pd. elegans* is evenly surrounded by a cingulum. The mesial accessory cusp of MHN.AIX.PV.2017.6.6 has cingula relatively weakly developed, like the P2 of other peradectid species (Fig. 3d-e). In lateral view, the mesial edge of the main cusp is convex and the crested distal edge is slightly concave near the apex (Fig. 3d, f). In the same view, there is a notch between the distal crista of the main cusp and the distal accessory cusp, as on all P2 and P3 known for *Peradectes*, namely *Pd. elegans* (AMNH 17383, pers. obs.), *Pd. gulottai* (Rose 2010: fig. 1) and *Peradectes californicus* (Stock, 1936) (Lillegraven 1976: fig. 6). By contrast, the distal crest and accessory cusp are highly connected in *Mimoperadectes* and in most herpetotheriids, so that this notch is absent in, for example, *Herpetotherium* (e.g., Lillegraven 1976: pl. 5, figs. 1-2; Sánchez-Villagra et al. 2007: fig. 1c; Korth 2018: figs. 1c, 9a), *Peratherium* (e.g., Crochet 1980b: fig. 205) and the type species of *Amphiperatherium* (Koenigswald 1970: fig. 16). In occlusal and distal views, the distal crista of the main cusp is slightly curved lingually, so that it distally terminates mesiolingually to the distal accessory cusp.

Upper molars: Upper molars are three-rooted. M1 are triangular in shape, almost as long as wide. M2 are shorter and wider than M1 (Table 2). In turn M3 are shorter and wider than M2, so that the length to width (L/W) ratio decreases from M1 to M3 on the holotype (Table 2). The low disparity of length to width ratio between M2 and M3 (= L/W M2 - L/W M3 < 0.10, Table 2) evidences a low discrepancy of proportions between upper molars of MHN.AIX.PV.2018.26.14. The protocone is strictly lingual to the paracone on M1 and M2, like *Pd. protinnominatus*, but unlike *Pd. elegans*, in which the protocone is distolingual to the paracone on these upper molar loci (Fig. 4), and is slightly distolingual to the paracone on M3

and M4 (Figs. 4c, 5t). The protocone may be more mesial on other M3 (e.g., UM-FDN-21, Fig. 5d; MNHN.F.SN18, Fig. 5q) or almost lingual to the centrocrista midpoint on the M3 of the holotype (Fig. 4c). The talon is more mesiodistally expanded on M1 and M2 than on M3. Among M3, the talon is distinctly mesiodistally narrow only on MNHN.F.SN78. A sharp ridge is present on the lingual edge of the acute protocone of the M3 of UM-FDN-21 (Fig. 5d). Such a sharp protocone ridge occurs at least in some other peradectid species (e.g., McGrew 1937: fig. 3). The protocone is always procumbent and lower than the paracone, on all upper molar loci (e.g., Fig. 5n, s). Both conules are relatively small. The metaconule is larger than the paraconule (e.g., Fig. 5n), although still low in distolingual view (Fig. 3c). The paraconule is positioned slightly more labially than the metaconule. The preparaconular crista extends labially to form the mesial edge of the paracingulum, and the postmetaconular crista ends lingually to the base of the metacone. Faint internal conular cristae often connect the conules to the base of the paracone or metacone, mostly on M1 (e.g., Figs. 4c, 5e, k). Such serial variation for the presence of the internal conular cristae is noted in the dental rows of *Pd. elegans* and *Pd. protinnominatus*, with their M3 lacking the internal conular cristae (Fig. 4b-c). Only one M3 of *Pd. crocheti* sp. nov. has an internal conular crista, on the metaconule (Smith et al. 2011: fig. 5.18B). A deep basin is present on the talon distolabially to the paraconule and mesiolabially to the metaconule of all upper molars.

The distal edge of M1-M3 is often emarginated between the talon and stylar shelf. This emargination is deep (e.g., UM-FNR2-1, Fig. 5k) to occasionally absent on Palette specimens (MHN.AIX.PV.2017.6.7 and MHN.AIX.PV.2018.26.20, Fig. 5g, m). The distal emargination is present on M3 of *Pd. protinnominatus*, but not on M3 of *Pd. elegans*, for which the postmetaconular crista extends distolabially to the lingual extremity of the metacone base (Fig. 4a; Krishtalka and Stucky 1983b: fig. 3) unlike the M3 of both *Pd. crocheti* sp. nov. and *Pd. protinnominatus*. The paracingulum is straight and mesiodistally long on most specimens,

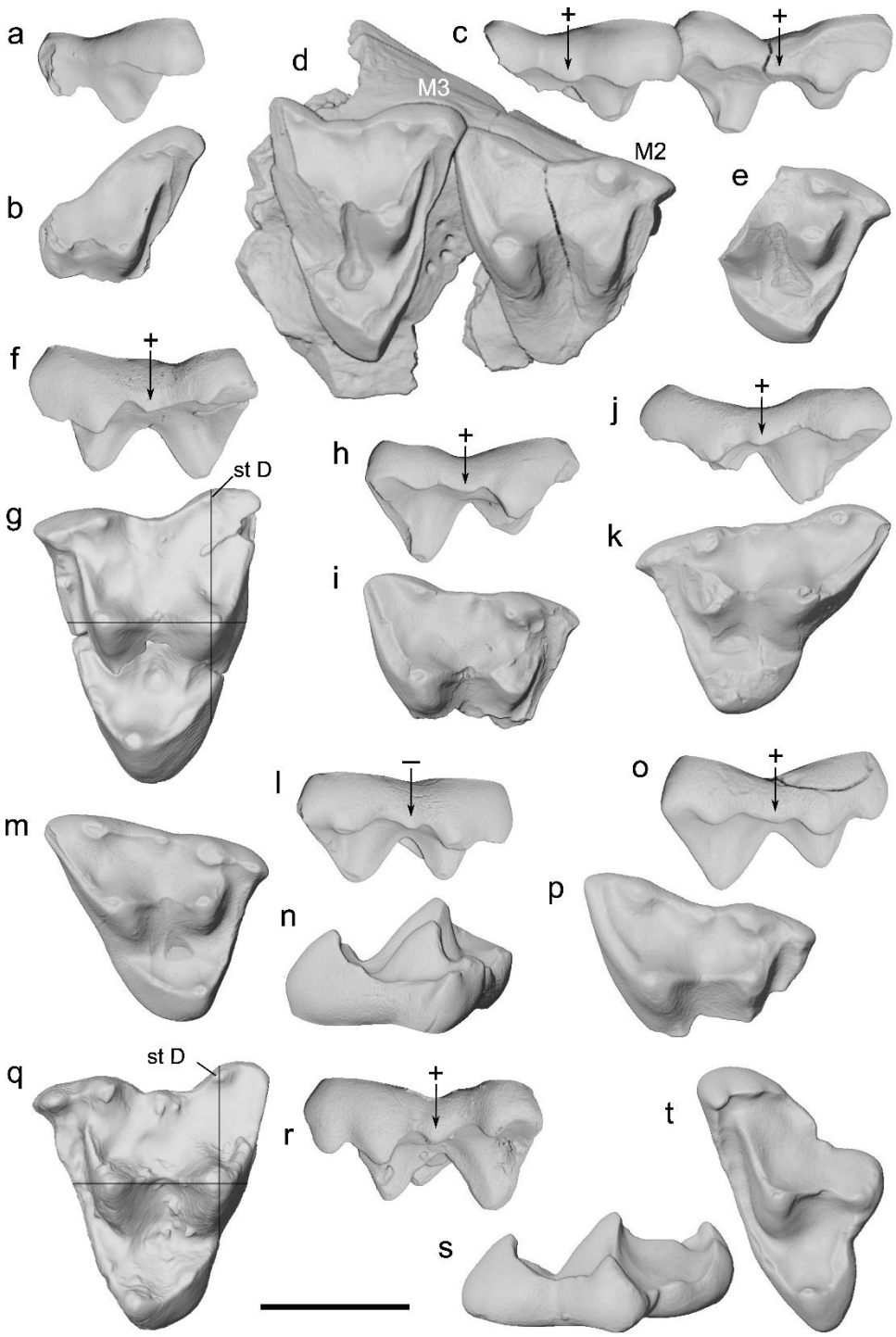

Fig. 5 Upper molars of *Peradectes crocheti* sp. nov. from Fordones, Fournes, Meudon, Palette and Soissons (France; MP7-MP8+9 interval). **a-b**. UM-FDN-286, labial fragment of right M4; **a**. labial view; **b**. occlusal view. **c-d**. UM-FDN-21, right partial maxillary with fragmentary M2-M3; **c**. labial view; **d**. occlusal view. **e**. UM-FDN-2, fragmentary right M1 in occlusal view. **f-g**. MHN.AIX.PV.2017.6.7, left M3 (surface model); **f**. labial view; **g**. occlusal view. **h-i**. UM-FDN-285, labial fragment of right M2; **h**. labial view; **i**. occlusal view. **j-k**. UM-FNR2-1, left M1; **j**. labial view; **k**. occlusal view. **l-n**. MHN.AIX.PV.2018.26.20, right M1; **l**. labial view;

m. occlusal view; **n**. mesial view. **o-p**. MNHN.F.Me15975, labial fragment of right M2; **o**. labial view; **p**. occlusal view. **q-r**. MNHN.F.SN18, left M3 (surface model); **q**. occlusal view; **r**. labial view. **s-t**. MNHN.F.Me16084, left M4; **s**. distal view; **t**. occlusal view. The arrows denoting the stylar cusp C on labial views are followed by '+' if the most ventral point on the st. C – st. D mesiodistal extension is reached on the st. C, and by '-' if this most ventral point is reached on the st. D. The segments on the occlusal views of MHN.AIX.PV.2017.6.7 and MNHN.F.SN18 (**g** and **q**) are positioned on the paracone – metacone axis and its perpendicular line. Abbreviation: **st D**, stylar cusp D. Scale bar equals 1 mm.

whereas the mesial edge is slightly emarginated mesially to the paracone on the M1 of the holotype (Fig. 3b), the M2 from Croydon (Hooker 2020: fig. 3G), and more strongly emarginated on the M1, M3 and one M4 from Fordones (UM-FDN-286, Fig. 5b; UM-FDN-21; Fig. 5d; UM-FDN-23; Marandat 1991: pl. 1, fig. 2). The height of the paracone and metacone varies for a given molar locus, but the paracone is always lower on M1-M3. For example, on the unworn M1 the paracone and metacone can be subequal in height, the paracone being slightly lower (e.g., MHN.AIX.PV.2017.6.11, MHN.AIX.PV.2018.26.20; Fig. 5l), or the paracone can be much lower than the metacone (e.g., MNHN.F.SN76). It is worth mentioning that a paracone and metacone that are subequal in height have also been documented in *Pt. constans* (e.g., Ladevèze et al. 2012: fig. 5Ga). The paracone is also less mesiodistally long than the metacone. The paracone and metacone are conical, with a convex labial edge contrary to herpetotheriids, where these main cusps are triangular. The labial edge of these cusps is narrower labiolingually than their lingual edge. The centrocrista is straight, unlike the V-shaped centrocrista of most herpetotheriids. Some upper molars have a less straight centrocrista than M1-M3 of the holotype, such as UM-FDN-1 for M1 (Fig. 5e), UM-FDN-21 for M2 (Fig. 5d), MNHN.F.SN18 for M3 (Fig. 5q) and MNHN.F.Me16084 for M4 (Fig. 5t). The same variation is established for *Pd. elegans* specimens, with the centrocrista of AMNH 17383 upper molars being more V-shaped (especially on the M3 and M4, Fig. 4a) with respect to the strictly straight

centrocrista of the upper molars of the paratype AMNH 17369 (Krishtalka and Stucky 1983b: fig. 3). The postmetacrista is generally low, and it does not define a distal wall on the less worn stylar shelf (e.g., MHN.AIX.PV.2017.6.7, Fig. 5g; MNHN.F.Me15975, Fig. 5p), except on two upper molars, namely the M1 MHN.AIX.PV.2018.26.20 (Fig. 5n) and the fragmentary M3 MNHN.F.SN78. Distal to the metacone, the distal margin of the tooth is mesiodistally long instead of being strictly vertical on one M3 and two M1 from Palette (MHN.AIX.PV.2017.6.7, Fig. 5g; MHN.AIX.PV.2017.6.11 and MHN.AIX.PV.2018.26.20, Fig. 5m). The same variation is seemingly also present in the herpetotheriid *Peratherium constans* Teilhard de Chardin, 1927 (Ladevèze et al. 2012: fig. 5Gb vs fig. 5Hb). The stylar shelf labiolingually widens relative to the talon from M1 to M4. It is approximately slightly narrower than the talon on M3, and subequal in width with the talon on the M4 MNHN.F.Me16084 (Fig. 5t).

The stylar line bears four stylar cusps, from stylar cusp A to stylar cusp D, in most specimens. However, there is a distinct stylar cusp E on a single specimen of the sample, MNHN.F.SN78, where it is as high as stylar cusps C and D, but less mesiodistally long. Stylar cusp B is dominant in size over the other stylar cusps in *Pd. crocheti* sp. nov. and *Pd. protinnominatus*, whereas it is subequal in length and width to stylar cusp A in *Pd. elegans* (Fig. 4b-c vs Fig. 4a). It is worth noting that stylar cusps A and B are of the same labiolingual width on the M3 of UM-FDN-21 (Fig. 5d). On M1-M3 of *Pd. crocheti* sp. nov., stylar cusp A is higher than stylar cusps C and D. The spur-like stylar cusp A can be mesiolabial or labial to the paracingulum on M1 (Figs. 3b, 5k vs Fig. 5m), M2 (Fig. 5d and UM-FNR2-2 vs Figs. 3b, 5i, p) and M3 (Fig. 5g, q vs Figs. 3b, 5d). Stylar cusp A bears a sharp mesial crest. Stylar cusp A is most frequently placed mesiolingually to stylar cusp B on M2 and M3, as in the European *Pd. louisi* and *Pd. russelli*, or *Peradectes chesteri* Gazin, 1952 (e.g., Murphey et al. 2018: fig. 13.3), and *Pd. californicus* (e.g., Lillegraven 1976: pl. 7, fig. 1c), whereas the two stylar cusps are most often aligned in *Pd. elegans* and *Pd. protinnominatus* (e.g., Fig. 4; see also comparison in Online Resource 3:

Fig. S10). An exception for *Pd. crocheti* sp. nov. is the M3 of UM-FDN-21 on which stylar cusp A is strictly mesial to stylar cusp B. From M1 to M4, the preparacrista elongates, stylar cusps A and B are increasingly close, and the relative height of stylar cusp A gradually increases, so that stylar cusp A is higher than stylar cusp B on the unworn M4 (Fig. 5s). All these tendencies are evidenced on the composite upper molar series from Fordones (Fig. 5a-e). On the holotype MHN.AIX.PV.2018.26.14, the preparacrista labially connects stylar cusp B on the M1 and M2, and stylar cusp A on the M3 (Fig. 4c). In the whole sample, the connection of the labial end of the preparacrista is as such in 6 out of 8 of the M1 (e.g., Fig. 5m), 4 out of 6 of the M2 with available preparacrista and stylar cusps A and B (e.g., Fig. 5i), and 4 out of 6 of the M3 (e.g., Fig. 5d, g). M1 to M3 specimens with a different labial connection of this crest have a preparacrista that labially ends in an intermediate position between stylar cusps A and B, namely UM-FDN-2 and UM-FNR2-1 for M1 (Fig. 5e, k), MNHN.F.Me15975 for M2 (Fig. 5p) and MNHN.F.SN18 and the upper molar from Sotteville-sur-Mer for M3 (Fig. 5q; Smith et al. 2011: fig. 5.18B). The M2 of the holotype of *Pd. protinnominatus* also has a preparacrista that labially ends in an intermediate position between the anterior stylar cusps (Fig. 4b). One M2 of *Pd. crocheti* sp. nov. (UM-FDN-21) has a preparacrista that connects to stylar cusp A (Fig. 5d). The preparacrista of most M1 and M2 connects to stylar cusp B through a thin crest situated on the lingual edge of stylar cusp B. Even without connection between these structures on M3, such a crest may be present (e.g., UM-FDN-21, Fig. 5d). On M1-M3, stylar cusp B is conical, lower than the paracone (labial views of Fig. 5) and generally positioned strictly labially to the paracone apex. Stylar cusp B is relatively slightly more mesial on the M3 of the holotype (Fig. 4c), on UM-FDN-23 and maybe on the M3 of UM-FDN-21 (Fig. 5d), but the broken metacone of the latter prevents unequivocal observation. Stylar cusp B is mesiolabial to the paracone apex on M1-M3 of Paleocene - Eocene North American peradectids, such as *Pd. elegans* (Fig. 4a; Krishtalka and Stucky 1983b: fig; 3), *Pd. protinnominatus* (Fig. 4b; McKenna

1960: fig. 18b; Bown 1979: fig. 40a right), and *Pd. chesteri* (e.g., West 1973: pl. 1, figs. c-d). We should mention that stylar cusp B is also strictly labial to the paracone apex on upper molars of *Pd. protinnominatus* from the Clarkforkian-3 (late Paleocene) and Wasatchian-M (early Eocene) localities of the northern Bighorn Basin (pers. obs.; Gingerich and Smith 2006: fig. 26E), and of cf. *Pd. protinnominatus* from the Wasatchian-0 of the southern Bighorn Basin (Rose et al. 2012: fig. 14A-C).

Stylar cusps C and D are more labiolingually pinched than stylar cusp B. Stylar cusp C is labial to the midpoint of the centrocrista. The single upper molar with a double stylar cusp C is the M2 from Abbey Wood (Hooker 2010: fig. 8a-b), on which the distal stylar cusp C is larger than the mesial one. The doubling of stylar cusp C is as rare as in *Pd. louisi* (see below); it is more frequent in herpetotheriids such as *Pt. constans* (Ladevèze et al. 2012) and *Amphiperatherium maximum* Crochet, 1979 (Crochet 1980b: p. 98-100), and seemingly in *Mimoperadectes* (M2 in Bown and Rose 1979: fig. 2; Gingerich and Smith 2006: fig. 15C; Beard and Dawson 2009: fig. 4A; M1 in Horovitz et al. 2009: fig. S1C). Stylar cusp C has an intermediate position between stylar cusps B and D, with the exception of two M1 where stylar cusps B and C are more closely appressed together (MNHN.F.SN76 and UM-FNR2-1; Fig. 5j-k). On a given molar locus, stylar cusps C and D can be highly connected or separated by a fossa (e.g., for M3, Fig. 5f vs Fig. 5r). In occlusal view, the area occupied by stylar cusp C is less important than the area of stylar cusp D on M1 and M2 (especially on M1, Figs. 4c, 5i, k, m, p). Stylar cusps C and D are subequal in width on M3. In labial view, the apex of stylar cusp C is as ventral or more ventral than the apex of stylar cusp D on all M1-M3, with the exception of the M1 MHN.AIX.PV.2018.26.20 (Fig. 5l; 1 out of 18 available specimens). Altogether, the relative heights of the stylar cusps of M1 to M3 of *Pd. crocheti* sp. nov. are mostly as follows: st. B > A ≥ C ≥ D (Table 3). Among ascertained peradectids, the apex of stylar cusp C is also at least as ventral as the apex of stylar cusp D only in the oldest *Peradectes* species, namely *Pd. minor*,

Table 3 Height relationships of stylar cusps (A to D) of all ascertained peradectid species for which M2 and/or M3 are known. See method [1] for estimating stylar cusp heights in Fig. 2a. Species positioned above the median horizontal line of the table have stylar cusp C apex at least as ventral as stylar cusp D apex; species positioned below the median horizontal line have stylar cusp C apex less ventral than stylar cusp D apex, at least on one locus, or have vestigial stylar cusp C. Height relationships of stylar cusps are partially in bold when stylar cusp B is not dominant over other stylar cusps. *, more than one specimen of the species (including illustrated specimens) has been observed in labial view in this study.

Species	Stylar height relationships	References
Armintodelphys dawsoni	M2: **B = C**	Krishtalka and Stucky (1984: p. 40)
*Mimoperadectes labrus**	M2: B > C ≥ D ≥ A M3: B > A > C > D [a]	Gingerich and Smith (2006: fig. 15C); Rose et al. (2012: fig. 12E)
Mimoperadectes sowasheensis	M2: B > A > C > D	Beard and Dawson (2009: fig. 4A)
Peradectes coprexeches	M3: **C ≥ B** > D	Williamson and Taylor (2011: fig. 6.7)
Peradectes crocheti sp. nov.*	M2-M3: B > A ≥ C ≥ D	this study; e.g., Smith et al. (2011: fig. 5.18A); Hooker (2020: fig. 3F)
Peradectes elegans	M2: **B = C** > A = D M3: B > A > C ≥ D	cast of AMNH 17383 (in Simpson 1935: fig. 3)
Peradectes minor	M2-M3: B = A > C > D	Clemens (2006: fig. 2C, E)
*Peradectes protinnominatus**	M2-M3: B > A = C = D	cast of UCMP 44077 (holotype); Gingerich and Smith (2006: fig. 26D)
Didelphidectes cf. *pumilis*	M3: B > D >> C (vestigial or absent)	Kihm and Schumaker (2015: fig. 13N-O)
Mimoperadectes houdei	M2: B > D >> A = C M3: B = A > D >> C	Horovitz et al. (2009: fig. S1C)
Nanodelphys hunti	M2-M3: B > D >> C (vestigial or absent)	McGrew (1939: 394, fig. 114); Korth (1994: 390, fig. 7.1-2)
Peradectes californicus	M3: B = A > D >> C	Lillegraven (1976: pl. 7, fig. 1a)
Peradectes chesteri	M2-M3: B >> C, D (vestigial or absent)	Krishtalka and Stucky (1983b, 1984); Murphey et al. (2018)
Peradectes gulottai	M2: B > A > D >> C M3: B = A > D >> C	Rose (2010: fig. 1.1)
*Peradectes louisi**	M2: B > A > D > C [b] M3: B > A >> D > C	this study
*Peradectes russelli**	M2: B > A = C = D M3: B > A > D > C	this study

[a] the relative height of stylar cusp A of M3 differs from the one reported by Bown and Rose (1979: p. 90) for the holotype.
[b] in one M2 specimen (MNHN.F.CB3228; Fig. 10i), stylar cusp C is lower than stylar cusp D.

Pd. coprexeches, *Pd. elegans*, *Pd. protinnominatus*, and in *Mimoperadectes labrus* and *M. sowasheensis* (Table 3). Stylar cusp C is also relatively prominent (equal in size to stylar cusp B) on the only upper molar attributed to *Armintodelphys* (Table 3). In labial view, the distal crest of stylar cusp C is always mesiodistally longer than its mesial crest on M1-M3. Stylar cusp D is distolabial to the metacone on M1 (labial to the metacone on M1 of *Pd. elegans* and *Pd.*

protinnominatus; Fig. 4) and strictly labial to the metacone on M3. Stylar cusp D of M2 can be strictly labial or distolabial to the metacone (e.g., Fig. 5i vs Figs. 4c, 5p). This variation may occur also in *Pd. protinnominatus* because unillustrated M2 attributed to this species by Gingerich and Smith (2006: p. 254) (UM 113378 and UM 113391, pers. obs. of corresponding casts) have a stylar cusp D distolabial to the metacone contrary to the holotype of *Pd. protinnominatus* (Fig. 4b). The relatively lowest stylar cusp D of the sample is on the M3 UM-FDN-23 (Marandat 1991: pl. 1, fig. 2). The ectoflexus is absent on all M1, which have a straight labial margin unlike M1 in *Pd. protinnominatus* (e.g., Fig. 4b vs Fig. 4c). M2 have shallower asymmetric ectoflexus than M3. The ectoflexus is always long and asymmetric on M3, with a metastylar wing more labially extended than the parastylar wing. Variations in the depth and degree of asymmetry of the ectoflexus of M3 exist, both in Palette (MHN.AIX.PV.2018.26.14, Fig. 4c vs MHN.AIX.PV.2017.6.7, Fig. 5g) and Fordones (UM-FDN-21, Fig. 5d vs UM-FDN-23, Marandat 1991: pl. 1, fig. 2). The metastylar wing is worn on the M2 and M3 of MHN.AIX.PV.2018.26.14, especially on the M3 (Fig. 4c), resulting in the weak asymmetry of the ectoflexus mentioned. The metastylar wing is acute on unworn M1-M3.

Additional description of the M4 can be made. This locus is documented by four specimens, of which only the left M4 from Meudon (MNHN.F.Me16084, Fig. 5s-t) is complete. The straight centrocrista of M4 is shorter than on more anterior molars, and this upper molar is mesiodistally shorter than others. On MNHN.F.Me16084, the protocone is lower than the paracone but higher than the metacone (Fig. 5s). On MHN.AIX.PV.2017.6.12, the protocone is higher than the metacone, and relatively more mesial than on MNHN.F.Me16084, so that it is strictly lingual to the paracone. A protocone higher than the metacone on M4 is known in other peradectids such as *Mimoperadectes labrus* (pers. obs., UM 66144) and *Pd. russelli*. The crescentiform paraconule is indistinct in lateral view on MHN.AIX.PV.2017.6.12, but present on MNHN.F.Me16084 (Fig. 5s). Both specimens have a tiny metaconule close to the lingual edge

of the metacone. The conules lack internal cristae. The distal edge of the talon of both MNHN.F.Me16084 and UM-FDN-289 is deeply emarginated (Fig. 5t), whereas it is straight on MHN.AIX.PV.2017.6.12. On all specimens, the paracone is much higher, longer and wider than the metacone. The labial edge of the paracone of UM-FDN-286 is almost as convex as the lingual edge, whereas MNHN.F.Me16084 has a more triangular paracone (Fig. 5s). The preparacrista is directed towards stylar cusp A but it ends distolingually to it. Stylar cusps A and B are placed mesiolabially to the paracone on both UM-FDN-286 and MNHN.F.Me16084. Stylar cusps A and B are separated by a shallow notch on MNHN.F.Me16084 (this area is worn on UM-FDN-286). On the specimen from Meudon, stylar cusp A is reduced in surface compared to stylar cusp B, which is mesiodistally long and doubled (Fig. 5t). The specimen from Fordones being worn in its most mesiolabial part, it is not possible to conclude whether the stylar cusps in the A and B positions are a relatively large stylar cusp B and small stylar cusp A, or a doubled stylar cusp B (Fig. 5b). Stylar cusp C is here the lowest stylar cusp, and there is no stylar cusp D. Stylar cusp C is positioned mesiolabially to the midpoint of the centrocrista in both specimens (Fig. 5b, t), as in *Pd. elegans* (Krishtalka and Stucky 1983b: fig. 3), but unlike, for example, certain European herpetotheriids in which it is strictly labial to the centrocrista (e.g., *Peratherium constans*, Ladevèze et al. 2012: figs. 4D, 5D; *Pt. elegans*, Ladevèze et al. 2012: fig. 7a; *Pt. cuvieri*, Selva and Ladevèze 2017: fig. 5Ab). Interestingly, stylar cusp C is also mesiolabial to the midpoint of the centrocrista in some herpetotheriid species (e.g., Crochet 1980b: figs. 109, 223). Stylar cusp C is more crescentiform on UM-FDN-286 than on MNHN.F.Me16084. The ectoflexus is well-developed, again as in *Pd. elegans*, which distinguishes the isolated M4 of *Pd. crocheti* sp. nov. from those of the coeval herpetotheriid *Pt. constans* or the type species of herpetotheriids, *Herpetotherium fugax* Cope, 1873 (e.g., Fox 1983: fig. 2a), which lack the ectoflexus.

Mandible and lower premolars: The right dentary MHN.AIX.PV.2017.6.8 is preserved from the canine alveolus to the m3 (Fig. 6). The canine alveolus is labially broken. The dentary bears an anterior mental foramen situated below the posterior root of the p1 (Fig. 6b-c), and a posterior mental foramen situated below the posterior root of the m1 (Fig. 6c). The presence of mental foramina below p1 and m1 (with slight variations) is almost always observed in peradectids and herpetotheriids (e.g., Korth 1994: fig. 8; Ladevèze et al. 2012: fig. 3A-B; Smith and Smith 2013: fig. 4A; Korth 2018: fig. 14f; but see Korth 1994: p. 393, for *Armintodelphys*). The depth of the dentary gradually increases posteriorly to the canine alveolus. The unfused mandibular symphysis extends posteriorly to a point ventral to the posterior alveolus of the p2 (Online Resource 6), as in *Pd. elegans* (Simpson 1935: fig. 2; pers. obs. of a cast of AMNH 17376) and alphadontids (e.g., Clemens 1966: figs. 58a, 61a; Cifelli and Muizon 1998: fig. 2B). The maximum posterior dorsoventral width value of the mandibular symphysis of *Peradectes* is lower than the value of the width between the most posterodorsal point of the symphysis and the posterior alveolus of p2 (Online Resource 6), contrary to figured alphadontid hemi-mandibles with a preserved symphysis (Clemens 1966: figs. 58a, 61a), in which these two width values appear at least subequal (but see the juvenile alphadontid specimen in Cifelli and Muizon [1998: fig. 2B]). The symphyseal angle between the long axis of the symphysis and the horizontal axis of the tooth row measures approximately 20°; this is close to the lowest values obtained from similar measurements performed in several fossil and extant marsupialiforms (Muizon and Ladevèze 2020: table 7). The posterior root of the p1 is preserved within its posterior alveolus. It is much smaller than the posterior root of p2 and p3, and it descends less deeply ventrally, within the dentary (Fig. 6d). The whole p1 was thus much smaller than the p2 and p3. There are no diastemata between the lower premolars. In occlusal view, the position of the anterior alveolus of the p1, mesially or distally to the inter-alveolar septum, is unclear (Fig. 6a). A similar uncertainty applies to the holotype of both *Pd. elegans* (AMNH 17376) and *Pd.*

californicus (Stock 1936: pl. 1, fig. 2a), so that the p1 of *Pd. elegans* was first considered to be single rooted (Simpson 1935: p. 10). In occlusal view of MHN.AIX.PV.2017.6.8 (Fig. 6a), alike in *Pd. elegans* (pers. obs. of a cast of AMNH 17376), the alveolus apparently anterior to the posterior root of the p1 is larger than expected for this premolar locus. The p1 is actually two rooted in both *Pd. elegans* (Fox 1983: fig. 3) and *Pd. crocheti* sp. nov. (Fig. 6d), with a smaller anterior than posterior root in cross section, as revealed by computed tomography study of MHN.AIX.PV.2017.6.8 for the European species. In *Pd. crocheti* sp. nov., the anterior root of the p1 is laterally adjacent to the inter-alveolar septum separating the canine alveolus from the p1 roots (Fig. 6b, d). Consequently, there is no diastema between between the p1 and lower canine, these two teeth being close together (Fig. 6b), as in *Pd. elegans* (Fox 1983).

Contrary to the lower molars, all lower premolars have mesiodistally curved roots (Fig. 6d). This character has not been studied so far for both peradectids and herpetotheriids. Interestingly, lower premolars of some Eocene herpetotheriids exhibit straight roots, similar to the lower molars (e.g., holotype of *Amphiperatherium fontense* Crochet, 1979 [Crochet 1980b: fig. 123]; pers. obs. of UM-BRT-574, *Amphiperatherium bourdellense* Crochet, 1979, Le Bretou, in Quercy). The posterior root of all preserved cheek teeth of MHN.AIX.PV.2017.6.8 is larger than the anterior root in cross section. The roots of all lower cheek teeth decrease in circumference ventrally to the crown. The unworn p2 and p3 of MHN.AIX.PV.2017.6.8 are the first lower premolar crowns allocated to European peradectids. The posterior heel of the p2 is broken. The p2 and p3 are similar in width, the p2 being only slightly wider (Table 2). The p3 is relatively labiolingually wider than in *Pd. elegans* (Krishtalka and Stucky 1983b: table 2). The apex of the p3, situated on the main cuspid, is slightly but distinctly higher than the apex of the p2 and of the m1, which is situated on the protoconid for the latter (Fig. 6c-d; Online Resource 6). On the p2 and p3, the apex overhangs its respective anterior root. The p2 is slightly procumbent, because its apex is positioned dorsomesially to the most ventral point of the

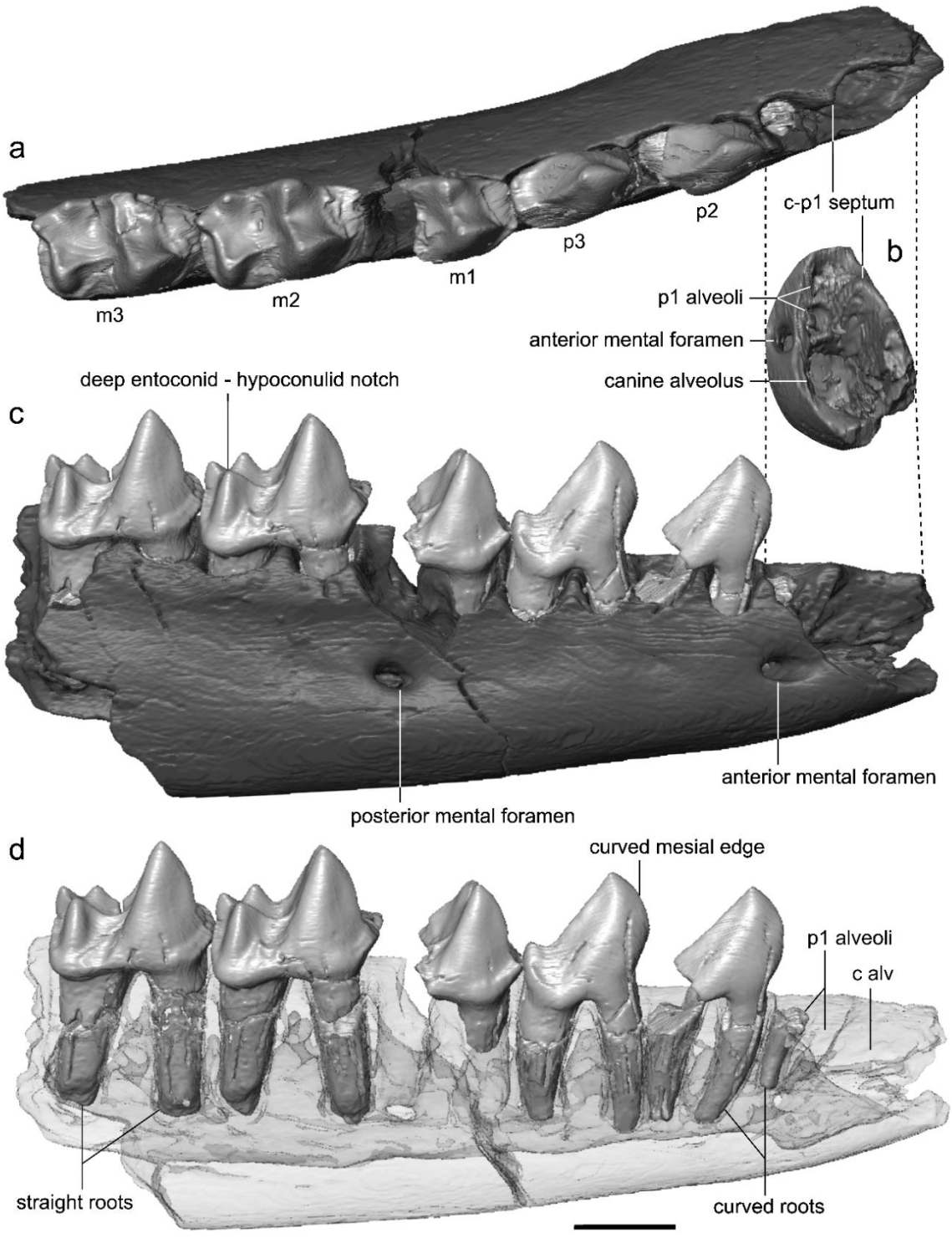

Fig. 6 Surface model of MHN.AIX.PV.2017.6.8, right hemi-mandible fragment with canine alveolus, posterior root of p1, partial p2, p3, partial m1, and m2-m3, of *Peradectes crocheti* sp. nov. from Palette (Provence; MP7-MP8+9 interval) in: **a**. occlusal (dorsal) view; **b**. mesiolabial (anterolateral) view with focus on c-p1 alveoli; **c**. labial (lateral) view; **d**. labial (lateral) view with transparent dentary. Abbreviation: **c alv**, canine alveolus. Scale bar equals 1 mm.

anterior root, whereas the apex of the p3 is strictly dorsal to the most ventral point of its anterior root. In lateral view, the main cuspid of the p2 and p3 forms the mesial edge of these teeth, which is projected mesially to the anterior root. It is curved as in other *Peradectes* species (e.g., AMNH 17376, holotype of *Pd. elegans*; UCMP 45950, paratype of *Pd. protinnominatus*), contrary to herpetotheriids in which it is V-shaped (e.g., Korth 1994: fig. 8.1 for *Herpetotherium fugax*). In mesial view, the main cuspid is bent lingually. The distal cristid of the main cuspid is straight in lateral view. The p3 is almost as long as high. The distal heel of the p3 is short and bears two accessory cuspids (Fig. 6a), whereas the described p3 of North American peradectids have only one accessory cuspid on their distal heel. The distal heel is lower in *Mimoperadectes* and *Armintodelphys* (see illustration in Online Resource 3: Fig. S1). Some rare herpetotheriid specimens also have double accessory cuspids on the heels of their lower premolars (e.g., Hooker 2010: fig. 8n-p). These accessory cuspids are positioned on the cingulid that surrounds the distal heel. The larger and higher distal cuspid, on the distal margin of the p3, is connected to the distal cristid of the main cuspid (Fig. 6a). This first accessory cuspid is pointed, dorsal to the ventralmost point reached by the distal cristid of the main cuspid. The second distal cuspid is smaller, and is positioned on the distolingual margin of the p3. The connection between the distal cristid of the main cuspid and the main accessory cuspid divides the heel into unequal lingual and labial parts, the labial surface being both lower and less laterally spread than the lingual surface. Both accessory cuspids of the heel of the p3 are connected by a high cristid formed by the heel cingulid. The lingual cingulid is mesiodistally longer than the labial cingulid. However, as in *Mimoperadectes* (Bown and Rose 1979: fig. 1), the lingual cingulid is much shorter than in *Pd. elegans* and *Pd. protinnominatus*, in which it ascends the distolingual edge of the main cuspid (e.g., Simpson 1935: fig. 2).

Lower molars: The description of the lower molars is primarly based on the two lower tooth rows from Palette (MHN.AIX.PV.2017.6.8, right, and MHN.AIX.PV.2017.6.9, left), possibly

representing the same individual. The partial right hemi-mandible MHN.AIX.PV.2017.6.9 (Fig. 7a-c) preserves a complete molar series (m1-m4). The m1 is smaller (in length and width) than the m2, which is in turn as large or slightly smaller than the m3 (Table 2). The m4 is the smallest locus of the lower molar row. The trigonid is narrower labiolingually than the talonid on the m1, the reverse on the m4. m2 have a labiolingually wider talonid than trigonid (e.g., MHN.AIX.PV.2017.6.9, Fig. 7a; MNHN.F.Ri221, Fig. 7g), with the exception of the m2 from Meudon (MNHN.F.Me16101, Fig. 7i), on which the trigonid and talonid are as wide. All m3 have a trigonid equal in labiolingual width to the talonid (e.g., MHN.AIX.PV.2017.6.9, Fig. 7a; MNHN.F.SN2508, Fig. 7k), as in *Pd. elegans* and contrary to the other European peradectid species. The trigonid is longer than the talonid on all molars. One of the three known m1, MNHN.F.SN121, has a trigonid less labiolingually wide than the m1 from Palette and Rians, with a relatively longer paracristid lingual segment, which is also found in *Pd. louisi* and *Pd. russelli*. On both molar rows from Palette (Figs. 6a, 7a), the m2 and m3 have a trigonid as mesiodistally long as labiolingually wide. Only one isolated m3, also from the type locality (MHN.AIX.PV.2017.6.10), exhibits a trigonid longer than wide.

On MHN.AIX.PV.2017.6.9, a groove on the mesial surface of the paraconid of the m3, lingual to the precingulid, contacts the hypoconulid of the m2. In anatomical position on the dentary, the apex of the hypoconulid of m2 is ventral to the apex of the paraconid of m3. The precingulid labiolingually extends from a point mesial or slightly mesiolabial to the apex of the paraconid, to a point mesial to the apex of the protoconid. In lingual view, the paraconid is less and less mesially projected from m1 to m4 (Fig. 7c), but its mesiolingual edge is always keel-like, as in all metatherians. The preparacristid is longer on the m2 from Meudon (Fig. 7i) than on the m2 of MHN.AIX.PV.2017.6.9. In occlusal view, the paracristid lingual segment elongates from m1 to m4. The postmetacristid shortens from m1 to m4 on occlusal view (Fig. 7a), so that it is almost vertical in lingual view on the m4 (Fig. 7c). On m1 and m2, the metaconid is longer than

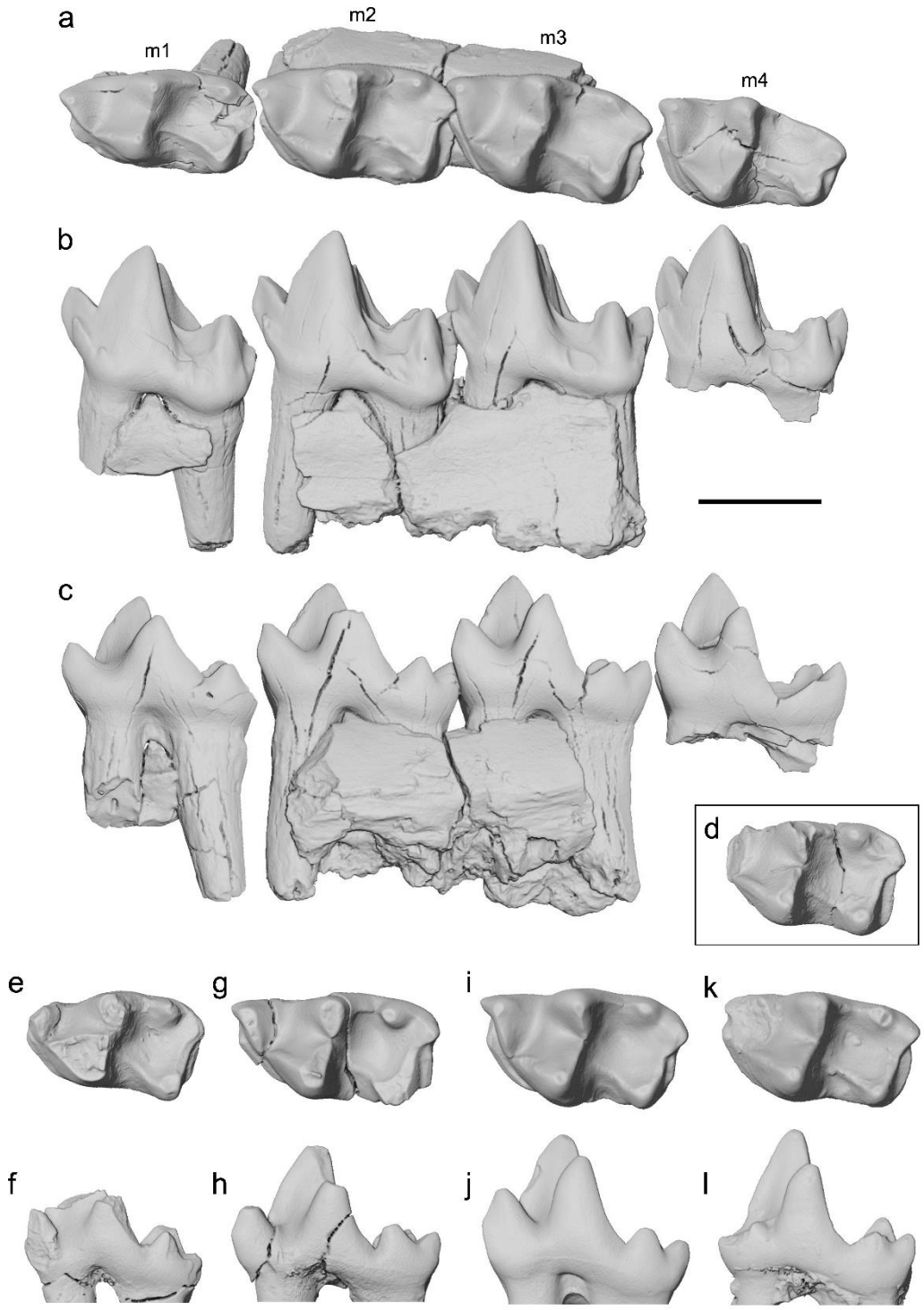

Fig. 7 Lower molars of *Peradectes crocheti* sp. nov. (except **d**) from Palette, Meudon, Rians and Soissons (France; MP7-MP8+9 interval). **a-c**. MHN.AIX.PV.2017.6.9, left m1-m4 row with fragments of dentary; **a**. occlusal view; **b**. labial view; **c**. reversed lingual view. **d**. comparison with UM-FDN-18, fragmentary right m2 from Fordones (Corbières) attributed to *Peratherium constans* (Marandat 1991: p. 68), in reversed occlusal view. **e-f**. MNHN.F.Ri516, right m1; **e**. reversed occlusal view; **f**. lingual view. **g-h**. MNHN.F.Ri221, left m2; **g**. occlusal

view; **h**. reversed lingual view. **i-j**. MNHN.F.Me16101, left m2; **i**. occlusal view; **j**. reversed lingual view. **k-l**. MNHN.F.SN2508, right m3; **k**. reversed occlusal view; **l**. lingual view. Scale bar equals 1 mm.

the paraconid, and longer than the metaconid of m3 and m4. The metaconid of m3 is only slightly longer than the paraconid. Those two cuspids are of equivalent length on m4. The protoconid is the highest cuspid of the trigonid on all lower molars. The metaconid is higher than the paraconid, their height difference being less marked on m4 than on anterior molar loci (Fig. 7c). The metaconid is either well distolingual to the protoconid (e.g., Fig. 7a) or relatively closer to it mesiolabially (e.g., Fig. 7g). The paracristid is always longer than the protocristid. On the mesial edge of the protoconid, the preprotocristid is convex in mesiolabial view (Fig. 6c-d), except on m4. The labial edge of the protoconid is weakly convex in mesial or distal view.

The protocristid notch opens more ventrally than both the paracristid notch and the lingual opening of the trigonid basin. The latter is always higher than the lingual opening of the talonid basin, unlike in herpetotheriids. The difference in height between those two lingual openings increases gradually from m1 to m4 (Fig. 7c). The talonid basin is a deep, rounded depression. None of the lower molars are labially emarginated. The lingual edge of the talonid is curved, with an entoconid that is obliquely positioned relative to the paraconid – metaconid axis, as in all late Paleocene – Eocene peradectids (e.g., Hough 1961: fig. 2A, for the late Eocene genus *Didelphidectes*). The lingual edge of the talonid is straight and the entoconid is not obliquely oriented in the early peradectids *Pd. minor* (e.g., Williamson et al. 2012: fig. 8A, 8D) and *Pd. coprexeches* (e.g., Williamson and Taylor 2011: fig. 7A, 7D, 7J), as in herpetotheriids.

The entoconid and hypoconulid are labiolingually pinched. The entoconid is often labial to the paraconid – metaconid axis (e.g., Fig. 7a, k) but the three cuspids are aligned on some m2

specimens (e.g., MNHN.F.Ri221, Fig. 7g; MNHN.F.Me16101, Fig. 7i). The pre-entocristid is always sharp and joins the postmetacristid on the postmetacristid – pre-entocristid notch. The postentocristid is absent on the m2, but present on the m3 of MHN.AIX.PV.2017.6.9. The entoconid is positioned more and more distally to the metaconid from m1 to m4, so that the metaconid – entoconid notch mesiodistally elongates from m1 to m4 (Fig. 7c). In occlusal view, the entoconid of m2 and m3 is in intermediate position between the distal edge of the trigonid and the distal margin of the tooth, whereas the entoconid is closer to the distolingual corner of the tooth on equivalent loci in *Pd. elegans* (e.g., Krishtalka and Stucky 1983b: fig. 4b for occlusal view, Mckenna 1960: fig. 17c [lower] for lateral view). The entoconid of m4 is closer to the distal margin of the tooth than from the distal wall of the trigonid. The entoconid has a symmetrical shape in lingual view, with equally long pre-entocristid and postentocristid. In absolute height, the entoconid of m1 and m2 are subequal (Fig. 7c, f, h), it is lower on m3 (e.g., Fig. 7l) and much lower on m4 (Fig. 7c).

The entoconid - hypoconulid notch is deep, as deep as the entoconid – metaconid notch on m2 (Fig. 6c), as in *Pd. protinnominatus* (e.g., Gingerich and Smith 2006: fig. 26a, c). In comparison, the lowest point of the entoconid – hypoconulid notch of *Pd. elegans* can be higher than the lowest point of the entoconid – metaconid notch (e.g., McKenna 1960: fig. 17c), even on m2 (e.g., pers. obs., AMNH 17376), or as high as the lowest point of the entoconid – metaconid notch (e.g., Fox 1983: fig. 3). The hypoconulid occupies approximately one third of the labiolingual width of the distal margin of the talonid on m2 and m3 and one half of it on m1 and m4 (Fig. 7a). The hypoconulid is lower than the entoconid on m1 and m2 (e.g., Fig. 7f, h, j), as high and as long on m3 (e.g., Fig. 7l), and much higher on m4 (see the increasing height of hypoconulid along the molar series, Fig. 7c). A lingual cristid of the hypoconulid descends on the entoconid – hypoconulid notch only on the m2 from Rians (MNHN.F.Ri221, Fig. 7g).

The hypoconid is mesiodistally pinched, with an angle of approximately 70° between the cristid obliqua and postcristid. This cuspid is mesiolabial to labial to the entoconid apex (e.g., Fig. 6a); distolabial to the protoconid on m1, m2, and m3, and strictly distal to the protoconid on m4. In distal view, the entoconid and hypoconid are subequal in height, unlike in herpetotheriids, in which the entoconid is higher (pers. obs.). The hypoconid of m4 is much lower than the hypoconid of more anterior lower molar loci. The cristid obliqua is curved on all loci, and its mesial end is positioned labially to the protocristid notch on all lower molar loci. The curvature of this crest is more pronounced on m4 than on more anterior molars (Fig. 7a). The cristid obliqua ascends slightly on the distal wall of the trigonid; it reaches approximately half the dorsoventral height of the distal wall of the trigonid, between the talonid basin and the protocrisid notch. The postingulid is lingually and labially convex; it attenuates labially to the hypoconulid instead of extending lingually towards it (see illustrations in Online Resource 3: Fig. S6). On the specimens from Palette, the hypoflexid is labiolingually wide, so that it is directly connected to the postcingulid. In this case, the hypoconid is totally internalized within the talonid (Figs. 6a, 7a).

Postcranial: The sole postcranial material attributed to *Peradectes crocheti* sp. nov. is a minute, complete right astragalus (MHN.AIX.PV.2017.6.14, Fig. 8) not found in association with dental remains of this species. This specimen has been confidently attributed to *Pd. crocheti* sp. nov. based on the following: i) compatibility of size (proximodistal length = 1.97 mm; mediolateral width = 1.59 mm); ii) morphological and size similarity with a left astragalus of cf. *Peradectes protinnominatus* from the Wasatchian-0 of the southern Bighorn Basin (Rose et al. 2012: fig. 11E-H) and with Wasatchian peradectid astragali described by Szalay (1994: fig. 6.10D-F); iii) *Pd. crocheti* sp. nov. is the only peradectid recorded in Palette, based on dental remains. In dorsal view (Fig. 8a), the trochlea is smooth and nearly ungrooved, and there is no

distal astragalar tubercle. The astragalar neck and head are relatively proximodistally long (Fig. 8a-b). In turn, the astragalar neck and head have the same mediolateral width, the two being well distinguished in ventrolateral view (Fig. 8c). In distal view, the astragalus is relatively flat (Fig. 8d). Its medial tibial facet is only gently sloping, so that there is a rounded angle between the medial and lateral tibial facets (Fig. 8d). The distal end of the lateral tibial facet is located on the astragalar neck.

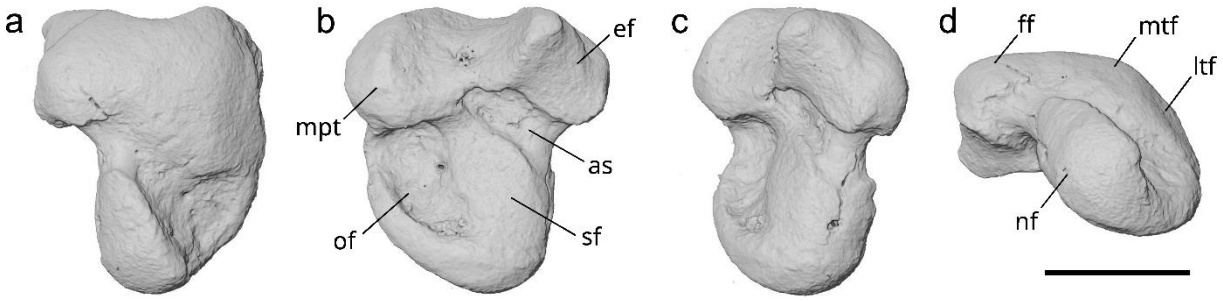

Fig. 8 Right astragalus of *Peradectes crocheti* sp. nov. from Palette (Provence, MP7-MP8+9 interval), MHN.AIX.PV.2017.6.14. **a**. dorsal view; **b**. ventral view; **c**. ventrolateral view; **d**. distal view. Abbreviations, terminology following Rose et al. (2012): **as**, astragalar sulcus; **ef**, ectal facet; **ff**, fibular facet; **ltf**, lateral tibial facet; **mpt**, medial plantar tubercle; **mtf**, medial tibial facet; **nf**, navicular facet; **of**, ovoid fossa; **sf**, sustentacular facet. Scale bar equals 1 mm.

In contrast to MHN.AIX.PV.2017.6.14, known herpetotheriid astragali are less dorsoventrally flat, and have a more grooved trochlea in addition to an almost vertical medial tibial facet (Rose 2012; Rose et al. 2012), characters which would be expected on astragali of the coeval herpetotheriid *Pt. constans* in Palette (only calcanei of *Pt. constans* are known from its type locality; Coillot et al. 2013). Unlike in cf. *Pd. protinnominatus* and *M. labrus*, the medial border of the astragalar neck of MHN.AIX.PV.2017.6.14, formed by the proximal extension of the large navicular facet, does not reach the trochlea (Fig. 8b-c). The ovoid fossa is thus more open medially than in cf. *Pd. protinnominatus*. The ovoid fossa of the composite drawing of Szalay (1994: fig. 6.10E) for Wasatchian peradectid astragali is also open, but relatively more distally.

MHN.AIX.PV.2017.6.14 compares better with the astragalus of cf. *Pd. protinnominatus* than with the one of the larger *Mimoperadectes labrus* (Rose et al. 2012: fig. 11A-D), for example in having an astragalar sulcus (narrower than in *Herpetotherium innominatum* [Simpson, 1928]) and shorter ectal facet with a rounded instead of triangular distlolateral extremity (Fig. 8b).

Peradectes louisi Crochet, 1979

Figures 9, 10, 11 (except 11g-h)

1977a *Peradectes* sp. nov. 1; Crochet: p. 359.

1979 *Peradectes louisi* Crochet; Crochet: p. 367, fig. 1.

1980b *Peradectes louisi* Crochet; Crochet: p. 39-42, figs. 6-13 (in part).

1980b *Peradectes* sp.; Crochet: p. 49-51, figs. 26-27, 29 (in part).

Holotype: left M3, MNHN.F.GL197, first figured by Crochet (1979: fig. 1, 1980b: fig. 9a, b) and housed in the collections of the Muséum National d'Histoire Naturelle, Paris.

Localities: Sables de Brasles (type locality), Avenay, Mutigny, Condé-en-Brie and Sézanne-Broyes; all in the eastern Paris Basin.

Age: middle Ypresian (middle early Eocene), MP8+9 and ~MP8+9 reference level (~ mammalian biozones PE IV and PE V).

Remarks: We here propose a revision of *Pd. louisi* based on a re-description of the holotype, and allocate to this species several new upper and lower molar remains from its type locality (Fig. 9), and other MP8+9 and ~MP8+9 Paris Basin localities in order to study polymorphism and enhance comparisons with other European peradectids.

Translation to English of the original French diagnosis (Crochet 1979): 'European species of small size. On M3, stylar cusp B subequal in height to C and D. Ectoflexus poorly formed

and symmetric; conules weak; M3 relatively long. Lingual opening of the prefossid higher than the entocristid notch located between the metaconid and entoconid. Except on m4, base of the hypoconid mesio-distally pinched and cristid obliqua with a concavity before joining the posterior base of the trigonid. m4 smaller than m3.'

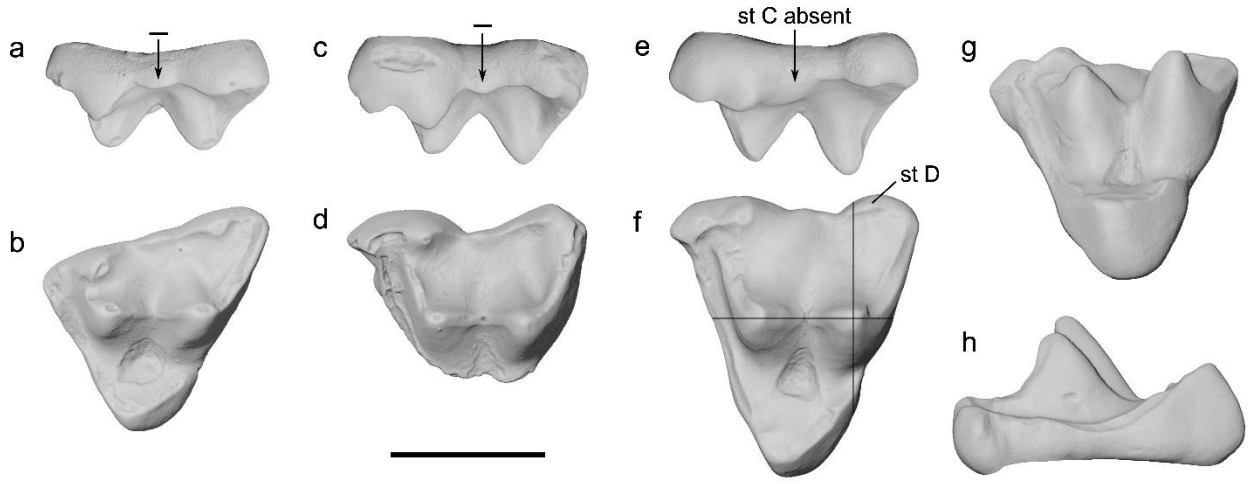

Fig. 9 Upper molars of *Peradectes louisi* from its type locality, Sables de Brasles (Aisne, France; ~MP8+9). **a-b**. MNHN.F.GL1, left M1; **a**. labial view; **b**. occlusal view. **c-d**. MNHN.F.GL272, labial half of left M2; **c**. labial view; **d**. occlusal view. **e-h**. MNHN.F.GL197, holotype, left M3; **e**. labial view; **f**. occlusal view, the segments are positioned on the paracone – metacone axis and its perpendicular line; **g**. lingual view; **h**. mesial view. The arrows denoting stylar cusp C on the labial views **a** and **c** are followed by '-', meaning the most ventral point on the [stylar cusp C – stylar cusp D] mesiodistal extension is reached on stylar cusp D. Abbreviations: **st C**, stylar cusp C; **st D**, stylar cusp D. Scale bar equals 1 mm.

New differential diagnosis: Differs from *Pd. crocheti* sp. nov. and *Pd. russelli* in having: (i) relatively mesiodistally longer lower molars; (ii) stylar cusp D distolabial to metacone apex on M3 (upper molars of '*Arm.*' *dufraingi* are unknown); and (iii) stylar cusp C less ventral than stylar cusp D apex on M1 and M2. Further differs from *Pd. crocheti* sp. nov. by: (i) stylar cusp C less ventral than stylar cusp D apex also on M3; (ii) presence of crown labial emargination on all lower molars; (iii) trigonid more labiolingually wide than talonid on m3; (iv) relatively lower entoconid and hypoconulid separated by a shallower notch; and (v) in lacking

postcingulid on m4. Further differs from *Pd. russelli* in being noticeably smaller. Differs from '*Armintodelphys*' *dufraingi* in: (i) being larger; in having (ii) talonid mostly labiolingually as wide or wider than trigonid on m2; (iii) entoconid higher than hypoconulid on m2 and as high as hypoconulid on m3; and (iv) larger postcingulid on m2 and m3.

Material: Additional material from Sables de Brasles: left M1 (MNHN.F.GL1, MNHN.F.GL296), worn left M1 (MNHN.F.GL57), worn right M2 (MNHN.F.GL154), labial half of left M2 (MNHN.F.GL272), worn right M3 (MNHN.F.GL265), right m1 (MNHN.F.GL136), left m3 (MNHN.F.GL261, MNHN.F.GL263), right m3 (MNHN.F.GL383), right m4 (MNHN.F.GL301).

Material from Mutigny: right dP3 (MNHN.F.Mu18005; Crochet 1980b: fig. 6), left M1 (MNHN.F.Mu18006; Crochet 1980b: fig. 26), left M2 (MNHN.F.Mu6511; Crochet 1980b: fig. 8), left worn M3 (MNHN.F.Mu18001).

Material from Avenay: left M1 (MNHN.F.Av16023, MNHN.F.Av16036; Crochet 1980b: fig. 7, UM-AV-1-SK, UM-AV-3-SK), right M1 (MNHN.F.Av16057, UM-AV-2-SK), mesial fragment of left M2 (MNHN.F.Av4582), left M2 (MNHN.F.Av18003), right M2 (MNHN.F.Av18004), left m1 (UM-AV-7-SK, UM-AV-12-SK), right m1 (MNHN.F.Av16028; Crochet 1980b: fig. 10, MNHN.F.Av7229), left m2 (MNHN.F.Av16016, MNHN.F.Av16044, MNHN.F.Av18001, MNHN.F.Av6830, UM-AV-10-SK, UM-AV-11-SK), right m2 (MNHN.F.Av16027; Crochet 1980b: fig. 11), left m3 (MNHN.F.Av18000, UM-AV-4-SK, UM-AV-5-SK), right m3 (MNHN.F.Av18002; Crochet 1980b: fig. 12, MNHN.F.Av16149, MNHN.F.Av16158, UM-AV-6-SK, UM-AV-9-SK), fragmentary right m3 (UM-AV-8-SK), fragment of left dentary with worn m3 and trigonid of m4 (MNHN.F.Av4642), left m4 (MNHN.F.Av16032, MNHN.F.Av16037; Crochet 1980b: fig. 13).

Material from Condé-en-Brie: left M2 (MNHN.F.CB1486, MNHN.F.CB3707, MNHN.F.CB3637), left worn M2 (MNHN.F.CB835, MNHN.F.CB4183), right M2 (MNHN.F.CB1080; Crochet 1980b: fig. 27, MNHN.F.CB3213, MNHN.F.CB3228), right M3 (MNHN.F.CB4182), left m1 (MNHN.F.CB962, MNHN.F.CB4391), right dentary with fragmentary m2-m4 (MNHN.F.CB226; Crochet 1980b: fig. 29), left m2 (MNHN.F.CB5090, MNHN.F.CB5092, MNHN.F.CB5097, MNHN.F.CB828), right m2 (MNHN.F.CB872, MNHN.F.CB878), left m3 (MNHN.F.CB5104, MNHN.F.CB959), right m3 (MNHN.F.CB4213).

Material from Sézanne-Broyes: right M3 (MNHN.F.SZ18005), worn left M3 (MNHN.F.SZ18000), left M4 (MNHN.F.SZ18004), left m1 (MNHN.F.SZ18003), left m2 (MNHN.F.SZ18001), left m3 (MNHN.F.SZ18006).

Comparative description

Remark: *Peradectes louisi* being similar to *Pd. crocheti* sp. nov., detailed comparisons of *Pd. louisi* with North American peradectids are not proposed, except where necessary (see 'Deciduous upper premolar' below).

Deciduous upper premolar: Only one isolated DP3, from Mutigny, is known for European peradectids (MNHN.F.Mu18005, Fig. 10a-b). This specimen was part of the hypodigm of *Pd. louisi* (Crochet 1979). Although *Pd. louisi* is coeval with *Pd. russelli* in Mutigny, MNHN.F.Mu18005 certainly belongs to *Pd. louisi* instead of *Pd. russelli* due to its small size (L = 1.54 mm; W = 1.26 mm). It is as long and less wide than the M1 of *Pd. louisi*. The dP3 is also identified as such by the long and wide stylar cusp A spur and the deep mesial emargination of the short paracingulum. Compared to dP3 of *Pd. chesteri* (Murphey et al. 2018: fig. 13.1) and *Pd. californicus* (Rothecker and Storer 1996: fig. 1O), the only other described and figured

peradectid dP3 with ascertained specific attribution, MNHN.F.Mu18005 is relatively longer. The ratio of the labiolingual width of dP3 to the labiolingual width of M1 is similar in *Pd. louisi* and *Pd. chesteri*. The protocone is strictly lingual to the midpoint of the centrocrista on MNHN.F.Mu18005. The paracone and metacone are identical in mesiodistal length and height, whereas the protocone is much smaller. Contrary to *Pd. chesteri*, the paraconule and the ectoflexus are absent, and the distal emargination of the crown is present. MNHN.F.Mu18005 retains a postparaconular crista reaching the base of the paracone. Stylar cusps C and D are present in this specimen. Stylar cusp C is vestigial compared to stylar cusp D, whereas stylar cusp C is absent in *Pd. chesteri* and *Pd. californicus* (note that the long stylar cusp in the D position in *Pd. chesteri* was interpreted as a stylar cusp C by Murphey et al. 2018). Stylar cusp D is placed slightly distolabially to the metacone apex on MNHN.F.Mu18005. Stylar cusp D is rather mesiolabial to the metacone apex in *Pd. californicus* according to the available illustration.

Upper molars: The protocone is lower than paracone and metacone as in other European peradectids (Fig. 9h). The trigon basin is in intermediate position between the protocone, paracone and metacone on M1 (Fig. 9b). The protocone is positioned more lingually on M3, so that the trigon basin is closer to the paracone and metacone (Fig. 9f). A sharp ridge is present on the lingual edge of the acute protocone of the M3 on which this cusp is mesiodistally pinched (MNHN.F.SZ18005, Fig. 10n-o). The paraconule is faint. The holotype bears a premetaconular crista unlike the other unworn M3, which lack internal conular cristae (the worn MNHN.F.GL265 retains internal conular cristae). Various M1 and M2 have faint internal conular cristae (e.g., Fig. 10d, f, h). The postmetaconular crista elongates from M1 to M3. Similar to *Pd. crocheti* sp. nov., the paracingulum is either of constant mesiodistal length or it is occasionally emarginated mesially to the paracone apex (e.g., MNHN.F.Mu6511, Fig. 10l for M2, MNHN.F.SZ18005, Fig. 10o for M3). The distal emargination of the crown is rarely

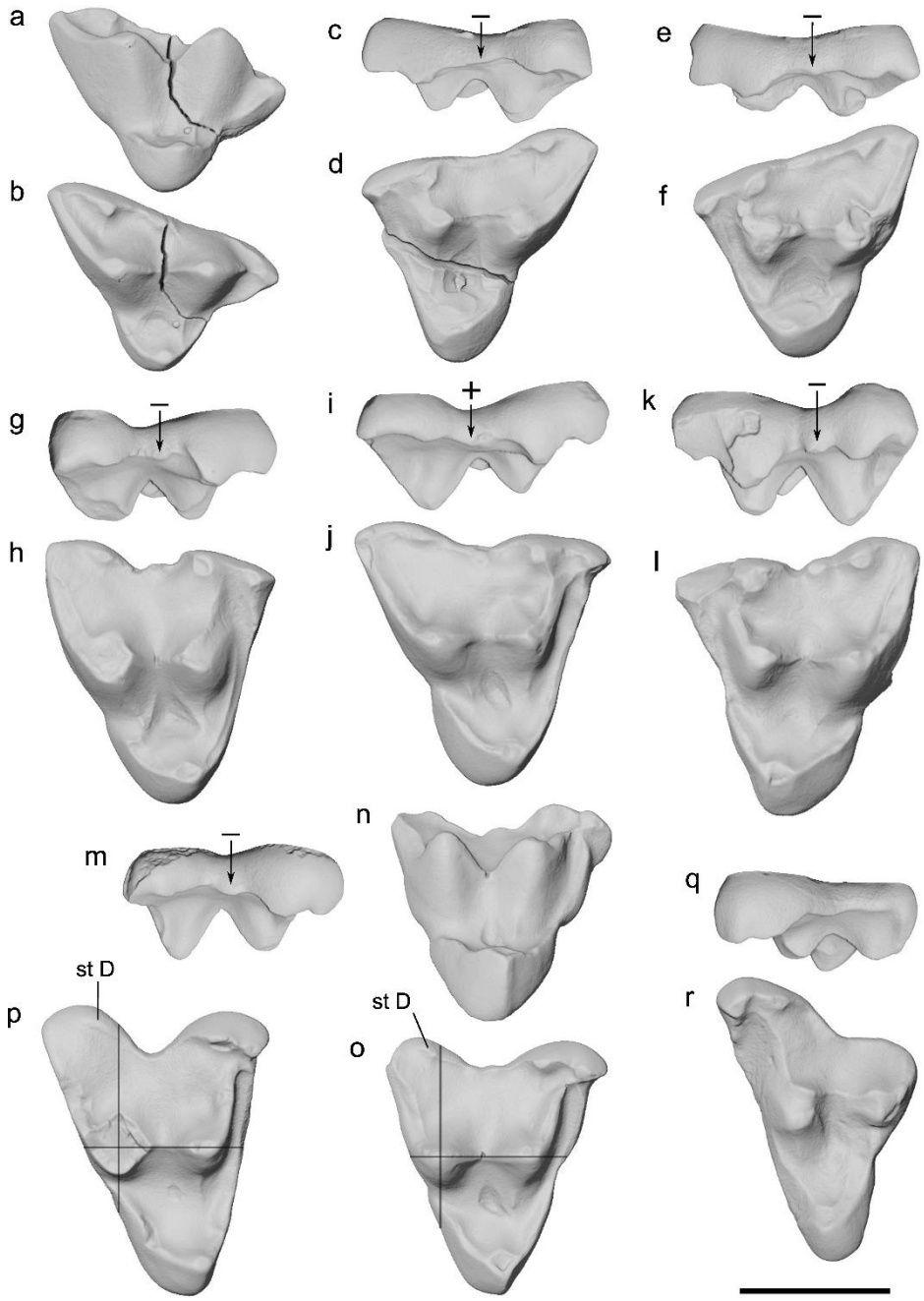

Fig. 10 Upper molars of *Peradectes louisi* from Avenay (MP8+9), Condé-en-Brie, Mutigny and Sézanne-Broyes (~MP8+9), all in the Paris Basin. **a-b**. MNHN.F.Mu18005, right dP3; **a**. lingual view; **b**. occlusal view. **c-d**. MNHN.F.Mu18006, left M1; **c**. labial view; **d**. occlusal view. **e-f**. UM-AV-1-SK, left M1; **e**. labial view; **f**. occlusal view. **g-h**. MNHN.F.CB3213, right M2; **g**. labial view; **h**. occlusal view. **i-j**. MNHN.F.CB3228, right M2; **i**. labial view; **j**. occlusal view. **k-l**. MNHN.F.Mu6511, left M2; **k**. labial view; **l**. occlusal view. **m-o**. MNHN.F.SZ18005, right M3; **m**. labial view; **n**. lingual view; **o**. occlusal view. **p**. MNHN.F.CB4182, right M3 in occlusal view. **q-r**. MNHN.F.SZ18004, left M4; **q**. labial view; **r**. occlusal view. The arrows denoting stylar cusp C on labial views are followed by '+' if the

most ventral point on the [stylar cusp C – stylar cusp D] mesiodistal extension is reached on stylar cusp C, and by '-' if this most ventral point is reached on stylar cusp D. The segments on the occlusal views of MNHN.F.SZ18005 (**o**) and MNHN.F.CB4182 (**p**) are positioned on the paracone – metacone axis and its perpendicular line. Abbreviation: **st D**, stylar cusp D. Scale bar equals 1 mm.

lacking, the distal margin being straight on the M1 MNHN.F.GL1 (Fig. 9b) and the M3 MNHN.F.CB4182 (Fig. 10p). The preparacrista elongates from M1 to M3 as illustrated on the molar series from the type locality (Fig. 9). This crest is connected to stylar cusp A on M1 and M2 and to stylar cusp B on M3 and M4. The M2 MNHN.F.GL272 has an unworn and salient postmetacrista forming a high distal wall on the stylar shelf (Fig. 9c-d), which is not found in *Pd. crocheti* sp. nov. This distal wall is absent in most specimens (e.g., Fig. 10n).

Stylar cusp A is positioned mesiolingually to stylar cusp B on M2 and M3, except for the M2 MNHN.F.CB3228 having a stylar cusp A strictly mesial to stylar cusp B (Fig. 10j). Stylar cusp B is more conical on the M3 holotype than on the M3 MNHN.F.CB4182 (Fig. 10p) or MNHN.F.SZ18005 (Fig. 10o) for which it is labiolingually pinched. This stylar cusp is labial to the paracone apex on M1 and M2, and mesiolabial to the paracone apex on M3. Stylar cusp B of the holotype (Fig. 9f) and of MNHN.F.SZ18005 has a small crest on its lingual edge directed towards the preparacrista, similar to the one connected to the preparacrista on M1 and M2.

Stylar cusp C is absent on the holotype (Fig. 9e-g) and on the M3 MNHN.F.CB4182. Variation in the positioning of this stylar cusp exists, as in *Pd. crocheti* sp. nov., so that it can be closer to stylar cusp B than to stylar cusp D (e.g., for M2, MNHN.F.CB1486 or MNHN.F.GL272, Fig. 9c vs MNHN.F.Mu6511, Fig. 10k). The doubling of stylar cusp C occurs only in one specimen (MNHN.F.CB1080, Crochet 1980b: fig. 27), as in *Pd. crocheti* sp. nov. Unlike other peradectid species, stylar cusp D is distolabial to the metacone apex on M3, in addition to M1 and M2

(e.g., molar series of Fig. 9). Conversely, M2 specimens from various localities have a stylar cusp D strictly labial instead of distolabial to the metacone apex (MNHN.F.Mu6511, Fig. 10l; MNHN.F.Av18004; MNHN.F.CB3213, Fig. 10h). On M2, stylar cusp D is either conical (e.g., Fig. 10l) or labiolingually pinched (Figs. 9d, 10j). The apex of stylar cusp C is less ventral than the apex of stylar cusp D on all M1 to M3, except on the M2 MNHN.F.CB3228 (Fig. 10i). Altogether, the relative heights of the stylar cusps A to D of M1 to M3 of *Pd. louisi* are mostly as follows: st. B > A > D > C (Table 3). Among ascertained peradectids, the apex of stylar cusp C is also less ventral than the apex of stylar cusp D on M2 and M3 only in *Pd. russelli* (only on M3), *M. houdei* (differs from *M. labrus* and *M. sowasheensis*, pers. obs.), *Pd. gulottai*, *Pd. californicus*, *Nanodelphys hunti* (Cope, 1873) (stylar cusp C is absent on the holotype, preserving M2 and M3 [McGrew 1937: figs. 3-4]) and *Didelphidectes* cf. *pumilis* (stylar cusp C is absent and stylar cusp D is present in the latter) (Table 3). Stylar cusp C is also vestigial in *Pd. chesteri* (Table 3). Stylar cusp E is notably present in UM-AV-1-SK, on which it is as high as stylar cusp D (Fig. 10e), and on UM-AV-2-SK. Stylar cusp E occurs more frequently than in *Pd. crocheti* sp. nov.

M1 lack the ectoflexus (e.g., Figs. 9b, 10f), except UM-AV-2-SK on which it is narrow and MNHN.F.Mu18006 with a longer ectoflexus (Fig. 10d). The ectoflexus is asymmetric on M3 as in other European peradectids (e.g., Fig. 9f), particularly on MNHN.F.SZ18000 with a metastylar wing much more labially extended than the parastylar wing. The asymmetry is less marked on MNHN.F.SZ18005 (Fig. 10o) from the same locality. The ectoflexus of M2 can be deeper than on M3 (e.g., Figs. 9d, 10h vs Fig. 9f).

We report the first M4 of *Pd. louisi*, from Sézanne-Broyes (MNHN.F.SZ18004, Fig. 10q-r). The ectoflexus is deep as in other peradectids. The talon is relatively labiolingually wider than on M4 of *Pd. crocheti* sp. nov. As in *Pd. russelli* (Crochet 1979: fig. 2) and contrary to *Pd. crocheti* sp. nov., stylar cusp C is greatly reduced (Fig. 10q). Stylar cusp A is the highest.

Contrary to the M4 of both *Pd. crocheti* sp. nov. and *Pd. russelli*, the metastylar wing is relatively larger, and the protocone is subequal in height to the metacone instead of being higher. The paracone and metacone are subequal in height, but both cusps are worn.

Lower molars: m2 have a talonid most often as labiolingually wide or wider than the trigonid (e.g., Fig. 11m, o), as in *Pd. crocheti* sp. nov. and almost all m2 of *Pd. russelli*. However, one m2 has a talonid slightly narrower than the trigonid (MNHN.F.SZ18001, Fig. 11k), resembling the condition seen in the m2 of '*Arm.*' *dufraingi*. The m3 MNHN.F.Av16149 has a trigonid relatively longer (L/W trigonid = 1.20) than any other m3 of *Pd. louisi*, for which the trigonid is most often as long as wide (e.g., Fig. 11r, t, v, x). The development of the precingulid varies for a given molar locus (e.g., Fig. 11r vs 11t). The protoconid is always markedly higher than on m4 of '*Arm.*' *dufraingi*. The metaconid is always distolingual to the protoconid. On m3, the paraconid and metaconid are either equal in mesiodistal length (e.g., Fig. 11s) or the metaconid is longer (e.g., Fig. 11y).

The cristid obliqua is almost straight on some m2 (e.g., MNHN.F.CB878, Fig. 11o; MNHN.F.Av16027, Crochet 1980b: fig. 11), m3 (e.g., MNHN.F.GL261; Fig. 11v) and m4 (MNHN.F.GL301; Fig. 11e), whereas it is curved on most lower molar specimens (Fig. 11). There is notable variation of the positionning of the mesial end of the cristid obliqua for a given molar locus. For example, the cristid obliqua ends mesially labial to the protocristid notch on the m3 MNHN.F.CB4213 (Fig. 11r), but is close to the protocristid notch on the m3 MNHN.F.Av18002 (Fig. 11t). The postcristid is straight instead of curved (i.e., the hypoconulid is weakly distally projected) on all m1 (e.g., Fig. 11a, c), 8 out of 13 m2 specimens (e.g., MNHN.F.CB828, Fig. 11m; MNHN.F.CB878, Fig. 11o), only 6 out of 17 m3 specimens (e.g., MNHN.F.Av4642, Fig. 11i; UM-AV-6-SK), and 2 out of 3 m4 specimens (MNHN.F.GL301, Fig. 11e; MNHN.F.Av16037, Crochet 1980b: fig. 13).

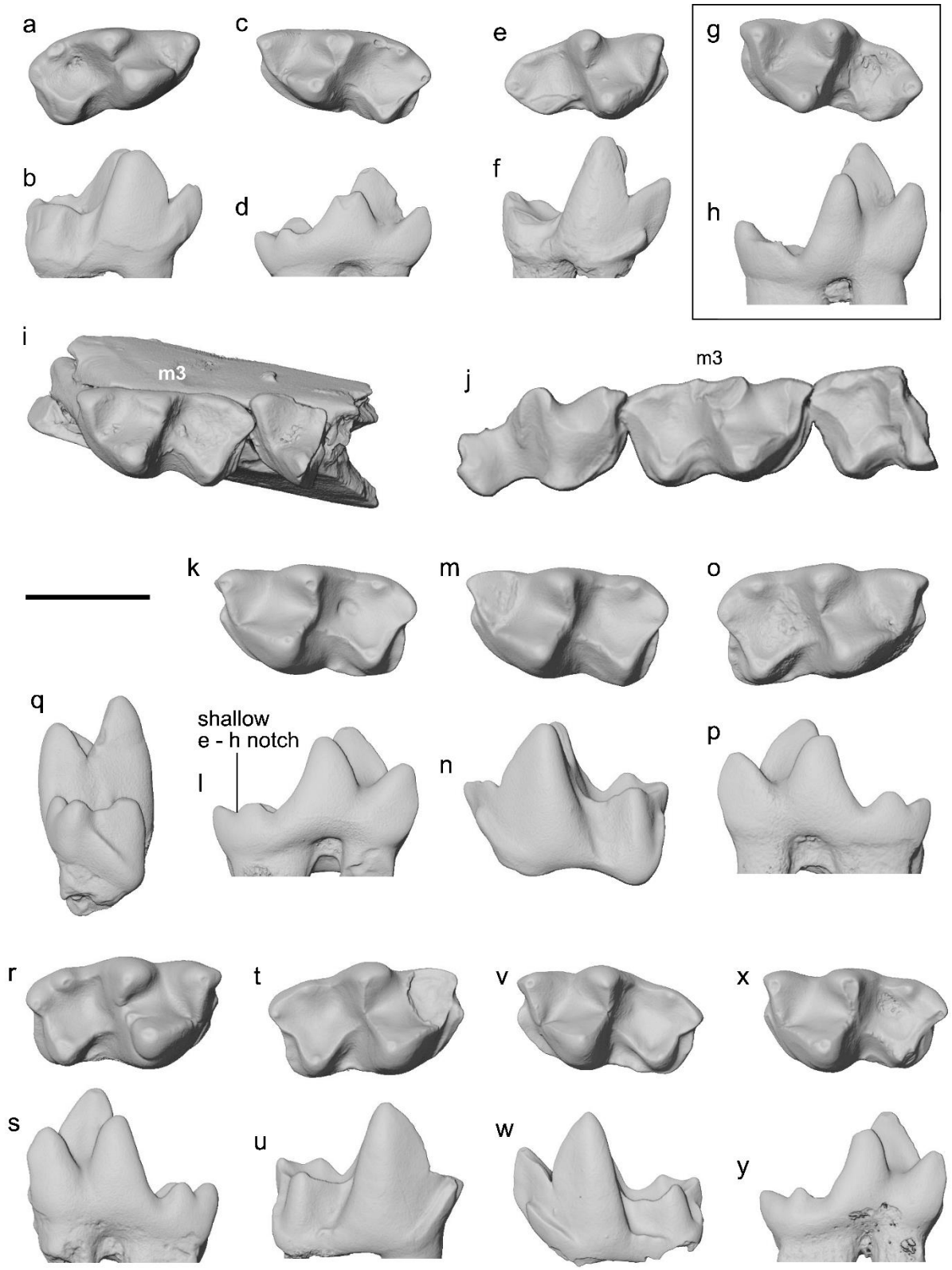

Fig. 11 Lower molars of *Peradectes louisi* (except **g-h**) from Avenay (MP8+9), Condé-en-Brie, Sables de Brasles, Sézanne-Broyes (~MP8+9) and of *Peradectes* cf. *louisi* from Saint-Agnan (MP8+9-MP10 interval), all localities being in the Paris Basin. **a-b**. MNHN.F.GL136, right m1; **a**. occlusal view; **b**. labial view. **c-d**. MNHN.F.SZ18003, left m1; **c**. occlusal view; **d**. lingual

view. **e-f**. MNHN.F.GL301, right m4; **e**. occlusal view; **f**. mesiolabial view. **g-h**, comparison with MNHN.F.STA296, left m4 of *Peradectes* cf. *louisi* from Saint-Agnan (Aisne, MP8+9-MP10 interval); **g**. occlusal view; **h**. lingual view. **i**. MNHN.F.Av4642, left hemi-mandible fragment with fragmentary trigonid of m2 and worn m3 in occlusal view. **j**. MNHN.F.CB226, m2-m4 from a right hemi-mandible fragment in occlusal view. **k-l**. MNHN.F.SZ18001, left m2; **k**. occlusal view; **l**. lingual view. **m-n**. MNHN.F.CB828, left m2; **m**. occlusal view; **n**. labial view. **o-p**. MNHN.F.CB878, right m2; **o**. occlusal view; **p**. lingual view. **q-s**. MNHN.F.CB4213, right m3; **q**. distal view; **r**. occlusal view; **s**. lingual view. **t-u**. MNHN.F.Av18002, right m3; **t**. occlusal view; **u**. labial view. **v-w**. MNHN.F.GL261, left m3; **v**. occlusal view; **w**. labial view. **x-y**. MNHN.F.GL263, left m3; **x**. occlusal view; **y**. lingual view. Abbreviation: **e – h notch**, entoconid – hypoconulid notch. Scale bar equals 1 mm.

On the partial hemi-mandible MNHN.F.CB226, the only partial molar row known for *Pd. louisi*, the m3 has a much smaller entoconid than the m2, so that the entoconid is minute on the m3 (Fig. 11j). The talonid is slightly labiolingually wider on the m2 than on the m3 on this specimen. The talonid is as labiolingually wide as the trigonid on most of the m2 specimens (see above), whereas the talonid is narrower than the trigonid on the m3 (e.g., Fig. 11k, m, o for m2 vs Fig. 11r, t, v, x for m3). Among the 46 lower molar specimens, 41 have a strong labial emargination of the crown. The emargination is weaker in five specimens with a relatively wider hypoflexid, namely the m1 MNHN.F.CB4391 and UM-AV-12-SK, the m2 MNHN.F.Av16016 and MNHN.F.CB5092, and the m3 MNHN.F.GL383. Among them, only MNHN.F.Av16016 and MNHN.F.GL383 have a labial emargination as weak as in equivalent molar loci in *Pd. crocheti* sp. nov.

The entoconid and hypoconulid are small on all molars, so that the entoconid – hypoconulid notch is shallow (Fig. 11l). These two cuspids are sometimes so minute on the m3 that the notch between them is shallower than on m1 and m2 (e.g., MNHN.F.GL261, Fig. 11w) to indistinct (e.g., MNHN.F.GL383, UM-AV-5-SK). The entoconid is asymmetrical in lateral view because the entoconid – metaconid notch is deeper than the entoconid – hypoconulid notch. The

postentocristid is sometimes absent on m2 (e.g., MNHN.F.CB878; Fig. 11o vs Fig. 11j, m) and m3 (e.g., MNHN.F.CB4213; Fig. 11r vs Fig. 11j, t, v), so that the entoconid and hypoconulid are not connected by a crest on the concerned specimens. Even on the m2 with a small entoconid (e.g., MNHN.F.SZ18001, Fig. 11l), the entoconid is always at least slightly higher than the hypoconulid. These two cuspids are mostly subequal in height on the m3 (Fig. 11s, u, w, y), but some specimens have a slightly higher entoconid as for the m2 (e.g., UM-AV-4-SK). The relative length of the entoconid of the m3 varies from shorter than the hypoconulid (e.g., MNHN.F.GL263, Fig. 11y) to as long as the hypoconulid (e.g., MNHN.F.CB4213, Fig. 11s). The entoconid is as high as the hypoconid in distal view (Fig. 11q). MNHN.F.Av18002 has a lingually unreduced postcingulid (Fig. 11t). The degree of lingual curvature of the talonid also varies, especially on m3 (e.g., Fig. 11v vs Fig. 11x).

The lower molar MNHN.F.Av16032 exhibits typical peradectid traits such as a lingually curved talonid and a hypoconid mesiolabial to entoconid, and is similar to other *Pd. louisi* m4 in occlusal view in having a small labiolingually pinched talonid with an almost centered hypoconulid on the distal margin of the talonid, and an absence of a prominent postcingulid reaching the base of the hypoconulid (e.g., MNHN.F.GL301, Fig. 11e). However, although other peradectid m4 have an entoconid much lower than the hypoconulid (Fig. 11f, h), and other *Pd. louisi* m4 (MNHN.F.GL301 and MNHN.F.Av16037) have a straight postcristid, on MNHN.F.Av16032 the entoconid is large, as high as the hypoconulid and higher than the hypoconid, and the postcristid is curved. Because the relative height of the entoconid varies as such in *Pt. constans* m4 (e.g., Ladevèze et al. 2012: fig. 6Hc vs fig. 6Ic) and because m4 of the closely related *Pd. crocheti* sp. nov. and *Pd.* cf. *louisi* have a curved postcristid (Figs. 7a, 11g), MNHN.F.Av16032 is identified as m4 of *Pd. louisi*. The hypoconid apex is placed slightly distolabially to the protoconid apex on MNHN.F.Av16032, this character being observed also in ascertained peradectid m4 (e.g., Fig. 11g). The preprotocristid is not convex in labial view

on two m4 specimens (MNHN.F.Av16037, Crochet 1980b: fig. 13a; MNHN.F.GL301, Fig. 11f) contrary to other molar loci (e.g., Fig. 11b vs Fig. 11f) and to the m4 MNHN.F.Av16032.

Peradectes cf. *louisi*

Figure 11g-h

? 1983 *Peradectes mutigniensis* Crochet; Louis and Laurain: p. 8.

Material: MNHN.F.STA296, left m4.

Locality and age: Saint-Agnan, Aisne, eastern Paris Basin; MP8+9 – MP10 interval (see Louis and Laurain 1983; Lecomte 1994; Escarguel 1999; Solé et al. 2018).

Description and comment: The only peradectid specimen from Saint-Agnan is the m4 MNHN.F.STA296. It is much smaller than the m4 of *Pd. russelli*, and larger and with a higher crown than the m4 of '*Arm.*' *dufraingi*. MNHN.F.STA296 does not differ in size and morphology from the m4 of *Pd. louisi* MNHN.F.GL301 and MNHN.F.Av16037 (e.g., Fig. 11e-f vs Fig. 11g-h; Online Resource 1: Table S2). However, peradectid m4 are rare and bear less diagnostic characters than m2 and m3. For example, the relative height of the entoconid and hypoconulid in addition to the morphology of the notch between them allow to distinguish the European species *Pd. crocheti* sp. nov., *Pd. lousi* / *Pd. russelli* and '*Arm.*' *dufraingi* based on m2 and m3. On m4, the configuration of these cuspids is the same for the four valid species and MNHN.F.STA296, with the entoconid much lower than the hypoconulid (Fig. 11h; except MNHN.F.Av16032). Because of this, and the lack of other molar loci from Saint-Agnan, MNHN.F.STA296 can only be tentatively ascribed to *Peradectes* cf. *louisi*. Furthermore, it is worth mentioning that undescribed peradectid species, also equivalent in size to *Pd. louisi*, probably occur in localities younger than MP8+9 (see Discussion, 'Revision of putative occurrences of typical MP8+9 and ~MP8+9 peradectids in MP10 and ~MP10 faunas').

Peradectes russelli Crochet, 1979

Figure 12

Remark: *Peradectes 'mutigniensis'* Crochet, 1979, is considered a junior synonym of *Pd. russelli* (see Discussion).

1977a *Peradectes* sp. nov. 2; Crochet: p. 359, pl. 1, fig. C.

1979 *Peradectes russelli* Crochet; Crochet: p. 367-368, fig. 2 (in part).

1979 *Peradectes mutigniensis* Crochet; Crochet: p. 368, fig. 3.

1980b *Peradectes louisi* Crochet; Crochet: fig. 4a (in part).

1980b *Peradectes russelli* Crochet; Crochet: p. 43-46, figs. 14-17 (no fig. 18) (in part).

1980b *Peradectes mutigniensis* Crochet; Crochet: p. 46-49, figs. 19-25.

1980b *Peradectes* sp.; Crochet: p. 51 (in part).

Holotype: MNHN.F.CB924, fragment of right maxilla with M3-M4, housed at the Muséum National d'Histoire Naturelle (Paris), and figured by Crochet (1977a: pl. 1, fig. C_3, 1979: fig. 2; 1980b: fig. 16).

Localities: Condé-en-Brie (type locality), Avenay, Mutigny, Sables de Brasles, Sézanne-Broyes; all in the eastern Paris Basin.

Age: middle Ypresian (middle early Eocene), MP8+9 and ~MP8+9 reference level (~ mammalian biozones PE IV and PE V)

Material: Additional material from Condé-en-Brie: left M1 (MNHN.F.CB2501; Crochet 1977a: pl. 1, fig. C_1, 1980b: fig. 14, MNHN.F.CB3275), right M1 (MNHN.F.CB3007), left M2 (MNHN.F.CB5103; Crochet 1977a: pl. 1, fig. C_2, 1980b: fig.15, MNHN.F.CB840, MNHN.F.CB850), right M2 (MNHN.F.CB3644), labial half of right M2 (MNHN.F.CB2753), left M3 (MNHN.F.CB742), right M3 (MNHN.F.CB2502), right m1 (MNHN.F.CB3021), right

m2 (MNHN.F.CB5098, MNHN.F.CB5100, MNHN.F.CB928), fragment of right dentary with worn m2 (MNHN.F.CB925).

Material from Avenay: left M1 (UM-AV-13-SK), right M1 (MNHN.F.Av16024; Crochet 1980b: fig. 19), right M3 (MNHN.F.Av4813; Crochet 1980b: fig. 4a, MNHN.F.Av6837), left m2 (MNHN.F.Av7235; Crochet 1980b: fig. 17, UM-AV-14-SK), right m2 (UM-AV-15-SK).

Material from Mutigny: left M1 (MNHN.F.Mu18004; Crochet 1980b: fig. 20), right M1 (MNHN.F.Mu5532), left M2 (MNHN.F.Mu18002; Crochet 1980b: fig. 21), right M3 (MNHN.F.Mu5521; Crochet 1980b: fig. 22), right m2 (MNHN.F.Mu18000; Crochet 1980b: fig. 23), left m3 (MNHN.F.Mu6451; Crochet 1980b: fig. 24), right m4 (MNHN.F.Mu18003).

Material from Sables de Brasles: right m2 (MNHN.F.GL92; Crochet 1980b: fig. 25), right m3 (MNHN.F.GL410).

Material from Sézanne-Broyes: left m1 (MNHN.F.SZ18002).

Translation to English of the original French diagnosis (Crochet 1979): 'European species of median size. On M3, stylar cusp B slightly higher than other stylar cusps. Ectoflexus symmetric, wide and well-developed, stylar cusp C reduced. Paraconule not very pronounced or absent, metaconule weak. In occlusal view, M3 with a rather massive aspect (stylar line relatively long, preprotocrista – postprotocrista angle quite open). On lower molars, lingual opening of the prefossid higher than the lowest point of the entocristid. m4 longer than m3.'

New differential diagnosis: Differs from the other European peradectid species in being significantly larger. Further differs from *Pd. crocheti* sp. nov. in having: (i) stylar cusp C apex less ventral than stylar cusp D apex on M3; (ii) crown labial emargination on m3 and m4, and often m2; (iii) trigonid more labiolingually wide than talonid on m3; and (iv) entoconid and hypoconulid separated by a shallower notch. Differs also from *Pd. louisi* and '*Arm.*' *dufraingi* in having relatively wider lower molars. Further differs from *Pd. louisi* in having: (i) stylar cusp

D strictly labial to metacone apex; and (ii) stylar cusp C apex as ventral as stylar cusp D apex on M1 and M2. Further differs from '*Arm.*' *dufraingi* notably by: (i) entoconid higher than hypoconulid on m2 and as high as hypoconulid on m3; and (ii) larger postcingulid on m2 and m3.

Comparative description

Remark: *Peradectes russelli* being similar to *Pd. crocheti* sp. nov. and *Pd. louisi*, detailed comparisons of *Pd. russelli* with North American peradectids are not proposed.

Upper molars: The mesiodistal length of the talon and of the centrocrista varies positively with the mesiodistal length of the specimens (e.g., MNHN.F.CB3007, Fig. 12b vs MNHN.F.CB3275, Fig. 12d for M1; MNHN.F.Av6837, Fig. 12f vs MNHN.F.CB2502, Fig. 12h for M3). The protocone of one M1 (MNHN.F.Av16024; Crochet 1980b: fig. 19b) and two M2 (MNHN.F.Mu18002, Crochet 1980b: fig.21; MNHN.F.CB850, Fig. 12j) is relatively more distally positioned than for other specimens (still mesiolingual to the midpoint of the centrocrista). The tiny paraconule preserved on molars of the holotype (Crochet 1979: fig. 2; pers. obs.) is indistinct on most other upper molars (Fig. 12b, d, f, h, j), as in *Pd. louisi*. M1 and M2 have a faint premetaconular crista in addition to the postmetaconular crista (e.g., Fig. 12b, d, j), the former being more marked on some specimens (e.g., MNHN.F.CB2501). The M3 MNHN.F.CB2502 has a doubled stylar cusp A (Fig. 12g-h). One of the two small cusps in the stylar cusp A position is directly mesial to stylar cusp B, and is connected to it by a crest; the second small A cusp is placed mesiolingually to stylar cusp B, as on other M3. Stylar cusp B is strictly labial to the paracone on the M3 of the holotype (MNHN.F.CB924; Crochet 1979: fig. 2) and mesiolabial to the paracone on the M3 MNHN.F.Mu5521, former holotype of *Pd. 'mutigniensis'* (Crochet 1979: fig. 3). Apart from MNHN.F.CB924, only the M3

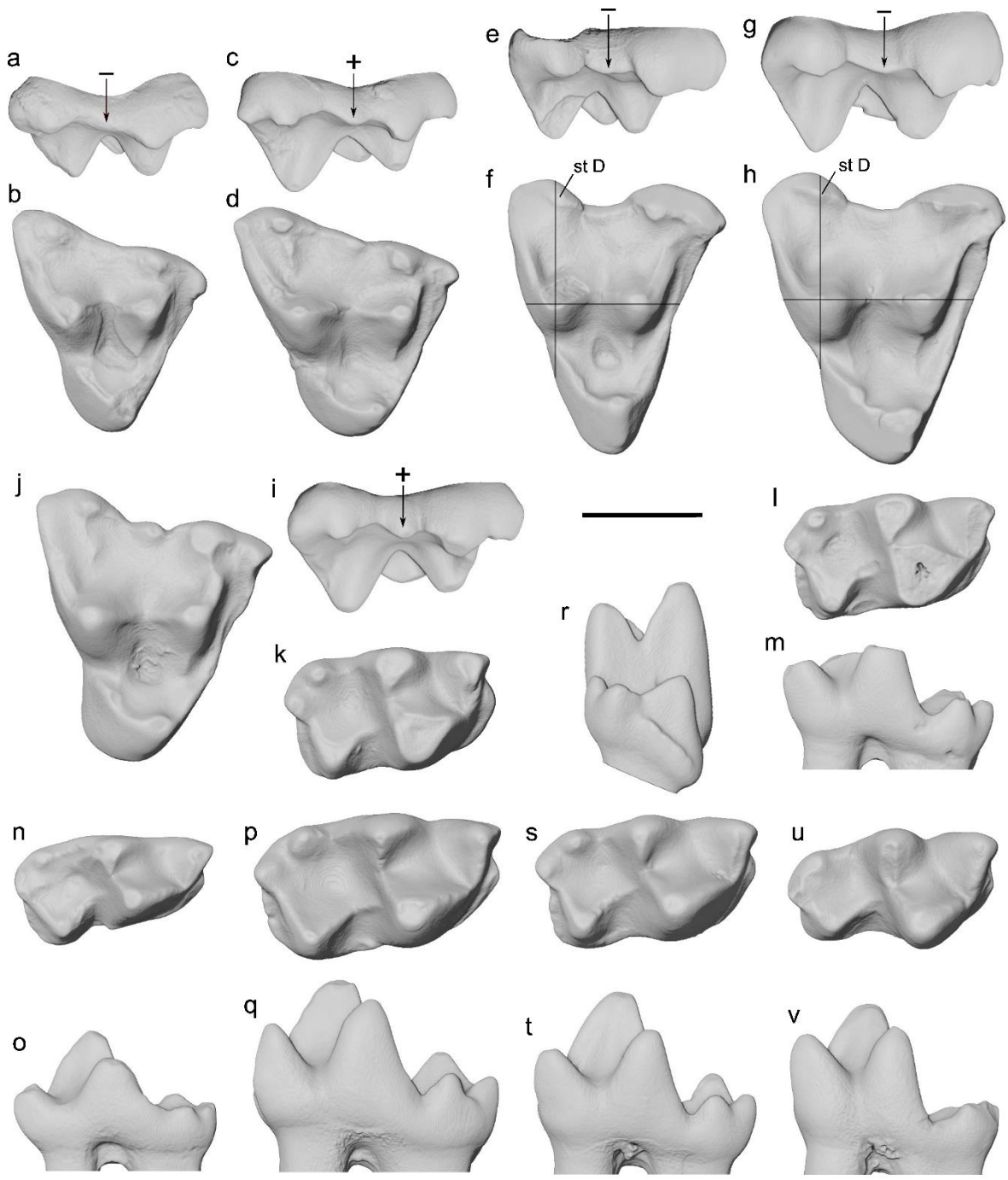

Fig. 12 Upper and lower molars of *Peradectes russelli* from Avenay (MP8+9), Condé-en-Brie, Mutigny, Sables de Brasles and Sézanne-Broyes (~MP8+9), all in the Paris Basin. **a-b**. MNHN.F.CB3007, right M1; **a**. labial view; **b**. occlusal view. **c-d**. MNHN.F.CB3275, left M1; **c**. reversed labial view; **d**. reversed occlusal view. **e-f**. MNHN.F.Av6837, right M3; **e**. labial view; **f**. occlusal view. **g-h**. MNHN.F.CB2502, right M3; **g**. labial view; **h**. occlusal view. **i-j**. MNHN.F.CB850, left M2; **i**. reversed labial view; **j**. reversed occlusal view. **k**. UM-AV-14-SK, left m2 in reversed occlusal view. **l-m**. MNHN.F.Mu18000, right m2; **l**. occlusal view; **m**. lingual view. **n-o**. MNHN.F.SZ18002, left m1; **n**. reversed occlusal view; **o**. reversed lingual

view. **p-q**. MNHN.F.CB928, right m2; **p**. occlusal view; **q**. lingual view. **r-t**. MNHN.F.GL410, right m3; **r**. distal view; **s**. occlusal view; **t**. lingual view. **u-v**. MNHN.F.Mu18003, right m4; **u**. occlusal view; **v**. lingual view. The arrows denoting the stylar cusp C on labial views are followed by '+' if the most ventral point on the st. C – st. D mesiodistal extension is reached on the st. C, and by '-' if this most ventral point is reached on the st. D. The segments on the occlusal views of MNHN.F.Av6837 (**f**) and MNHN.F.CB2502 (**h**) are positioned on the paracone – metacone axis and its perpendicular line. Abbreviation: **st D**, stylar cusp D. Scale bar equals 1 mm.

MNHN.F.Av4813 (Crochet 1980b: fig. 4a) has a stylar cusp B strictly labial to the paracone (2 out of 6 M3 specimens). This character state is present on all M1 and M2 as in *Pd. crocheti* sp. nov. and *Pd. louisi*. In occlusal view, stylar cusp C is closer to stylar cusp B than to stylar cusp D on 4 out of 7 M1 (MNHN.F.CB2501; MNHN.F.CB3275, Fig. 12c; MNHN.F.Mu18004; MNHN.F.Mu5532) and 2 out of 5 M2 (MNHN.F.CB5103; MNHN.F.CB850, Fig. 12i). The apices of stylar cusps C and D are equally ventral on both M1 and M2 contrary to *Pd. louisi*, except for the M1 MNHN.F.CB3007 on which stylar cusp D is more ventral than the vestigial stylar cusp C (1 out of 12 M1 to M2 specimens, Fig. 12a). The height relationships of stylar cusps of *Pd. russelli* are as follows: st. B > A = C = D for M2, and st. B > A > D > C for M3 (e.g., Fig. 12e) (Table 3). On 5 out of 18 isolated M1-M3 (MNHN.F.Mu18004 and MNHN.F.CB3275 for M1, MNHN.F.CB850 for M2, MNHN.F.CB742 and MNHN.F.CB924 for M3), stylar cusp D has a lingual crest of variable labiolingual length (e.g., Fig. 12d, j), which is unseen in *Pd. crocheti* sp. nov. and *Pd. louisi*. The ectoflexus is relatively deep on 4 out of 7 M1 (e.g., MNHN.F.CB3007, Fig. 12b), especially on UM-AV-13-SK. The M4 (MNHN.F.CB924, Crochet 1979: fig. 2) lacks stylar cusp C unlike *Pd. crocheti* sp. nov. and *Pd. louisi*, and has minute stylar cusps A and B. The M4 lacks internal conular cristae. As in *Pd. crocheti* sp. nov. and *Pd. louisi*, stylar cusp A of M4 is higher than stylar cusp B and there is a deep ectoflexus.

Lower molars: The m1 and m4 described here are the first reported for this species. m1 have a relatively long paracristid and a metaconid much higher than the paraconid. The m1 from Sézanne-Broyes (MNHN.F.SZ18002, Fig. 12n-o) is significantly larger than the m1 of *Pd. louisi* from the same locality (MNHN.F.SZ18003, Fig. 11c-d). As in *Pd. louisi*, m2 differ from m3 in having as labiolingually wide trigonid and talonid instead of a narrower talonid, and entoconid higher than the hypoconulid instead of equal in height (e.g., Fig. 12l-m, p-q vs Fig. 12s-t). The talonid is as labiolingually wide or wider than the trigonid on m2, except for MNHN.F.GL92, for which the talonid is slightly narrower than the trigonid (Crochet 1980b: fig. 25). The metaconid is longer than the paraconid on m1 and m2 (Fig. 12o, q), these two cuspids are subequal in length on m3 (Fig. 12t), and the paraconid is longer than the metaconid on the single available m4 (Fig. 12v). The labial emargination of the crown is present in one out of the two m1 (MNHN.F.SZ18002, Fig. 12n), slightly on 4/9 m2 (e.g., UM-AV-14-SK , Fig. 12k vs MNHN.F.Mu18000, Fig. 12l) and all m3-m4 (Fig. 12s, u). The entoconid and hypoconid are of the same height in distal view (e.g., Fig. 12r), with the exception of the m2 MNHN.F.CB928, with a hypoconid higher than the entoconid. The hypoconid is unambiguously mesiolabial instead of labial to the entoconid on some lower molars (e.g., Fig. 12k, l, n, u), as in *Pd. louisi*. On m2, the entoconid can be positioned either close to the distolingual corner of the molar (e.g., UM-AV-14-SK, Fig. 12k or MNHN.F.Mu18000, Fig. 12l) or intermediate between the distal edge of the trigonid and the distal margin of the molar (e.g., MNHN.F.CB928, Fig. 12p). The entoconid – hypoconulid notch is slightly higher than the metaconid – entoconid notch on m2 (e.g., MNHN.F.CB928, Fig. 12q) and much higher on m3 (e.g., MNHN.F.GL410, Fig. 12t). m1 and m4 have a straight postcristid, whereas it is curved on m2 and m3. The m4 has a relatively long paracristid lingual segment, a relatively high paraconid and a labiolingually narrow talonid (Fig. 12u), as in *Pd. crocheti* sp. nov. and *Pd.*

louisi. The mesial end of the cristid obliqua of m4 is slightly labial to the protocristid notch on the trigonid wall. There is no distinct postcingulid on m4, as in *Pd. louisi*.

Results

Quantitative comparisons

Size and proportions of molars. Univariate statistics based on molar measurements for the three studied peradectid species are presented in Table 4. The two complete and unworn upper molars from Palette are the M1 MHN.AIX.PV.2018.26.20, which is smaller than the M1 of the holotype, and the M3 MHN.AIX.PV.2017.6.7, which is larger than the M3 of the holotype (Online Resource 1: Table S1). In particular, the length and width of MHN.AIX.PV.2018.26.20 represent the minimum of the observed range values for M1, and the width of MHN.AIX.PV.2017.6.7 is the maximum of the observed range values for M3 (material from all localities included). Thus, most of the size variation of *Pd. crocheti* sp. nov. is represented in its type locality. The disparity of length to width ratio between the M2 and M3 (= L/W M2 - L/W M3) is weak based on mean values (i.e., < 0.10) for *Pd. louisi* and *Pd. russelli* (isolated molars only). Because of the low number of specimens with calculated L/W ratios for M2 of *Pd. crocheti* sp. nov. (two specimens, including the holotype), only the disparity of M2-M3 from the type specimen is retained for comparisons of this character between *Pd. crocheti* sp. nov. and other peradectids (Table 2). The m1 of *Pd. crocheti* sp. nov. and *Pd. louisi* are a mean of 9% mesiodistally shorter than the m2, whereas this value is 12.5% for *Pd. russelli* (Table 4).

The standard deviation and coefficient of variation values for the length of the M2 of *Pd. crocheti* sp. nov. are relatively higher than for the other molar loci, probably because the M2 from Croydon (Hooker 2020) is much larger than other M2 specimens ascribed to this species. However, the normal distribution for the length of the M2 of *Pd. crocheti* sp. nov. is not

Table 4 Univariate statistics associated with measurements (in mm) of upper and lower molars of *Peradectes crocheti* sp. nov., *Pd. louisi* and *Pd. russelli*. Abbreviations: **N**, number of specimens measured; **OR**, observed range; **SD**, standard deviation; **CV**, unbiased coefficient of variation (%); **W**, Shapiro–Wilk normality test (**ns**, normal distribution cannot be rejected; **s**, normal distribution is rejected; $P < 0.05$).

Peradectes crocheti sp. nov								*Peradectes louisi*								*Peradectes russelli*							
Locus		N	OR	Mean	SD	CV	W	Locus		N	OR	Mean	SD	CV	W	Locus		N	OR	Mean	SD	CV	W
M1	L	5	1.51-1.71	1.60	0.079	4.91	ns	M1	L	9	1.47-1.65	1.56	0.060	3.86	ns	M1	L	7	1.62-1.97	1.81	0.117	6.45	ns
	W	6	1.40-1.59	1.49	0.093	6.27	s		W	9	1.45-1.66	1.55	0.070	4.50	ns		W	7	1.78-2.09	1.89	0.099	5.25	ns
	L/W	5	0.97-1.21	1.06	0.092	8.67	ns		L/W	9	0.94-1.07	1.01	0.042	4.19	ns		L/W	7	0.88-1.03	0.96	0.048	5.01	ns
M2	L	7	1.45-1.81	1.57	0.117	7.46	ns	M2	L	6	1.52-1.71	1.61	0.068	4.23	ns	M2	L	5	1.82-2.11	1.97	0.110	5.58	ns
	W	3	1.66-1.85	1.74					W	9	1.69-1.87	1.77	0.067	3.79	ns		W	4	2.07-2.27	2.19	0.097	4.43	ns
	L/W	2	0.88-0.98	0.93					L/W	4	0.86-0.98	0.91	0.056	6.15	ns		L/W	4	0.85-0.92	0.88	0.030	3.38	ns
M3	L	5	1.40-1.60	1.53	0.078	5.10	ns	M3	L	4	1.41-1.63	1.51	0.093	6.17	ns	M3	L	6	1.78-2.02	1.92	0.096	5.01	ns
	W	6	1.77-1.98	1.85	0.083	4.49	ns		W	4	1.72-1.92	1.83	0.083	4.53	ns		W	6	2.27-2.52	2.36	0.103	4.36	ns
	L/W	4	0.77-0.87	0.82	0.044	5.44	ns		L/W	4	0.77-0.88	0.82	0.051	6.23	ns		L/W	6	0.78-0.86	0.81	0.030	3.74	ns
M4	L	2	1.12-1.26	1.19				M4	L	1	1.33					M4	L	1	1.35				
	W	1	1.79						W	1	1.88						W	1	2.36				
	L/W	1	0.70						L/W	1	0.71						L/W	1	0.57				
m1	L	2	1.47-1.57	1,52				m1	L	8	1.40-1.56	1.50	0.063	4.19	ns	m1	L	2	1.65-1.71	1.68			
	W	3	0.86-0.94	0.91					W	8	0.76-0.85	0.81	0.038	4.73	ns		W	2	0.89-0.92	0.91			
	L/W	2	1.69-1.71	1.70					L/W	8	1.75-2.03	1.85	0.087	4.69	ns		L/W	2	1.79-1.92	1.86			
m2	L	4	1.64-1.69	1.67	0.026	1.58	ns	m2	L	13	1.54-1.73	1.65	0.060	3.66	ns	m2	L	9	1.75-2.05	1.92	0.114	5.94	ns
	W	3	0.99-1.04	1.02					W	14	0.87-1.00	0.94	0.044	4.62	ns		W	9	1.04-1.25	1.14	0.074	6.49	ns
	L/W	3	1.59-1.71	1.63					L/W	13	1.61-1.83	1.74	0.060	3.45	ns		L/W	9	1.62-1.79	1.69	0.053	3.14	ns
m3	L	5	1.53-1.66	1.60	0.068	4.24	ns	m3	L	18	1.47-1.66	1.57	0.050	3.20	ns	m3	L	2	1.74-1.85	1.80			
	W	5	0.87-1.06	0.97	0.078	8.02	ns		W	16	0.84-0.95	0.89	0.036	4.02	ns		W	2	1.05-1.11	1.08			
	L/W	5	1.58-1.77	1.65	0.077	4,66	ns		L/W	16	1.62-1.87	1.77	0.063	3.58	ns		L/W	2	1.66-1.67				
m4	L	1	1.55					m4	L	3	1.44-1.53	1.48				m4	L	1	1.75				
	W	1	0.92						W	3	0.78-0.85	0.83					W	1	1.00				
	L/W	1	1.68						L/W	3	1.74-1.85	1.80					L/W	1	1.75				

rejected. The low standard deviation value for the length of the m2 of *Pd. crocheti* sp. nov. is most likely because two out of the four specimens included probably represent the same individual (MHN.AIX.PV.2017.6.8 and MHN.AIX.PV.2017.6.9). The normal distribution is rejected for the width of M1 of *Pd. crocheti* sp. nov. (Table 4). This is most likely because no size continuum is recorded between the six M1 forming two clusters for *Pd. crocheti* sp. nov. (Online Resource 1: Table S1). For all other molar measurements, the normal distribution is not rejected (see Table 4).

The observed ranges for dental measurements of *Pd. crocheti* sp. nov. and *Pd. louisi* are alike, except for the labiolingual width values of the lower molars, which are lower in the latter (Table 4). There is a statistically significant difference between the L/W ratios of lower molars of the coeval *Pd. louisi* and *Pd. russelli*, either when m1 to m4, m2 to m3 or only m2 are taken into account (Table 5). However, the mean L/W ratio for lower molars of *Pd. russelli* and *Pd. crocheti* sp. nov. do not differ significantly (Table 5). Similarly to *Pd. crocheti* sp. nov., the lower molars of *Pd. russelli* are relatively labiolingually wider than those of *Pd. louisi*, except for m1 (Table 4). For the three species studied, the m2 are larger than the m3 in mean (Table 4, Fig. 13). The m2 to m4 of *Pd. louisi* are larger than equivalent loci in '*Arm.*' *dufraingi* (Table 4 vs Smith and Smith 2013: p. 304).

Taking into account all molar loci, the size distributions of *Pd. louisi* and *Pd. russelli* show almost no overlap (Fig. 13a-b). Only one M1 of *Pd. russelli* (MNHN.F.CB3007) is similar in size to M2 and M3 of the smaller *Pd. louisi* (Online Resource 1: Table S3). In the same way, the two m1 of *Pd. russelli* (MNHN.F.CB3021 and MNHN.F.SZ18002) are closer in size to both m2 and the largest m3 of *Pd. louisi* (Fig. 13b). However, M1 and m1 of *Pd. louisi* and *Pd. russelli* form two distinct size clusters. MNHN.F.SZ18004, the single M4 of *Pd. louisi*, is

attributed to this species in part because it is closer in width to the M3 of *Pd. louisi* than to the M3 of *Pd. russelli* (Fig. 13a).

Table 5 Results of Welch's *t*-test for comparisons of mean length to width ratio values between lower molars of *Peradectes louisi* and *Peradectes russelli*. The equality of mean L/W ratios is rejected for the three subsamples (which differ in the molar loci included) comparing lower molars of *Pd. louisi* and *Pd. russelli*, but not for the sample comparing lower molars of *Pd. crocheti* sp. nov. and *Pd. russelli*. Abbreviations: **d.f.**, degree of freedom; **L**, length; **N**, number of lower molars; **P**, p-value; **ns**, mean values not significantly different; **s**, mean values significantly different, $P < 0.05$; **t**, Welch Two Sample *t*-test value; **W**, width.

Compared samples for L / W ratio	Result of Welch's *t*-test
m1-4 *Pd. louisi* (N = 40) vs *Pd. russelli* (N = 14)	s (t = 2.58, d.f. = 21.79, P = 0.017)
m2-3 *Pd. louisi* (N = 29) vs *Pd. russelli* (N = 11)	s (t = 3.79, d.f. = 23.32, P = 0.001)
m2 *Pd. louisi* (N = 13) vs *Pd. russelli* (N = 9)	s (t = 2.11, d.f. = 18.68, P = 0.049)
m1-4 *Pd. crocheti* sp. nov. (N = 11) vs *Pd. russelli* (N = 14)	ns (t = 1.88, d.f. = 22.99, P = 0.073)

MNHN.F.Mu5521, former holotype of *Pd. 'mutigniensis'*, is the M3 of *Pd. russelli* with the lowest length and width, whereas the M3 of the holotype of *Pd. russelli* (MNHN.F.CB924) has the highest width value of the sample (Fig. 13a). *Peradectes russelli* occupies a larger length x width space than *Pd. louisi* (Fig. 13a-b), probably due to its larger size. In particular, the M3 and M4 of the holotype MNHN.F.CB924 differ greatly in length, more than what would be expected for the same molar loci in *Pd. louisi* based on available M3 and M4 specimens (Fig. 13a). The M2 and M3 overlap more in width in *Pd. louisi* than in *Pd. russelli*. Conversely, the M2 and M3 overlap more in length in *Pd. russelli* than in *Pd. louisi*.

Absolute basal heights of stylar cusps C and D. In the whole sample, the values of the absolute basal height of stylar cusp C to the absolute basal height of stylar cusp D are comprised in a range from 0.215 (i.e., the absolute basal height value of stylar cusp C is more than four times lower than for stylar cusp D; M1 MNHN.F.CB3007 of *Pd. russelli*) to 1,939 (i.e., the absolute basal height value of stylar cusp C is almost two times higher than for stylar cusp D;

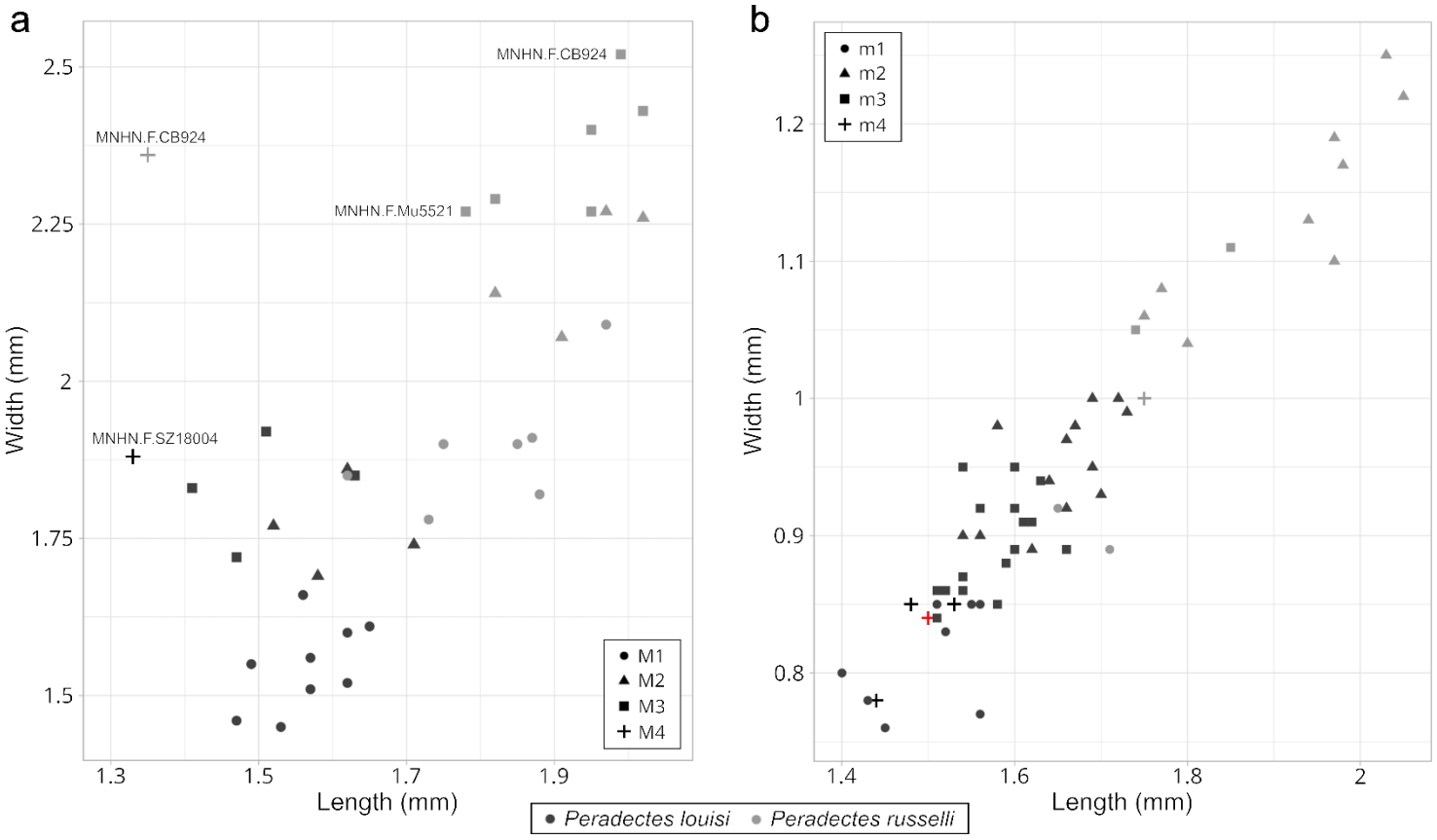

Fig. 13 Bivariate graphs (length x width) of upper molars (**a**) and lower molars (**b**) of the two species of *Peradectes* (*Pd. louisi* and *Pd. russelli*) from MP8+9, ~MP8+9 and MP8+9-MP10 interval localities of the Paris Basin. For upper molars (**a**), specimen numbers indicate the holotype of *Pd. russelli* (MNHN.F.CB924), the former holotype of *Pd. 'mutigniensis'* chosen by Crochet (1979) (MNHN.F.Mu5521) and the M4 of *Pd. louisi* (MNHN.F.SZ18004). For lower molars (**b**) the m4 specimen representing *Peradectes* cf. *louisi* is plotted in red. All measurements are from isolated molars with the exception of MNHN.F.CB924.

M3 UM-FDN-23 of *Pd. crocheti* sp. nov.) (Fig. 14; Online Resource 1: Table S4). The values equal or lower than the first quartile are only those of some M1 or M2 for *Pd. crocheti* sp. nov., whereas it concerns also some M3 specimens for the distributions of the values of *Pd. louisi* (MNHN.F.Mu18001) and *Pd. russelli* (MNHN.F.Av6837; MNHN.F.CB742). Conversely, the values equal or higher than the third quartile concern only M3 (five specimens) for *Pd. crocheti* sp. nov.; M1 (one specimen), M2 (three specimens) and M3 (one specimen) for *Pd. louisi*, with only M2 specimens as outlier values; and M1 (one specimen) and mostly M2 (four specimens)

for *Pd. russelli* (Fig. 14). It is worth noting that fewer M3 specimens are known for *Pd. louisi* (five specimens) than for the two other species. Among these specimens, two lack stylar cusp C (MNHN.F.GL197 and MNHN.F.CB4182), one is damaged in the stylar cusp C area, and only two have measurable absolute basal heights for stylar cusps C and D (MNHN.F.Mu18001 and MNHN.F.SZ18005; Online Resource 1: Table S4). *Peradectes russelli* differs from *Pd. crocheti* sp. nov. and *Pd. louisi* in having a lower value for the interquartile range, almost equal mean and median values, and the lowest ratio values of the whole sample (the M1 MNHN.F.CB2501 and MNHN.F.CB3007, and the M3 MNHN.F.CB742; Online Resource 1: Table S4).

There is a statistically significant difference between the rank sum of the absolute basal height of stylar cusp C to the absolute basal height of stylar cusp D of *Pd. crocheti* sp. nov. and *Pd. louisi* (Fig. 14; Wilcoxon-Mann-Whitney test; W = 226, P = 0.043), and *Pd. crocheti* sp. nov. and *Pd. russelli* (Wilcoxon-Mann-Whitney test; W = 256, P = 0.0004). We should mention that without including the *Pd. crocheti* sp. nov. M3 UM-FDN-23, which has a high value for the calculated ratio (Online Resource 1: Table S4), there is no statistically significant difference between *Pd. crocheti* sp. nov. and *Pd. louisi* for this character (Wilcoxon-Mann-Whitney test; W = 208, P = 0.072), and the statistical difference still occurs between *Pd. crocheti* sp. nov. and *Pd. russelli* (Wilcoxon-Mann-Whitney test; W = 239, P = 0.0007). There is no statistically significant difference between the rank sum of the calculated ratios of *Pd. louisi* and *Pd. russelli* (Wilcoxon-Mann-Whitney test; W = 204, P = 0.096). Noteworthy, a statistically significant difference is recovered between *Pd. louisi* and *Pd. russelli* using a parametric instead of a non-parametric test (Welch's *t*-test; t = 2.11, d.f. = 28.49, P = 0.044). Finally, the range of variation for the absolute basal height of the stylar cusp C for *Pd. russelli* (0.033 mm – 0.123 mm) is included in the one of *Pd. crocheti* sp. nov. (0.030 mm – 0.131 mm) (Online Resource 1: Table S4), although the former species is larger than the latter.

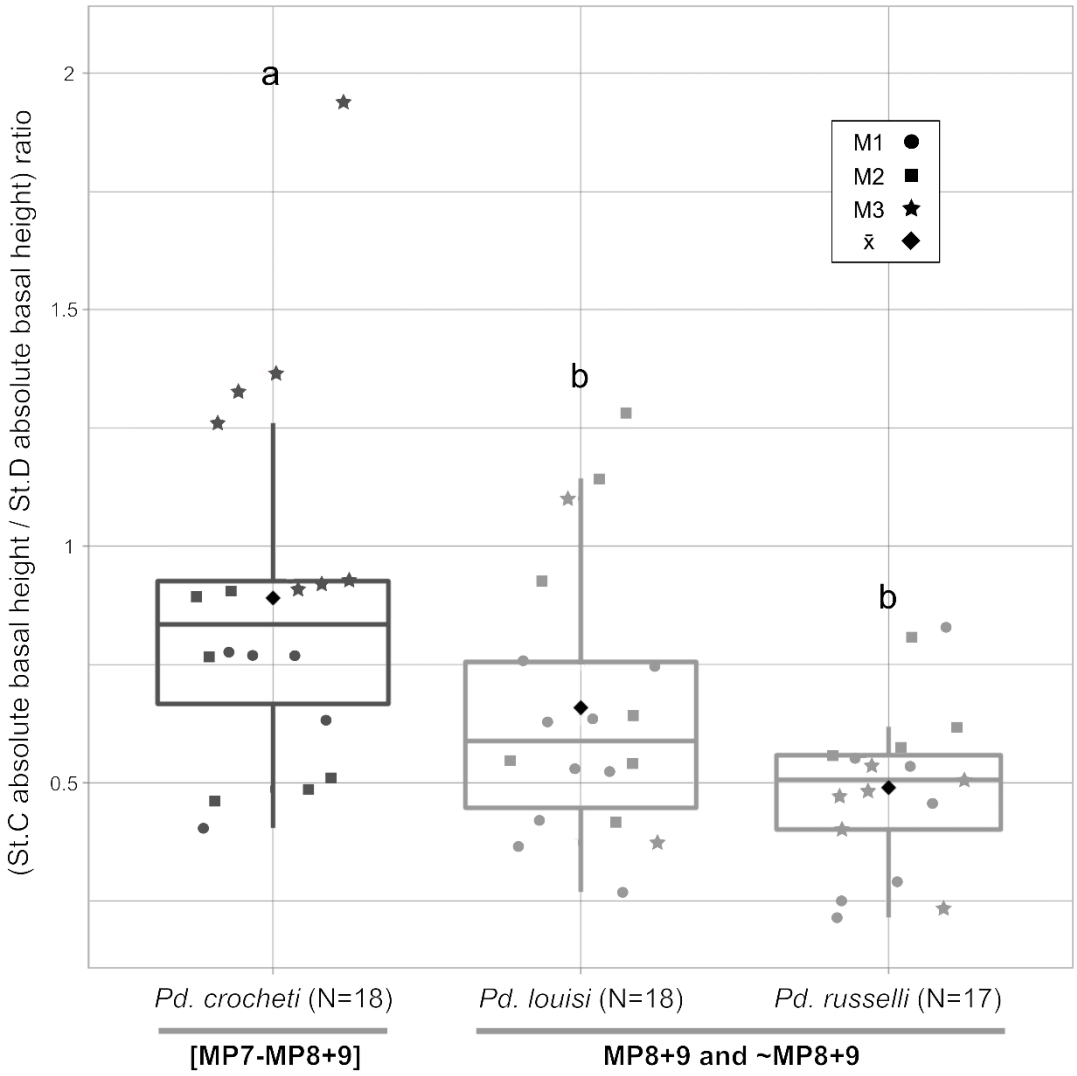

Fig. 14 Boxplots showing the distribution of the ratio values of the absolute basal height of stylar cusp C to the absolute basal height of stylar cusp D for *Peradectes crocheti* sp. nov. (MP7-MP8+9 interval), *Pd. louisi* and *Pd. russelli* (MP8+9 and ~MP8+9). M1 to M3 loci are considered. The value of the calculated ratio for each specimen is displayed for each box. The rank sum of ratio values of *Pd. crocheti* sp. nov. statistically significantly differs (letter 'a' above the box) from those of *Pd. louisi* and *Pd. russelli* (letter 'b') (non-parametric Wilcoxon-Mann-Whitney tests, $P < 0.05$; see main text). Abbreviation: **[MP7-MP8+9]**, time interval between MP7 and MP8+9 reference levels.

Height of the dentary. The dentary of MNHN.F.CB226 (*Pd. louisi*) is relatively higher below m2-m3 than those of MHN.AIX.PV.2017.6.8 (*Pd. crocheti* sp. nov.) and MNHN.F.CB925 (*Pd. russelli*) (Online Resource 1: Table S5). In turn, the dentary of *Pd. crocheti* sp. nov. is relatively

lower than the one of *Pd. russelli*. No conclusion can be made out of these height data, because of the small number of specimens, and because the height of the dentary and its elongation in opossum and 'opossum-like' metatherians may vary depending on the age and sex of the individuals (e.g., Hough 1961; Crochet 1980b: p. 35, fig. 5).

Intrafamilial phylogenetic analysis

Main cladistic analysis. The heuristic search yielded a single most-parsimonious tree (MPT) of 103 steps (Fig. 15), with a consistency index (CI) of 0.563 and a retention index (RI) of 0.526, which are indicative of high level of homoplasy in the dental characters used. A value of RI just above 0.5 indeed indicates that almost half of the similarities coded in the data matrix correspond to homoplasy (Farris 1989a, 1989b). The single MPT supports the monophyly of the ingroup, the Peradectidae, with a Bremer value of 4. 7 out of 37 (= 19%) characters are not parsimony informative for resolving relationships between the ingroup taxa. Within the ingroup (late Paleocene – middle Eocene peradectids), *Pd. elegans* is the earliest diverging offshoot of the branching sequence formed with *Pd. protinnominatus* and its sister-clade, which includes strictly Eocene *Peradectes* species as well as *Armintodelphys* and *Mimoperadectes* (hereafter designated as the 'Eocene' peradectid clade; Fig. 15). All late Paleocene – middle Eocene species distinct from *Pd. elegans* form a clade (Bremer index [BI] = 2, relatively to the mean Bremer value of 2.1) and share the following non-ambiguous synapomorphies: m1 slightly shorter (< 10%) than the m2 (4^1), postcingulids that attenuate labially to the hypoconulid (16^1), and stylar cusp A distinctly smaller than stylar cusp B on M3 (32^1).

The 'Eocene' clade is supported (BI = 2) by three non-ambiguous synapomorphies: p3 higher than m1 (3^0), the low disparity between the L/W ratios of M2 and M3 (22^1), and stylar cusp D placed distolabially to the metacone apex on M1 (35^1); two of these are non-homoplasic (3^0,

35^1). The four European species (*Pd. crocheti* sp. nov., *Pd. russelli*, *Pd. louisi* and '*Armintodelphys*' *dufraingi*) are clustered in a clade that is unambiguously supported (BI = 2) by four synapomorphies: the entoconid has an intermediate position, between the distal edge of the trigonid and the distal margin of m2 and m3 (21^1, non-homoplasic), stylar cusp A most frequently positioned mesiolingually to stylar cusp B on M2 or M3 (31^1, convergent), stylar cusp B positioned strictly labially to the apex of the paracone, at least on M1 and M2 (33^1, non-homoplasic), and the ectoflexus of their M3 is asymmetric (37^1, convergent). The relationships within the European clade are well-resolved despite the high amount of missing data for '*Arm.*' *dufraingi* (17 out of 37 [= 46%] scored characters). Within this clade, *Pd. crocheti* sp. nov. is the earliest diverging species. The clade comprising *Pd. russelli*, *Pd. louisi*, and '*Arm.*' *dufraingi* is supported (BI = 2) by two non-ambiguous synapomorphies: the presence of a straight postcristid at least on one m2-m4 locus (15^0, convergent) and the relatively small stylar cusp C compared to stylar cusps B and D (34^1, convergent). The less inclusive clade *Pd. louisi* + '*Arm.*' *dufraingi* is also supported (BI = 2) by two non-ambiguous synapomorphies: relatively long m2 or m3 with a L/W ratio equal to or higher than 1.75 (5^1, convergent) and the mesial end of the cristid obliqua sometimes ventral to the protocristid notch on m4 (11^1, convergent).

The sister group of the European peradectids is formed by a clade that includes the strictly Eocene North American peradectids (*Mimoperadectes labrus*, *Armintodelphys blacki* Krishtalka & Stucky, 1983a, *Armintodelphys dawsoni* Krishtalka & Stucky, 1983a, *Pd. chesteri*, *Pd. gulottai* and *Pd. californicus*). This clade is supported (BI = 2) by the following non-ambiguous synapomorphies: small distal heel on lower premolars (1^1, non-homoplasic), hypoconulid higher than the entoconid on m3 and m4 (19^1, convergent with '*Arm.*' *dufraingi*), and postmetacrista subequal in length or shorther than the preparacrista on M2 or M3 (29^0, with intraclade reversion). North American *Armintodelphys* species are more closely related to the strictly Eocene North American *Peradectes* species than to *Mimoperadectes labrus* based on

the absence of internal cristae on the conules (26^0, with intraclade reversion). The p3 lower than the m1 (3^2) is an ambiguous non-homoplasic character which supports the latter clade with the accelerated transformation (Acctran) optimization, or only the Eocene North American *Peradectes* clade with the delayed transformation (Deltran) optimization. The genus *Armintodelphys* is recovered as monophyletic based on two non-ambiguous synapomorphies not observed in '*Arm.*' *dufraingi*, namely a trigonid as wide as the talonid on m3 (7^1) and a talonid as long as the trigonid on m4 (8^1, non-homoplasic within the ingroup). In this topology, the genus *Peradectes* is not monophyletic, because a subclade of three *Peradectes* species is well nested (BI = 2) within the 'Eocene' North American clade that also includes *Mimoperadectes* and *Armintodelphys*. One of the most strongly supported clades of the ingroup is *Pd. gulottai* + *Pd. californicus* (BI = 3), although *Pd. gulottai* is the taxon with the least complete scoring (15 out of 37 [~ 41%] scored characters).

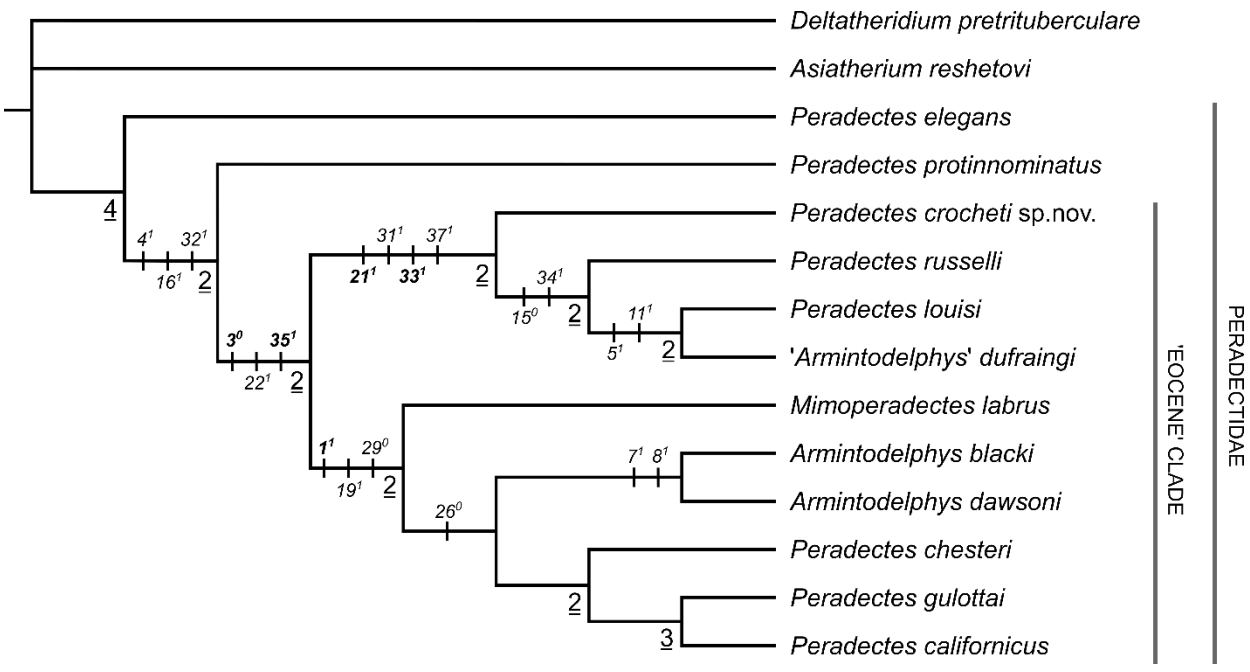

Fig. 15 Single most-parsimonious tree of 103 steps (CI = 0.563, RI = 0.526) from the first cladistics analysis (non-polymorphic characters 11, 31, 36 and 37; all characters unweighted and unordered). Underlined values under the branches at nodes are Bremer indices (BI) when > 1. The non-ambiguous synapomorphies are figured at the nodes of interest in this work, within

the ingroup. The character states in superscript are summarized in Online Resource 3. The non-ambiguous and non-homoplasic synapomorphies (CI = RI = 1) are in bold.

Subsequent cladistic analyses dealing with more characters concerned by polymorphic coding, implied weighting or ordered characters. A single MPT with the same topology is recovered from the second analysis (111 steps, CI = 0.604, RI = 0.517), for which the frequencies of observation were replaced by polymorphisms in the scoring of the characters 11, 31 and 36 (Online Resource 5: Fig. S1 and text). The differences with the first analysis concern notably (but not exclusively) two non-ambiguous synapomorphies of the first analysis that become ambiguous synapomorphies at their respective node with the accelerated transformation optimization, which are: stylar cusp A positioned mesiolingually to the stylar cusp B on the M2 or M3 (31^{1}) for the European peradectid clade, and the presence of a mesial end of the cristid obliqua ventral to the protocristid notch on the m4 (11^{1}) for the clade *Pd. louisi* + '*Arm.*' *dufraingi*. Numerous clades have a value of Bremer index decreasing from BI = 2 to BI = 1, namely the European clade, the *Pd. russelli* + *Pd. louisi* + '*Arm.*' *dufraingi* clade, the *Pd. louisi* + '*Arm.*' *dufraingi* clade, the strictly Eocene North American peradectid clade and the strictly Eocene North American *Peradectes* clade. The value of the Bremer index of the clade *Pd. gulottai* + *Pd. californicus* also decreases from 3 to 2.

As for the third analysis (addition of a polymorphic scoring for the character 37 to changes of the second analysis; see Online Resource 5), two different MPTs of 112 steps each (CI = 0.607, RI = 0.511) are obtained, and the strict consensus tree is weakly resolved, with no Bremer index values higher than BI = 1 within the ingroup (Online Resource 5: Fig. S2), and a large polytomy at the base of the 'Eocene' clade. *Peradectes crocheti* sp. nov. branches at this polytomy with other strictly Eocene peradectids, and thus does not form a clade with the other European species. *Peradectes louisi*, *Pd. russelli* and '*Arm.*' *dufraingi* still form a clade on the strict

consensus tree, but its internal topology is also unresolved. A monophyletic North American *Armintodelphys* is retained. One of the two MPTs has the same topology as the single MPT found in the previous analyses.

The fourth analysis of identical parameters and scoring as the previous one (which has the highest frequency of polymorphisms in its scoring), but with downweighted homoplasic characters instead of unweighted characters, resulted in a single MPT. The topology obtained is the same as in the main and second analyses (Fig. 15), and is that of one of the two trees of the third analysis; it is here favored for this reason. The same tree length, CI and RI scores as those of the third analysis are recovered. Finally, the fifth analysis with characters 3 and 34 ordered recovered a single MPT (105 steps, CI = 0.552, RI = 0.505), again with the favored topology. The only differences with the first analysis are as follows: i) the p3 higher than m1 (3^0) becomes homoplasic, and an ambiguous instead of non-ambiguous synapomorphy (Acctran optimization) supporting the 'Eocene' clade (for which BI = 1 instead of BI = 2); ii) the Bremer value of the 'Eocene' North American clade decreases from BI = 2 to BI = 1; iii) the acquisitions of a well-developed stylar cusp C (34^2) in the ingroup (still non-ambiguous) and of a p3 lower than m1 (3^2) in the *Armintodelphys* + 'Eocene' North American *Peradectes* clade (still ambiguous with Acctran optimization) take two steps instead of one each.

Discussion

Characters and spatiotemporal distribution of the earliest European peradectid species, *Peradectes crocheti* sp. nov.

The earliest occurrence of Peradectidae in Europe. Two *Peradectes* species were recognized in the Sotteville-sur-Mer fauna from the Mortemer Formation (~MP7, Normandie, Paris Basin;

Smith et al. 2011), each represented by a single specimen. The Sotteville-sur-Mer locality being considered as intermediate in age between Dormaal and both Soissons and Meudon (Smith et al. 2011; Marandat et al. 2012; Hooker 2015), both of these *Peradectes* species were proposed as the first European peradectids. *Peradectes* sp. 1 was identified after a fragment of a small left dentary, preserving a complete worn molar and a worn talonid (Smith et al. 2011: fig. 5.17), and would be the smallest peradectid recorded so far in Europe (Smith et al. 2011). On the molar designated as m3, the trigonid is mesiodistally narrow, much shorter than the talonid, the small protoconid is almost strictly labial to the metaconid, and the preprotocristid is rectilinear in mesiolabial view. On the putative m3 and better-preserved talonid of m2, the hypoconid is distolabial to the entoconid on the anteroposterior axis of the molar. The hypoconulid, though worn, is much lower than the entoconid, and these cuspids are not connected. Here, we rule out the attribution of this specimen to *Peradectes* because of the absence of the aforementioned characters in peradectids (Table 6). Furthermore, the low and mesiodistally pinched paraconid lacks the mesiolingual paraconid keel, a distinctive feature of metatherian mammals and of some basal therians and eutherians (Averianov et al. 2013; Averianov 2015: p. 175). The metaconid is subequal in height to the protoconid, but to our knowledge, no Laurasian metatherian with a metaconid subequal to or higher than the protoconid on lower molars exists. This feature occurs in, for example, some Paleocene South American metatherians from Tiupampa (e.g., Goin et al. 2003: p. 873; Muizon and Ladevèze 2022: p. 631-632), and is a synapomorphy of Eutheria (O'Leary et al. 2013). Finally, the entoconid and hypoconulid are not as twinned as in metatherians on the most anterior molar, and the postcingulid is absent, as seen in earliest marsupialiforms (e.g., Vullo et al. 2009) and eutherians, which also indicate the eutherian nature of this material.

Regarding the upper molar with a rectilinear centrocrista referred to as *Peradectes* sp. 2 (Smith et al. 2011: fig. 5.18), the depth of the ectoflexus and the relative length of the preparacrista

indicate it is a M3 rather than a M2. According to the authors, this molar is comparable in size and morphology to both *Pd.* '*mutigniensis*' (= *Pd. russelli*; MP8+9 and ~MP8+9 localities of the Paris Basin) and *Pd. protinnominatus* (Clarkforkian and early Wasatchian of the Bighorn Basin). However, among European peradectids, *Peradectes* sp. 2 from Sotteville-sur-Mer (L = 1.58 mm, W= 1.91 mm) is smaller than M2 and M3 of *Pd.* '*mutigniensis*', and closer in size to the holotype of *Pd. louisi*, as stated by Hooker (2020), and to the M3 of *Pd. crocheti* sp. nov. As in *Pd. crocheti* sp. nov. and *Pd. protinnominatus*, and contrary to *Pd. louisi*, stylar cusp D is labial instead of distolabial to the metacone apex, and stylar cusp C is much higher instead of subequal or lower than stylar cusp D. Although *Peradectes* sp. 2 and *Pd. protinnominatus* are almost the same size, *Peradectes* sp. 2 has a stylar cusp B positioned labially to the apex of the paracone on the stylar shelf, and the ectoflexus is asymmetric, as seen on M3 of *Pd. crocheti* sp. nov. from Palette. On the holotype of *Pd. protinnominatus* (UCMP 44077; McKenna 1960: fig. 17a) and on M3 from the Bighorn Basin (Bown 1979: fig. 40a right) attributed to *Pd. protinnominatus* in the last comprehensive revision of the species (Krishtalka and Stucky 1983b: p. 246-247), stylar cusp B is located mesiolabially to the paracone, and the ectoflexus has a symmetric shape (Fig. 4). It is worth mentioning that Gingerich and Smith (2006) did not report ascertained M3 of *Pd. protinnominatus* from the Bighorn Basin localities they studied. Considering its size and morphology, *Peradectes* sp. 2 is consequently better assigned to *Pd. crocheti* sp. nov., and it represents the earliest occurrence of this species. Therefore, *Pd. crocheti* sp. nov. is definitely the oldest European peradectid currently known (see Smith et al. 2011).

Recognition of other synonyms of *Peradectes crocheti* sp. nov. All other here proven peradectid dental material of MP7-MP8+9 interval localities attributed to *Peradectes* sp. (Russell et al. 1988; Marandat 1991; Hooker 2010) and *Pd. louisi* (Godinot 1981; Hooker 2020) have been allocated to *Pd. crocheti* sp. nov. in this study. These specimens conform to the size

range and morphological variation observed in *Pd. crocheti* sp. nov. from Palette. In Hooker's view, the labial fragment of upper molar from Abbey Wood (London, Blackheath Formation) he considered as *Peradectes* sp. (Hooker 2010: p. 17, fig. 8a-b) differs from all upper molars of the French *Peradectes* species in its much weaker stylar cusps and its more gracile metacone. The relative heights of the stylar cusps have been used here instead of the absolute height of the stylar line as diagnosic features of European peradectid species. Although both stylar cusps C and D are low on the M2 from Abbey Wood (e.g., compared to stylar cusp B), as on most upper molars of *Pd. crocheti* sp. nov. and *Pd. louisi* (Figs. 5, 9-10), the most ventral point of the stylar cusp C – D mesiodistal extension in labial view is on stylar cusp C, which is consequently higher than stylar cusp D, as in almost all specimens of *Pd. crocheti* sp. nov. (Fig. 5) and unlike *Pd. louisi* (Figs. 9-10). It is worth noting that Hooker (2020: p. 461) made the same observation for the relative heights of the stylar cusps of the M2 from Croydon (here re-referred as *Pd. crocheti* sp. nov.), which was however attributed to *Pd. louisi*. Furthermore, the metacone of the specimen from Abbey Wood is not significantly more gracile when compared with other unworn M2 of *Pd. crocheti* sp. nov. (e.g., MNHN.F.Me15975, Fig. 5o-p); thus, the shape of this cusp on the specimen from Abbey Wood is not exclusively shared with *Pd. protinnominatus* (*contra* Hooker 2010). Peradectid upper molars from Fordones (UM-FDN-1 and UM-FDN-23) were first found to be more similar to *Peradectes* sp. from MP8+9 and ~MP8+9 localities of the Paris Basin (= *Pd. louisi* in part, see below) than to any other peradectids then known, because, as on the M1 from Mutigny (MNHN.F.Mu18006; Fig. 10d), they are mesiodistally pinched at the base of the main cusps (Marandat 1991: p. 67, pl. 1, figs. 1-2), i.e., the distal edge of these upper molars is emarginated. The shape of the distal edge or mesiodistal constriction of the upper molars is here regarded as variable within the European *Peradectes* species. For example, the M1 UM-FDN-2 (Fig. 5e) of *Pd. crocheti* sp. nov., first assigned to a herpetotheriid by Marandat (1991: p. 71), shows a relatively long talon and a weak

distal emargination, which is the opposite condition to UM-FDN-1. Since this character varies substantially in the European peradectid species, its use to diagnose peradectid species (e.g., Horovitz et al. 2009) may be doubtful.

The two lower molars from Fordones would also be similar to the MP8+9 and ~MP8+9 *Peradectes* sp. due to the lingual position of the hypoconulid (Marandat 1991: p. 67, pl. 1, fig. 18). However, in addition to this character, the distolingual orientation of the hypoconulid, the entoconid higher than the hypoconid in distal view, the hypoconid positioned distolabially to the entoconid, and the pronounced labial emargination of the crown are more evocative of a herpetotheriid species. The presence of subequally-sized entoconid and hypoconulid as seen on these specimens is known to be not exclusive to Peradectidae (it also occurs in e.g., Herpetotheriidae [Crochet 1980b: p. 149, fig. 162] and 'Alphadontidae' [Johanson 1996: p. 1028]), and thus does not prevent the attribution of the lower molars from Fordones to herpetotheriids (*contra* Marandat 1991). Fragmentary lower molars of peradectids and herpetotheriids may be particularly difficult to distinguish in occlusal view. For example, a fragmentary lower molar from Fordones, lacking the paraconid and ascribed to the herpetotheriid *Pt. constans* (UM-FDN-18, Fig. 7d; Marandat 1991: p. 68) exhibits a curved lingual edge of the talonid with a relatively labiolingually wide hypoconulid, which may be superficially evocative of peradectids. If the metaconid and entoconid apex are considered aligned as on, for example, MNHN.F.Me16101 (Fig. 7i), the lingual edge of the talonid appears straight between the entoconid and metaconid (i.e., not fully curved) on UM-FDN-18, and its hypoconid is distolabial instead of labial or mesiolabial to its entoconid. In labial and lingual views, the entoconid is relatively higher and the entoconid – hypoconulid notch is deeper than in m2 of *Pd. crocheti* sp. nov. (Figs. 6, 7) and some m2 of *Pd. protinnominatus* (Gingerich and Smith 2006: fig. 26A-C). The postcingulid is also less convex than on figured peradectid m2 on which this cingulid is entirely preserved. These subtle differences probably led to confusion

Table 6 Summary of the main morphological differences between cheek teeth of ascertained late Paleocene – middle Eocene Peradectidae and Eocene Herpetotheriidae (and *Herpetotherium fugax*), deduced from comparisons of peradectid material described in this study. The character states in bold are documented absent in one or more species of the concerned group. Comparative data for *Herpetotherium fugax*: Korth (1994: fig. 8.1) for lower premolars, cast of AMNH 5254 (holotype) and Korth (2018: fig. 6b) for lower molars, Sánchez-Villagra et al. (2007: fig. 1c; *Herpetotherium* cf. *fugax*) for upper premolars, e.g., Green and Martin (1976: fig. 2), Fox (1983) and Korth (2018: fig. 6a) for upper molars.

	late Paleocene – middle Eocene Peradectidae	Eocene Herpetotheriidae + *Herpetotherium fugax*
Lower premolars		
Shape of mesial edge in labial or lingual view	curved	V-shaped, at least on one locus
Shape of roots	curved	straight
Upper premolars (P2-P3)		
Distal crista and accessory cusp configuration	**separated by a notch**	highly connected
Lower molars		
Preprotocristid shape on m1-3	fully convex	almost vertical
Metaconid most frequent position	**distolingual to protoconid**	almost strictly lingual to protoconid
Lingual opening of trigonid basin on m2	higher than metaconid-entoconid notch	as high as metaconid-entoconid notch
Entoconid vs hypoconid height in distal view	subequal	entoconid higher
Hypoconid position compared to entoconid on m2 or m3	mesiolabial to labial	labial to distolabial
Lingual edge of talonid on m2 or m3	curved, with oblique entoconid	straight, without oblique entoconid
Postcingulid lingual shape on m1-3	**attenuates labially to the hypoconulid**	**extends lingually towards hypoconulid tip**
Upper molars		
Protocone relative height on M1-M3	lower than paracone	subequal to higher than paracone
Conules relative size and structure	small, with rare internal cristae	larger, with frequent internal cristae
Paracone and metacone shape	conical, convex labial edge	triangular, flat labial edge
Centrocrista	rectilinear	strongly ‘v’-shaped
Doubling of stylar cusp C or D	**rare**	**frequent**
Stylar cusp D position on M1	**distolabial to metacone**	labial or mesiolabial to metacone
Ectoflexus on M4	present and deep	absent or weak

with herpetotheriids. As a matter of fact, the difficulty in differentiating early peradectids from early herpetotheriids, based on lower molars with subtle differences, has often been pointed out (Johanson 1996: p. 1030; Williamson and Lofgren 2014; but see Rose et al. [2012: p. 17] for an opposing view). In an attempt to overcome this issue, we summarize here (Table 6) the morphological differences between the cheek teeth of European Peradectidae and Herpetotheriidae, deduced from our comparisons of the peradectid material here described. Among the late Paleocene – Eocene peradectids, *Pd. crocheti* sp. nov. displays a combination of both derived features, mainly on upper molars, and primitive features, mostly but not exclusively on lower molars.

Intra-European paleobiogeographic and biostratigraphic implications. A biotic provincialism between northwestern European (Anglo-Belgian and Paris Basins) and southwestern European (south of France and Iberian Peninsula) mammal faunas was proposed based on occurrences of most of the eutherian taxa around the reference level ~MP7 (Marandat 1997; Smith 2000; Solé et al. 2011, 2013, 2018; Marandat et al. 2012). Exceptions are limited to two cases when considering only recent taxonomic revisions. The teeth of the artiodactyl *Diacodexis* from Dormaal (Belgium) and Palette (Provence) show strong similarities (Boivin et al. 2018), and the three plesiadapiform species *Arcius fuscus* Russell, Louis & Savage, 1967, *Arcius lapparenti* Russell, Louis & Savage, 1967, and *Arcius zbyszewskii* Estravís, 2000, have been documented in several deposits in northwestern and southwestern Europe (e.g., López-Torres and Silcox 2018). As for metatherians, *Peradectes crocheti* is newly recorded from localities closer in age to MP7 than to MP8+9, which are located in both northwestern Europe (Abbey Wood, Croydon, Meudon, Soissons and Sotteville-sur-Mer) and southwestern Europe (Fordones and Palette) (Fig. 1a). The herpetotheriid *Peratherium constans* also probably did not follow this dispersal pattern if both earliest Eocene (MP7) and MP7-MP8+9 interval occurrences are considered (Godinot et al. 1987; Marandat 1991; Estravís 2000; Ladevèze et

al. 2012). *Amphiperatherium* cf. *maximum*, smaller than the typical MP8+9 and ~MP8+9 species *A. maximum* (Crochet 1979, 1980b), is also found in the MP7-MP8+9 interval localities of Soissons in the northwestern European province (Louis 1996) and Fournes and Rians in the southwestern European province (Godinot 1981; Marandat 1991). Whether the northern form from Soissons represents the same species as the southern form from Fournes and Rians has yet to be thoroughly tested. Note that *Amphiperatherium* cf. *maximum* represents one of the earliest occurrences of *Amphiperatherium* since *A. brabantense* Crochet, 1979 (Dormaal), was synonymized with *Pt. constans* (Ladevèze et al. 2012). Altogether, the definition of *Pd. crocheti* sp. nov. reveals that none of the earliest species of the three metatherian genera present in Europe from the MP7 reference level to slightly after (*Peradectes crocheti* sp. nov. in Peradectidae, *Peratherium constans*, and *Amphiperatherium* cf. *maximum*, if indeed a single species, in Herpetotheriidae) seems to be affected by biotic provincialism, a conclusion challenging the bioprovinces scheme of Marandat et al. (2012), at least for metatherian mammals. Three herpetotheriid species have recently been demonstrated to be widespread between western and southeastern European assemblages, as early as the latest Eocene based on the occurrences of *Amphiperatherium exile* (Gervais, 1848-1852), contrary to coeval rodents which are mainly represented by distinct species from these two parts of Europe (Wessels et al. 2024). This reinforces the originality of the dispersal patterns of Laurasian metatherians compared to most coeval eutherians, as supported here.

Peradectes crocheti sp. nov. is the only peradectid documented in the MP7-MP8+9 localities where the family is present. It is unrecorded from younger localities from the Paris Basin (MP8+9 and ~MP8+9) that yielded exclusively *Pd. louisi* and *Pd. russelli*, the last occurrences of *Pd. crocheti* sp. nov. being from Fournes and Rians, after the ETM2 (see Material and methods). This documents the first well-supported species turnover for an early European metatherian lineage during the early Ypresian, as it is known at the same period for some

eutherian groups, but at the generic level (e.g., Solé 2014: fig. 3; Solé et al. 2018: table 10; Bronnert and Métais 2023: table 1). This peradectid species turnover is characterized, among other morphological characters, by a clear decrease of the mean absolute basal height of stylar cusp C relative to the mean absolute basal height of stylar cusp D during the early to middle early Eocene (MP7-MP8+9 interval to ~MP8+9) (Fig. 14).

Phylogenetic relationships between late Paleocene – middle Eocene peradectids

Origin and endemism of European peradectids. An apparent lack of support for the monophyly of European peradectids has been a consequence of previous studies regarding their taxonomic status (Crochet 1980b; Smith and Smith 2013). Crochet (1980b: p. 54, fig. 33), based on the morphology of upper molars only, suggested stronger affinities between *Peradectes elegans*, *Pd. louisi* and *Pd. russelli* on the one hand, and between *Pd. protinnominatus* and *Pd. 'mutigniensis'* on the other hand. The conclusions of Crochet (1980b) hence involved at least two independent peradectid dispersals of unspecified direction between North America and Europe. Smith and Smith (2013) described a new peradectid species from Egem (Belgium, ~MP8+9, 51-52 Ma, during the Early Eocene Climatic Optimum [EECO]) attributed to the North American genus *Armintodelphys* ('*Arm.*' *dufraingi*), and thus argued for an *Armintodelphys* dispersal from North America to Europe around the Early Eocene Climatic Optimum. However, most of our phylogenetic analyses have recovered the four European species *Pd. crocheti* sp. nov., *Pd. louisi*, *Pd. russelli* and '*Arm.*' *dufraingi* forming a clade nested within other late Paleocene to middle Eocene peradectids, with *Pd. crocheti* sp. nov. as the earliest diverging species (Fig. 16). Even in the less resolved third analysis, '*Arm.*' *dufraingi* forms a clade with *Pd. louisi* and *Pd. russelli*, rather than being included in the North American *Armintodelphys* clade. These results suggest that *Armintodelphys* did not disperse between

North America and Europe (*contra* Smith and Smith 2013), and that late Paleocene to Eocene peradectids have experienced a unique dispersal from North America to Europe during their evolutionary history (*contra* Crochet 1980b; Smith and Smith 2013). These conclusions imply that European peradectids certainly evolved as an endemic group until their extinction on this continent (the putative South American record of *Armintodelphys* compared with '*Arm.*' *dufraingi* [see Carneiro and Oliveira 2023: p. 37-38, fig. 15] has been reinterpreted as a putative herpetotheriid taxon; Carneiro et al. 2024), as European herpetotheriids probably also did (Ladevèze et al. 2012, 2020), at least until the middle early Eocene (MP8+9 or close in age, to MP8+9-MP10 interval). New dental material of late early Eocene (MP10 to MP11 reference levels) peradectids is further needed to definitely verify this hypothesis, because paleobiogeographic analyses of nyctitheriids show that dispersal events of small mammals from North America to Europe may have occurred multiple times and later than the middle early Eocene (Manz and Bloch 2015: p. 27-28, fig. 7).

The dispersal of peradectids perhaps occurred later than the arrival of herpetotheriid metatherians in Europe from North America, so far envisioned during the Paleocene-Eocene Thermal Maximum (PETM) for the latter, because peradectids are still unknown in the MP7 localities of Erquelinnes (Missiaen et al. 2013), Dormaal (Ladevèze et al. 2012), Le Quesnoy (Nel et al. 1999; pers. obs.) and Silveirinha (Estravis 2000), the last three having yielded the earliest herpetotheriid metatherians of Europe to date. According to the known fossil record, a putative dispersal event including peradectids by the Thulean route (a land bridge connecting North America and Europe via Greenland; Brikiatis 2014), probably followed (and was triggered by) the PETM, and took place between the PETM and ETM2, as has been established so far for paromomyid plesiadapiforms and the mesonychid *Pachyaena* (Fig. 16; Smith et al. 2011; Hooker 2015; Solé et al. 2018: p. 31). The finding of a peradectid astragalus in Palette (Fig. 8), with a nearly ungrooved trochlea (Fig. 8b) and a sloping medial tibial facet (Fig. 8d)

suggesting tibioastragalar mobility (Rose 2012), shows that the first European peradectids were probably already arboreally adapted, like their small (the body mass of *Pd. crocheti* is estimated between approximately 26-30 g, using the lengths of the four available unworn M3 [Online Resource 1: Table S1] in the appropriate predictive equation of Gordon [2003: fig. 7]), similarly sized, contemporaneous North American counterparts during the late Paleocene – early Eocene (Szalay 1994; Rose 2012), and like possible peradectid specimens from Messel (Kurz 2005). The Palette astragalus is very similar to astragali of small earliest Eocene North American peradectids (Rose et al. 2012), which provide further support to the close phylogenetic affinities between North American and European peradectids. A dispersal of peradectids from North America to Europe during the PETM or slightly later is also congruent with our phylogenetic framework, since the earliest offshoots of the European and strictly Eocene North American peradectid clades, namely *Pd. crocheti* sp. nov. and *M. labrus* respectively, together with the more basal *Pd. protinnominatus*, are recovered from early Eocene localities of similar age (Fig. 16). In particular, *Pd. crocheti* sp. nov. and *M. labrus* are not formally documented earlier than the early Eocene (Fig. 16; but see Rose 1981: p. 36), which supports the occurrence of a global cladogenesis event during or immediately after, and thus potentially driven by, the PETM in the evolutionary history of peradectids.

Definitions of *Peradectes, Armintodelphys,* and Peradectidae. The intrafamilial phylogenetic analysis highlighted disentangles relationships between all late Paleocene – middle Eocene peradectids. First, we concur with Williamson et al. (2012, 2014) in evidencing a lack of support for the monophyly of the genus *Peradectes*. It was recovered as polyphyletic in their phylogenetic analyses, including all valid North American *Peradectes* species, whereas it is paraphyletic in the analysis here performed, which does not include the earliest North American *Peradectes* species (early Paleocene, Danian), *Pd. minor* and *Pd. coprexeches* (Clemens 2006; Williamson and Taylor 2011; Williamson et al. 2012). The paraphyletic status of *Peradectes*,

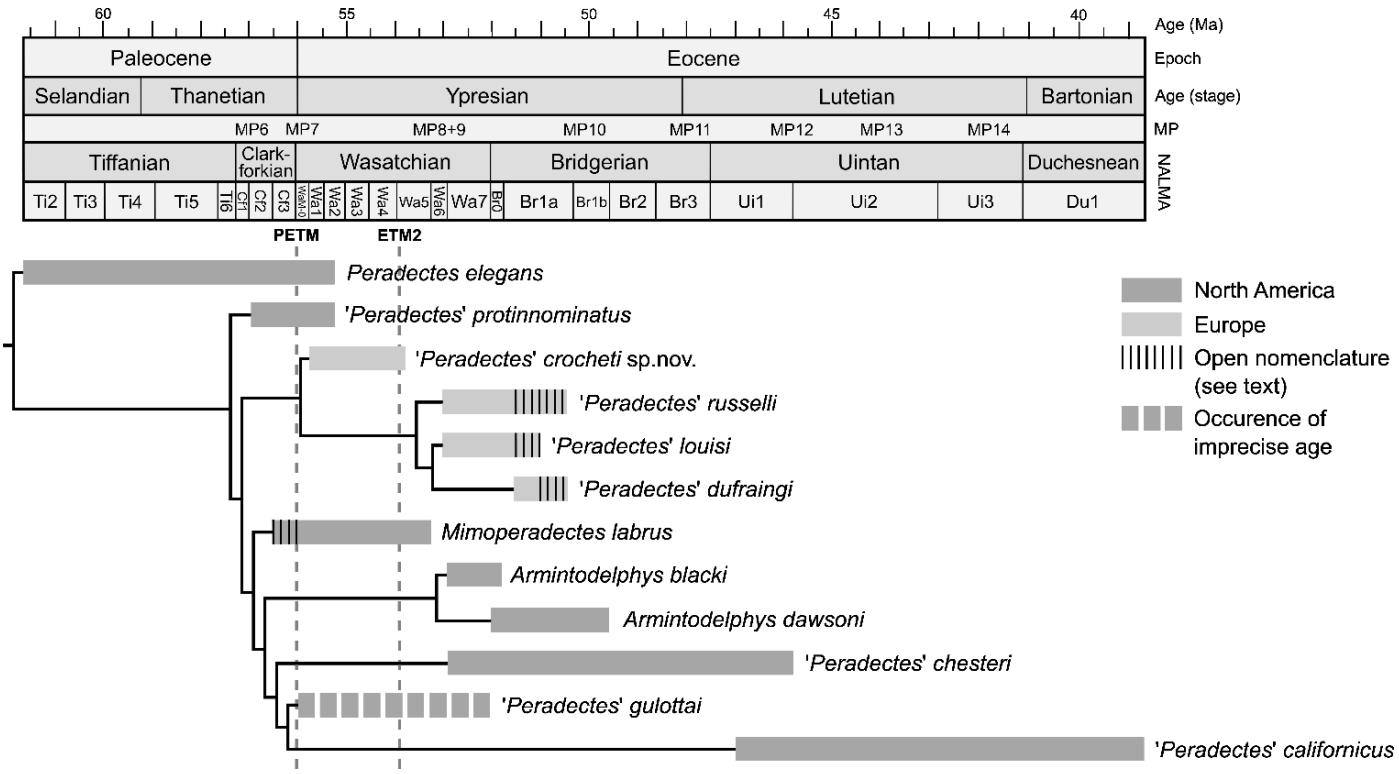

Fig. 16 Favored topology of the peradectid ingroup, recovered from four out of the five analyses, mapped on the Paleogene time scale (Speijer et al. 2020) and with the geographic distribution of species and selected thermal maxima of the early Eocene (PETM and ETM2). The European peradectid clade probably differentiated immediately after the PETM. *Peradectes* appears paraphyletic with the generic attributions here retained. Temporal extensions of taxa are detailed in Online Resource 2.

the genus being here valid if monospecific (i.e., restricted to *Pd. elegans*) or alternatively if it includes the species of the genera *Mimoperadectes* and *Armintodelphys* (and potentially *Didelphidectes* and *Nanodelphys*, which have not been included in our analyses), has long been suggested by an early diagram of the probable relationships between peradectid species (Krishtalka and Stucky 1983b: fig. 6), in the same way as in the topology obtained from most of our analyses. Second, Williamson et al. (2012: p. 629) proposed a phylogenetic definition of Peradectidae, as 'the most inclusive clade containing *Peradectes elegans*, but not *Herpetotherium fugax*, *Pediomys elegans* or *Didelphis virginiana*'. Contrary to the

phylogenetic analyses of Williamson et al. (2012, 2014), our topology recovering only relationships among peradectids is fully resolved, and *Peradectes elegans* and *Pd. californicus* (which form the clade Peradectidae in Williamson et al. [2012, 2014], according to the definition of Williamson et al. [2012]) are not found as sister taxa. This implies that a Peradectidae clade as originally conceived (e.g., Krishtalka and Stucky 1983b: fig. 6) or similar to that recovered in this study (Fig. 16), more inclusive than *Pd. elegans* + *Pd. californicus* as found by Williamson et al. (2012, 2014), could effectively exist, as Williamson et al. (2012: p. 632) suggested themselves. For these reasons, a broader phylogenetic analysis encompassing all *Peradectes* species nested in the whole Metatheria will be needed, but it is beyond the scope of this paper. Pending further study, we take a conservative and convenient approach in maintaining the use of the genus name *Peradectes*, even for European species. This encompasses '*Arm.*' *dufraingi*, here rereferred to *Peradectes* (*Pd. dufraingi*; see below).

Armintodelphys appears polyphyletic if the species *dufraingi* is included, but is monophyletic when this European species is not considered (as in Williamson et al. [2012, 2014]), or not included in the genus (this study). The lower molars of *Pd. dufraingi* and *Pd. louisi* are relatively more elongated than any late Paleocene to middle Eocene peradectid, *Armintodelphys* included (L/W of m3 > 1.75, see Table 4 for *Pd. louisi*), and the two European species share a labial emargination of lower molars that is absent in m3 of *Arm. blacki* and *Arm. dawsoni* (pers. obs., *contra* Krishtalka and Stucky 1983a). A relatively minute entoconid, lower than the hypoconulid on molar loci more anterior than m4, that has been proposed as a diagnostic character of *Armintodelphys* (Krishtalka and Stucky 1983a), is not only present in the *Armintodelphys* species and *Pd. dufraingi*, but also in other Eocene peradectids such as *Mimoperadectes labrus* (Bown and Rose 1979: fig. 1B; Rose et al. 2012: fig. 12H), *Pd. californicus* (Lillegraven 1976: pl. 9, fig. 2b) and *Didelphidectes* (Korth 1994). In turn, the characters here supporting the monophyly of North American *Armintodelphys* were not

mentioned in the diagnosis of the genus by Krishtalka and Stucky (1983a). The morphological similarities pointed out between *Pd. louisi* and *Pd. dufraingi*, in addition to the subtle differences of their lower molars (see diagnosis of *Pd. louisi*), do not justify assigning the species *Pd. dufraingi* to a genus other than that of the species *Pd. louisi* (hence *Peradectes*).

Limits of phylogenetics analyses. A caveat is in order on the phylogenetic analyses of peradectids, which are only based on dental characters due to the current lack of cranial and postcranial material for the group. Past research has shown that the dominance of dental characters in matrices may lead to inaccurate phylogenies, potentially due to higher levels of homoplasy in this anatomical partition (Sansom et al. 2017; Brocklehurst and Benevento 2020). The high homoplasy levels detected in our analyses (RI~0.5) do not contradict these cautionary statements. In addition, small cusps were mentioned to be possibly poorly reliable for reconstructing phylogenies due to their late occurrence in the patterning cascade of cusp development (Jernvall and Jung 2000). Whether this can apply to the stylar cusps present on upper molars of peradectids remains to be investigated, but our observations in the present study are suggestive of the presence of some phylogenetic signal in the subtle variation of these structures, for their relative position (representing 3 out of 37 characters used in the phylogenetic analyses), length and width (1 out of 37 characters), and height (1 out of 37 characters). In particular, the two methods employed to evaluate the relative height of the stylar cusps C and D produced an identical main result (the relative shrinking of the stylar cusp C between the MP7-MP8+9 interval and ~MP8+9). Meanwhile, the difficulty of accurately scoring complex dental variation (e.g., Billet and Bardin 2019) and the presence of high levels of homoplasy urge caution when interpreting current phylogenetic results on peradectids. The discovery of more complete fossils (like the material from Palette), and the use of geometric morphometric methods to characterize dental variation within peradectids, would allow to propose more robust characters in further studies.

Diagnostic characters and taxonomic status of the middle early Eocene European peradectids, *Peradectes louisi* and *Peradectes russelli*.

Systematics of *Peradectes louisi*. Crochet (1979) chose the left M3 MNHN.F.GL197 as the holotype of *Pd. louisi*, which was then the sole available M3 for this species (Crochet 1980b). An isolated M3 from Avenay (MNHN.F.Av4813) was referred to *Pd. louisi* earlier in his work (Crochet 1980b: fig. 4a) but was not included in the material referred to this species (Crochet 1980b: table 3). MNHN.F.Av4813 is of the size of the larger *Pd. russelli*, and is here allocated to this species. The original diagnostic characters of the upper molars of *Pd. louisi* were thus explicitly based on MNHN.F.GL197 alone (Crochet 1979, 1980b: p. 39). We have proposed a new description and figuration of the holotype (Fig. 9f). On a drawing of MNHN.F.GL197 in labial view from Crochet (1980b: fig. 9a), the stylar cusps B, C and D are subequal in height. Contrary to the original diagnosis and figure of Crochet (1980b), and although the stylar shelf of this M3 is worn, its stylar cusp B is clearly dominant in height over stylar cusp D, and stylar cusp C is absent or entirely worn (Fig. 9e-g). The slightly elevated surface interpreted as the summit of stylar cusp C of MNHN.F.GL197 by Crochet (1980b) is actually lingual to the stylar line. Moreover, the M3 of *Pd. louisi* MNHN.F.CB4182 also lacks stylar cusp C (Fig. 10p). The relative heights of the stylar cusps of MNHN.F.GL197 are similar on all the upper molars here attributed to *Pd. louisi* (Fig. 10), stylar cusp B being the highest, and stylar cusp C being most often lower than stylar cusp D or absent. As mentioned by Crochet (1979) in the diagnosis, the ectoflexus of MNHN.F.GL197 is weakly developed, but the newly reported M3 of *Pd. louisi* from Condé-en-Brie (MNHN.F.CB4182, Fig. 10p) and Sézanne-Broyes (MNHN.F.SZ18000, MNHN.F.SZ18005, Fig. 10o) have deeper ectoflexi. A similar variation of this trait is here noted on the M3 of *Pd. crocheti* sp. nov. from Palette and Fordones. The ectoflexus was also considered symmetric on M3 of *Pd. louisi* (Crochet 1979, 1980b). Here again, the new

description of the holotype and a more comprehensive sampling of M3, all properly oriented, show that the ectoflexus of this dental locus is asymmetric in *Pd. louisi* (Figs. 9f, 10p, o), although this asymmetry is, on average, less pronounced than in *Pd. crocheti* sp. nov. The relative weakness of the conules of the upper molars described by Crochet (1979, 1980b) was interpreted as a synapomorphy of peradectids by various authors (e.g., Krishtalka and Stucky 1983b; Korth 2008), rather than a diagnostic character at the species level. Finally, the M3 is not relatively longer than other upper molar loci of *Pd. louisi*, or M3 of other European *Peradectes* species (Table 4) (*contra* Crochet 1979, 1980b).

As for lower molars, a lingual opening of the trigonid basin higher than the lingual opening of the talonid basin was also proposed as a specific feature of *Pd. louisi* (Crochet 1979, 1980b). However, this character is also present in *Pd. crocheti* sp. nov. and *Pd. russelli*, and consequently the relative heights of the lingual opening of the trigonid versus talonid basin cannot be used to discriminate between European *Peradectes* species. Moreover, since only (at least) some ascertained herpetotheriids (i.e., from the earliest Eocene; Ladevèze et al. 2012), such as *Peratherium* and *Herpetotherium*, exhibit the reverse condition of this character (the trigonid and talonid basin open lingually at the same level), the character state of *Pd. louisi* is rather interpreted as a symplesiomorphy for the whole of Metatheria. According to Crochet (1979, 1980b), the hypoconid is mesiodistally pinched and the cristid obliqua is curved on the lower molars of *Pd. louisi*, except on m4. Nonetheless, we did not make the same observation based on the two m4 from the original hypodigm we consulted (MNHN.F.Av16032 and MNHN.F.Av16037). In particular, on MNHN.F.Av16037 the cristid obliqua is curved near the distal edge of the trigonid contrary to the drawing of Crochet (1980b: fig. 13). Characters of the talonid of m4 of *Pd. louisi* are probably highly impacted by polymorphism, as for m4 of other metatherians (e.g., Martin 2005: fig. 4). Moreover, the shape of the cristid obliqua varies among the m3 of *Pd. louisi*. Finally, as noted by Crochet (1979, 1980b), the m4 of *Pd. louisi* are smaller

than the m3, but the new report of m4 of *Pd. crocheti* sp. nov. and *Pd. russelli* in the present study shows that it is the same for these species. Altogether, none of the characters proposed by Crochet (1979, 1980b) are diagnostic of *Pd. louisi*; they are either actually not observed on the material, or are plesiomorphies. However, *Peradectes louisi* is definitely distinct from all other peradectid species in combining a stylar cusp D located distolabially to the metacone on the stylar shelf of M3, a stylar cusp C relatively lower than the stylar cusp D on M1-M3, and relatively long m3 with subequal entoconid and hypoconulid.

With the exception of the peradectid M2 from Coulondres (Southern France, ~MP10; UM-CLR-1; Crochet 1980b: fig. 28), the m1 MNHN.F.CB3021 here referred to *Pd. russelli* (interpreted as a dp3 by Crochet 1980b), and one possible m4 not found in collections (see Crochet 1980b: p. 49, bottom), all molars attributed to *Peradectes* sp. (Crochet 1980b: p. 49-51, figs. 26-27, 29) are here better allocated to *Pd. louisi*. According to Crochet (1980b: p. 49), two worn and fragmentary lower molar rows (MNHN.F.Av4642 and MNHN.F.CB226, Figs. 11i-j) differ from *Pd. louisi* in having a talonid with a rectilinear lingual edge and a hypoconulid more lingually positioned, hence characters for which a lingual axis of reference is needed to relatively locate structures. However, on both specimens the metaconid is totally worn (MNHN.F.Av4642, Fig. 11i) or incomplete (MNHN.F.CB226, Fig. 11j) on m3, the best preserved molar of each row, which probably prevented Crochet (1980b: fig. 29b) from describing them with an accurate orientation. With a corrected orientation, these specimens resemble *Pd. louisi*, with a subequal entoconid and hypoconulid on a relatively long m3. The differences in shape of the entoconid and cristid obliqua pointed out by Crochet (1980b) have been shown here to be typical variable traits of *Pd. louisi* (Fig. 11). All differences noted by Crochet (1980b) between upper molars of *Peradectes* sp. and *Pd. louisi*, such as the doubling of stylar cusp C on one specimen (Crochet 1980b: fig. 27), or the small size of stylar cusp D (Fig. 10i-j) are here interpreted as variable features of *Pd. louisi*. In fact, the doubling of stylar

cusp C is known to be as rare in other *Peradectes* species with various upper molars described, namely *Pd. coprexeches* (Williamson and Taylor 2011: p. 13, fig. 6.2) and *Pd. crocheti* sp. nov. (a single specimen concerned; this study). Note that the doubling of stylar cusp C is probably more frequent in *Mimoperadectes* (see Comparative description of *Pd. crocheti* sp. nov.), and in the oldest *Peradectes* species, *Pd. minor* (Clemens 2006: p. 28), than in other peradectid species.

Larger European peradectids, *Peradectes russelli* versus *Peradectes 'mutigniensis'*. Based on their original diagnoses (Crochet 1979) and comparisons (Crochet 1980b: p. 52), *Pd. russelli* and *Pd. 'mutigniensis'* would appear to differ in possessing (i) M3 relatively wider for *Pd. 'mutigniensis'* (i.e., with a mesiodistally shorter centrocrista and ectoflexus), (ii) M3 with a symmetric versus asymmetric ectoflexus, (iii) a lingual opening of the trigonid basin higher versus not higher than the lingual opening of the talonid basin (metaconid-entoconid notch) on lower molars and (iv) a less curved cristid obliqua on m2 and m3 of *Pd. 'mutigniensis'*. We disagree with these four arguments. First, the length to width ratio here calculated for M3 reported by Crochet (1980b) to both species are similar (Online Resource 1: Table S3). In particular this ratio is almost identical for the M3 of the holotype of *Pd. russelli* (MNHN.F.CB924, L/W = 0.79) and the 'holotype' of *Pd. 'mutigniensis'* (MNHN.F.Mu5521, L/W = 0.78). Second, the ectoflexus of the M3 of the holotype of *Pd. russelli* and all specimens originally attributed to this species is asymmetric, with a metastylar wing more labially expanded, when the paracone and metacone are aligned (e.g., MNHN.F.CB2502, Fig. 12h). Third, as in all peradectids, the trigonid basin of lower molars of *Pd. 'mutigniensis'* actually opens higher lingually than the talonid basin (e.g., MNHN.F.Mu18000, Fig. 12m). Fourth, although the single m3 of *Pd. 'mutigniensis'* has effectively a weakly curved cristid obliqua (MNHN.F.Mu6451; Crochet 1980b: fig. 24), a variation in the curvature of this cristid has been noted in the coeval *Pd. louisi*. It is worth mentioning that molars originally attributed to *Pd.*

russelli are slightly larger or subequal in size to those of *Pd. 'mutigniensis'* (Online Resource 1: Table S3), with one exception (the M3 MNHN.F.CB742 of *Pd. 'mutigniensis'* is larger than the M3 MNHN.F.Av4813 of *Pd. russelli sensu* Crochet [1980b]). Altogether, all characters proposed by Crochet (1979, 1980b) to distinguish *Pd. russelli* from *Pd. 'mutigniensis'* either are not observed on the concerned specimens or represent intraspecific morphological variation. The species name *Peradectes russelli* has page priority and is thus valid over its junior synonym *Pd. 'mutigniensis'* (see Crochet 1979: p. 367-368). Morphological variation found in molars of *Pd. russelli* are here documented, as for other European *Peradectes* species. Notably, some M1 to M3 of *Pd. russelli* have a transverse accessory crista on their stylar shelf, lingual to stylar cusp D (see Comparative description of *Pd. russelli*). This reminds the recent observation of transverse cristae variably present between the metacone and stylar cusp D in various herpetotheriid species (Wessels et al. 2024: p. 15, figs. 3h-j, 6a).

Crochet (1980b: p. 52, tables 4-5) argued that m4 of *Pd. russelli* and *Pd. 'mutigniensis'* are larger than m3. Among the collections of the MNHN, two specimens interpreted as m4 of *Pd. russelli* by Crochet (1980b: table 4) were found, namely MNHN.F.CB5114 from Condé-en-Brie and MNHN.F.Av9019 from Avenay. However, the lingual edge of their talonid is straight, and their talonid is relatively mesiodistally longer than in ascertained European metatherian m4. MNHN.F.CB5114 also exhibits as high protoconid and metaconid. MNHN.F.CB5114 and MNHN.F.Av9019 are most likely respectively m2 and m3 of an eutherian mammal taxon that lacks the paraconid keel of metatherians. We did not find the figured m4 specimen of *Pd. russelli* (Crochet 1980b: fig. 18) in the collections, but it is more similar to a herpetotheriid than to a peradectid metatherian considering characters such as the lingual alignment of the paraconid, metaconid and entoconid with a straight distolingual edge of the talonid, the transversally aligned protoconid and metaconid, and the mesiodistally long entoconid (Table 6). The two specimens reported as m4 of *Pd. 'mutigniensis'* by Crochet (1980b: table 5, fig.

25), MNHN.F.CB5100 and MNHN.F.GL92, lack the relative labiolingual reduction of the talonid compared to the other lower molar loci, which is a characteristic of m4 of most marsupialiforms. MNHN.F.CB5100 and MNHN.F.GL92 are here better interpreted as m2 of *Pd. russelli*, given the relative width of their trigonid and talonid. The single true isolated m4 of *Pd. russelli* is the newly reported MNHN.F.Mu18003 (Fig. 12u-v), which is subequal in length and shorter, respectively, than the two ascertained m3 of *Pd. russelli*.

Paleoecological and biostratigraphic implications. *Peradectes louisi* and *Pd. russelli* are coeval and are the only two peradectid species in MP8+9 and ~MP8+9 localities from the Paris Basin (Avenay, Condé-en-Brie, Mutigny, Sables de Brasles and Sézanne-Broyes), while Crochet (1980b) recognized up to four *Peradectes* species (*Pd. louisi*, *Pd. russelli*, *Pd. 'mutigniensis'* and *Peradectes* sp.) in Avenay and Condé-en-Brie. *Peradectes louisi* and *Pd. russelli* represent two distinct species that differ in a few morphological characters in addition to size difference, namely in the proportions of their lower molars (Table 5), and in two discrete features, namely the relative positioning of stylar cusp D on M3, and the relative ventral extension of stylar cusps C and D on M1 and M2 (Fig. 10 vs Fig. 12). Because the area of stylar cusps C and D is known to have minor functional importance during molar occlusion (e.g., Crompton and Hiiemae 1970: fig. 5A; Crochet 1980a: fig. 2a; Davis 2011: fig. 1B; Wessels et al. 2024: p. 15, fig. 8b) and because *Pd. louisi* and *Pd. russelli* group into two distinct size clusters (Fig. 13), these two species could probably partition their ecological niches (hypothetical arboreal and insectivorous to frugivorous small mammals, as partly deduced from the peradectid-like taxon from Messel; Kurz 2005) mostly based on size (body masses estimated to 22.9 – 31.4 g for *Pd. louisi*, and 41.2 – 60.6 g for *Pd. russelli*, using lengths of the unworn M3 [Online Resource 1: Tables S2-S3] in the appropriate predictive equation of Gordon [2003: fig. 7]). Similar cases of sympatry in the MP8+9 and ~MP8+9 mammal faunas studied, between two morphologically similar species that differ in size, concern other taxa, such as

(among recent revisions) the plesiadapiform *Arcius*, because *Arc. fuscus* and the larger *Arc. lapparenti* co-occur in Mutigny, Avenay, Condé-en-Brie, Sables de Brasles, and Sézanne-Broyes (López-Torres and Silcox 2018), and the theridomorph rodent *Euromys*, because *E. thaleri* (Michaux, 1964) and the larger *E. woodi* (Michaux, 1964) co-occur in Mutigny, Avenay and Condé-en-Brie (Escarguel 1999; Vianey-Liaud and Marivaux 2021). The coexistence of two peradectid species differing in size apparently continues during the EECO (~MP10; Vianey-Liaud et al. 2024).

European peradectid species larger than the small *Pd. crocheti* sp. nov. first occur in Mutigny (~MP8+9, PE IV), with *Pd. russelli*. The mammalian faunas of Mutigny and Avenay are considered to exhibit major differences based on two herpetotheriid lineages, still unrevised, following the conclusions of Crochet (1980b) (Schmidt-Kittler et al. 1987: p. 21), and also on the absence of *Pd. russelli sensu* Crochet (1980b) in Mutigny (Crochet 1980b: fig. 30). This diffence in faunal composition is here reduced because *Pd. russelli* is recorded in both localities, and molars of this species from Mutigny, such as M1, do not significantly differ in size from *Pd. russelli* of other MP8+9 and ~MP8+9 localities (Online Resource 1: Table S3).

Revision of putative occurrences of typical MP8+9 and ~MP8+9 peradectids in MP10 and ~MP10 faunas

Peradectes louisi was recorded in Grauves (MP10) by two isolated lower molars which were not described (Crochet 1980b: table 3). The right m1 MNHN.F.Gr10010 is completely worn. This specimen effectively displays a peradectid-like outline shape for a m1, with a trigonid much longer than the talonid, the hypoconid mesiolabial to the entoconid, the convex distolingual margin of the talonid, and the lingual opening of the trigonid basin higher than the talonid one (see Table 6). MNHN.F.Gr10010 (L = 1.56 mm, W = 0.79 mm) is similar in size to

lower molars of *Pd. louisi* and *Pd. dufraingi*. However, this is not sufficient to propose a specific allocation, in part because the m1 of the slightly smaller *Pd. dufraingi* is so far undocumented.

MNHN.F.GR10013 (Fig. 17b-c; L = 1.56 mm, W = 0.85 mm) was listed as a left m4 (Crochet 1980b). It is less worn than MNHN.F.GR10010, especially on the talonid. MNHN.F.GR10013 is more likely a m3, rather than a m2 or m4, given that its talonid is relatively not as wide as on m2 of peradectids and also unreduced compared to m4 of peradectids (Fig. 17b). The lingual margin of the talonid is less worn than the rest of the molar, and preserves a minute entoconid smaller than the hypoconulid (Fig. 17c). Contrary to all m3 of *Pd. louisi*, the entoconid is lower than the hypoconulid. This character is exclusively shared with *Pd. dufraingi*, from the Egem locality (Smith and Smith 2013: fig. 4B-G). Because MNHN.F.GR10013 differs from m3 of *Pd. dufraingi* only in being larger (but is as long and wide as m3 of *Pd. louisi*), and in its stronger postcingulid (also similar to *Pd. louisi* in this respect), we here tentatively attribute this peradectid m3 from Grauves to *Peradectes* aff. *dufraingi*. Regarding the exhibited features of this material, *Pd. louisi* is hence clearly absent from Grauves. If the attribution we propose is correct, and following the conclusion of Smith and Smith (2013: p. 308-309) on the age of the Egem locality, MNHN.F.GR10013 would represent a species close to *Pd. dufraingi*, occurring in the MP10 reference level (instead of ~MP8+9 for *Pd. dufraingi*), and a second peradectid species with a minute entoconid recorded around the EECO.

Peradectes louisi was also recorded in Cuis (~MP10; = Grauves?, see Material and methods) by Crochet (1980b: table 3), by an unlabeled right upper molar (Fig. 17a; L > 1.37 mm, W = 1.73 mm), the sole metatherian tooth from this locality, for which only a cast is available in the fossil collections of the MNHN. The specimen is completely worn on its main cusps, stylar cusps, and conules. The most distolabial part of the metastylar wing and stylar cusp A are broken. Given the depth and asymmetry of the ectoflexus of this specimen, and the length of the preparacrista, it is most likely a M2 as listed by Crochet (1980b). It is similar in size to both

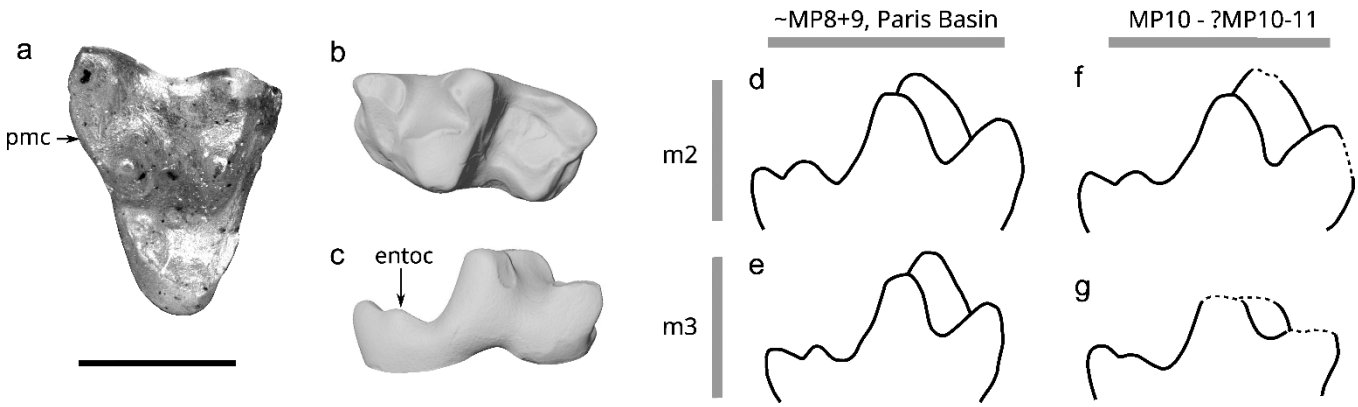

Fig. 17 Revision and comparisons of peradectid molars from MP10 and ?MP10-11 faunas. **a-c**. molars from the MP10 faunas of Cuis and Grauves (Paris Basin) attributed to *Peradectes louisi* by Crochet (1980b). **a**. cast of an unlabelled right M2 from Cuis in occlusal view. **b-c**. MNHN.F.GR10013, left m3 here attributed to *Peradectes* aff. *dufraingi*; **b**. occlusal view; **c**. lingual view. The arrows (**a** and **c**) denote character states discussed in the main text. **d-g**. comparisons of outline of lingual views of m2 and m3 from the MP10 and ?MP10-11 faunas to those of typical m2 and m3 from MP8+9 and ~MP8+9 faunas of the Paris Basin. Note differences in the relative height and length of the entoconid; **d**. right m2 (reversed) MNHN.F.CB878 (*Pd. louisi*); **e**. left m3 MNHN.F.CB4213 (*Pd. louisi*); **f**. left m2 UM-VIE-106 (?*Pd. mutigniensis* in Legendre et al. 1992); **g**. left m3 MNHN.F.GR10013. Abbreviations: **pmc**, postmetacrista; **entoc**, entoconid. All outlines are to scale. Scale bar equals 1 mm.

upper molars of *Pd. louisi* and *Peradectes* sp. from Azillanet (Minervois, southern France, ~MP10), the latter being limited to one M3 (Marandat 1986: pl. 1, fig. 2). The unworn M3 from Azillanet differs from all upper molars of *Pd. louisi* in having a slightly V-shaped centrocrista (distinct from the V-shaped centrocrista of herpetotheriids), as in *Peradectes* specimens in open nomenclature from the ~MP10 southern France localities of Coulondres and Mas de Gimel (UM-CLR-1 and UM-MGL-716; Crochet 1980b: fig. 28; Vianey-Liaud et al. 2024: fig. 2C), and in its more curved and distally projected postmetacrista relatively to the paracone – metacone axis. On the M2 from Cuis, the centrocrista is completely worn and cannot be described, but the postmetacrista is curved and distally projected (Fig. 17a), in the same way as for the M3 from Azillanet. The M2 from Cuis sharing this character with the unnamed species

from Azillanet and being highly worn on all cusps, the presence of *Pd. louisi* in Cuis is here no longer supported with confidence. Altogether, the revision of peradectids from Grauves and Cuis shows that *Pd. louisi* is most likely absent from the MP10 and ~MP10 localities where it was reported to date. The MP8+9-MP10 interval locality of Saint-Agnan yielded a possible *Pd. louisi* specimen here described as *Peradectes* cf. *louisi*. The occurrences of *Pd. louisi* are hence formally limited to MP8+9 and ~MP8+9 localities of the Paris Basin (Mutigny, Avenay, Condé-en-Brie, Sables-de-Brasles, and Sézanne-Broyes).

A fragment of a peradectid m4 from Mas de Gimel (~MP10; Montpellier, France) was attributed to *Peradectes* cf. *mutigniensis* (UM-MGL-320; Vianey-Liaud et al. 2024: fig. 2D). Based on the morphology of the mesiolingual part of the trigonid (the only well-preserved part of the molar) and the apparently labiolingually pinched talonid, UM-MGL-320 is similar in size and morphology, only to the m4 of *Pd. russelli* (MNHN.F.Mu18003, Fig. 12u), and is thus tentatively re-attributed to *Peradectes* cf. *russelli*. A lower molar belonging to a peradectid was reported from the Vielase fauna (?MP10-11, Quercy) as ?*Peradectes mutigniensis* (Legendre et al. 1992). This specimen (UM-VIE-106; L = 1.73 mm, W = 0.99 mm) is a m2, given the relative width of the talonid. It is comparable in size to the largest m2 of *Pd. louisi* (e.g., MNHN.F.CB5092; Online Resource 1: Table S2) rather than the m2 of *Pd. russelli* (= *Pd. 'mutigniensis'*), which are larger. The entoconid and hypoconulid of UM-VIE-106 are small, identical in height and mesiodistal length (Fig. 17f), whereas the entoconid is most often higher and always mesiodistally longer than the hypoconulid on all m2 of the MP8+9 and ~MP8+9 European peradectids (e.g., Fig. 17d). The m2 from Vielase thus might belong to a different unnamed peradectid species. The comparison with *Peradectes* aff. *dufraingi* from Grauves is difficult because the cuspids of the talonid are described only for the m3 of this taxon.

Altogether, the peradectid m2 from Vielase and m3 from Grauves here revised, both of which are late Ypresian in age, exhibit a configuration of the entoconid and hypoconulid that differs

from any peradectid molar of equivalent locus from the MP8+9 reference locality and ~MP8+9 localities of the Paris Basin, with a relatively less high entoconid (Fig. 17d-g). This may highlight a second species turnover among European peradectids, between middle early Eocene (MP8+9 or close in age) and late early Eocene (MP10 or close in age), although more dental material from MP10 and ~MP10 localities would be needed to update their tentative taxonomic status and confidently assess this hypothesis. To date, such low entoconids have been documented for *Peradectes dufraingi* (absent from the MP8+9 or localities close in age of the Paris Basin) from the Egem fauna, which would correlate with MP8+9 and the Early Eocene Climatic Optimum according to Smith and Smith (2013).

Peradectids are represented in southern France only in the MP7-MP8+9 interval localities that yielded *Pd. crocheti* sp. nov. and in MP10, ~MP10 and younger localities (Crochet 1977a, 1980b; Marandat 1986; Legendre et al. 1992). They are still unrecorded from southern France localities close in age to the MP8+9 of the Paris Basin, namely La Borie (= Saint-Papoul; Laurent et al. 2010) and Sainte-Eulalie (Danilo et al. 2013) probably due to the scarcity of small mammals in such localities. So far, only the ~MP8+9 locality of La Borie yielded an isolated lower molar of metatherian, belonging to a herpetotheriid (Crochet 1980b: p. 69).

Conclusion

European peradectids long remained less well documented than both the coeval North American peradectids and the also superficially 'opossum-like' Herpetotheriidae, in terms of spatial distribution and completeness of available fossil material. The fossils described here for the early peradectid *Peradectes crocheti* sp. nov., widespread in Western Europe and being represented by dental rows, enhance our knowledge of the ancestral morphotype of European peradectids, through accurate comparisons with the later occurring species *Pd. louisi* and *Pd.*

russelli, and the tentative characterization of morphological intraspecific variation. We encourage further quantification of characters based on isolated molars, because it may enable to decipher cryptic diagnostic features between coeval metatherian species (e.g., Table 5) or to support evidenced species turnover (e.g., Fig. 14) for a given lineage (e.g., Fig. 15). In the same way, the study of the relative heights of the stylar cusps of metatherian upper molars also appears meaningful to resolve systematics, at least for peradectids (Fig. 5 vs Fig. 10 vs Fig. 12).

Altogether, the evolution of peradectids in Europe appears simpler than suggested by previous studies. In fact, the newly recorded species turnovers between the early (MP7-MP8+9 interval), middle (MP8+9 and ~MP8+9) and late (MP10 and ~MP10) early Eocene (Figs. 14, 17) must have resulted from the endemic evolution of a European lineage, originating from an unique dispersal from North America to Europe possibly triggered by the PETM, which is consistent with the monophyly of European peradectids (Fig. 16), rather than from a more complicated evolutionary history punctuated by multiple dispersals. In turn and although the precise relationships between the late Paleocene – middle Eocene peradectids are here established, their complex taxonomy at the generic level is to be addressed. These conclusions regarding the evolutionary history of peradectids are derived from the definition of multiple relevant dental characters for the first time, which provide support for many peradectid clades. Such effort will be crucial for understanding the origin and phylogenetic affinities of peradectids in the whole of Marsupialiformes.

To date, the last putative European peradectids are known by three complete specimens from Messel (~MP11, ~47.2 to ~47.6 Ma for the Middle Messel Formation; Kaboth-Bahr et al. 2024) preserving the skeleton, skull and teeth rows, but still of unclear taxonomic status (Kurz and Habersetzer 2004; Kurz 2007; Beck et al. 2022: p. 315). Furthermore, peradectids are known by only eight isolated teeth regarding MP10 and ~MP10, and ?MP10-11 localities (Crochet 1980b; Marandat 1986; Legendre et al. 1992), which represent the youngest ascertained record

of this family in Europe so far. For these reasons, the last steps of the evolution of peradectids in Europe until their extinction, possibly after the MP11, remain blurry, awaiting for more fossil material to be described. This work is a prelude of the complete systematic revision of metatherians from the early Eocene of Europe.

Supplementary informations The online version contains supplementary material available at https://doi.org/10.1007/s10914-024-09724-5.

Acknowledgments This article is dedicated to the memory of Jean-Yves Crochet, who passed away on 21 October 2023. As a long time colleague of the Institut des Sciences de l'Evolution – Montpellier (ISEM) and friend, he greatly improved our knowledge of metatherian and insectivorous mammals. We are indebted to the Rougier family, owner of the Palette site, who kindly provided access, help and support for paleontological research on this locality. We acknowledge Y. Dutour and N. Vialle (Muséum d'Histoire Naturelle of Aix-en-Provence), Q. Vautrin (Parc Naturel Régional UNESCO Global Geopark Causses du Quercy), C. Bronnert and R. Vacant (MNHN), and E. Turini and L. Mohring for their precious help during these excavations. R. Vacant also carefully treated the sediments from Palette collected in 2018, that yielded the holotype of *Peradectes crocheti* sp. nov. We warmly thank A.-L. Charruault (ISEM), who performed the µ-CT-scanning and segmentation of this holotype specimen. V.N. Pernègre (MNHN) managed the allocation of various new MNHN specimen numbers. G. Escarguel (LENHA, Lyon) sampled the locality of Fournes 2. We are grateful to T. Smith and A. Folie (Royal Belgian Institute of Natural Sciences, Brussels) for access to comparative material and casts of the two specimens from Sotteville-sur-Mer here revised. We thank V.D. Crespo and an anonymous reviewer, as well as the editors R.M.D. Beck and D.A Croft, for their constructive remarks on an early version of the manuscript. This is ISEM publication n° 2024-118.

Author contributions KG and RT designed the study. KG prepared the figures and wrote the manuscript, which was completed by comments and feedbacks from GB, EG, MG, BM, SL and RT. Field expeditions in the Palette locality were conducted by GB, EG and RT. The peradectid specimens

labelled MHN.AIX.PV.2017- were isolated by KG after processing sediments. Data acquisition (including CT-scans) and analyses were performed by KG. All authors read and approved the final manuscript.

Funding This research was financially supported by a PhD thesis funding from the French Ministry of Higher Education, Research, and Innovation, and also in part by the ANR project EDENs (ANR-20-CE02-0007). Recent excavations at Palette were funded thanks to the Actions Transversales du Muséum (ATM Palette, MNHN funding). Three-dimensional data acquisition was performed using the micro-computed tomography (μ-CT) facilities of the MRI platform member of the national infrastructure France-BioImaging supported by the French National Research Agency (ANR-10-INBS-04, 'Investments for the future'), the labex CEMEB (ANR-10-LABX-0004) and NUMEV (ANR-10-LABX-0020). The Leica optical and digital station used to take photographs was acquired as part of the ANR-ERC PALASIAFRICA (ANR-08-JCJC-0017). A CC-BY public copyright license has been applied by the authors to the present document and will be applied to all subsequent versions up to the Author Accepted Manuscript arising from this submission, in accordance with the grant's open access conditions.

Data availability The 3D surface models of the most complete or informative specimens of *Peradectes crocheti* sp. nov. from Palette, namely the holotype (maxillary MHN.AIX.PV.2018.26.14), the P2 (MHN.AIX.PV.2017.6.6), a M3 (MHN.AIX.PV.2017.6.7), the two lower dental rows (MHN.AIX.PV.2017.6.8 and MHN.AIX.PV.2017.6.9), and the astragalus (MHN.AIX.PV.2017.6.14), are available on MorphoMuseuM. The other 3D surfaces and data are available upon request to the corresponding author. The character – taxon matrix used in the first phylogenetic analysis is available in MorphoBank (project 5399).

Competing interests The authors declare no competing interests.

References

Abello MA (2013) Analysis of dental homologies and phylogeny of Paucituberculata (Mammalia:

Marsupialia). Biol J Linn Soc 109:441-465. https://doi.org/10.1111/bij.12048

Averianov AO, Martin T, Lopatin AV, Krasnolutskii SA (2013) Stem therian mammal *Amphibetulimus* from the Middle Jurassic of Siberia. Paläontol Z 89:197–206. https://doi.org/10.1007/s12542-013-0217-x

Averianov AO (2015) Taxonomic revision of tribosphenic mammals from the Lower Cretaceous Antlers Formation of Texas and Oklahoma, USA. Proc Zool Inst RAS 319:141–181. https://doi.org/10.31610/trudyzin/2015.319.2.141

Beard KC, Dawson MR (2009) Early Wasatchian mammals of the Red Hot local fauna, uppermost Tuscahoma Formation, Lauderdale County, Mississippi. Ann Carnegie Mus 78:193–243. https://doi.org/10.2992/007.078.0301

Beck RMD (2023) Diversity and phylogeny of marsupials and their stem relatives (Metatheria). In: Cáceres NC, Dickman CR (eds) American and Australasian Marsupials. Springer, Cham, Switzerland, pp 23–88. https://doi.org/10.1007/978-3-031-08419-5_35

Beck RMD, Voss RS, Jansa SA (2022) Craniodental morphology and phylogeny of marsupials. Bull Am Mus Nat Hist 457:1-350. https://doi.org/10.1206/0003-0090.457.1.1

Billet G, Bardin J (2019) Serial homology and correlated characters in morphological phylogenetics: modeling the evolution of dental crests in placentals. Syst Biol 68:267–280. https://doi.org/10.1093/sysbio/syy071

BiochroM'97 (1997) Synthèse et tableaux de corrélation. In: Aguilar JP, Legendre S, Michaux J (eds) Actes du Congrès BiochroM'97, Mémoires et travaux de l'EPHE 21. Montpellier: Ecole Pratique des Hautes Etudes, Institut de Montpellier, pp 769–805.

Boivin M, Orliac MJ, Telles Antunes M, Godinot M, Laurent Y, Marandat B, Vidalenc D, Tabuce R (2018) New material of *Diacodexis* (Mammalia, Artiodactyla) from the early Eocene of Southern Europe. Geobios 51:285–306. https://doi.org/10.1016/j.geobios.2018.06.003

Bown TM (1979) Geology and mammalian paleontology of the Sand Creek Facies, lower Willwood Formation (lower Eocene), Washakie County, Wyoming. Geol Surv Wyo Mem 2:1–151.

Bown TM, Rose KD (1979) *Mimoperadectes*, a new marsupial, and *Worlandia*, a new dermopteran, from the lower part of the Willwood Formation (early Eocene), Bighorn Basin, Wyoming. Contr Mus Paleontol Univ Mich 25:89–104.

Bremer K (1994) Branch support and tree stability. Cladistics 10:295–304. https://doi.org/10.1111/j.1096-0031.1994.tb00179.x

Brikiatis L (2014) The De Geer, Thulean and Beringia routes: key concepts for understanding early Cenozoic biogeography. J Biogeogr 41:1036-1054. https://doi.org/10.1111/jbi.12310

Brocklehurst N, Benevento GL (2020) Dental characters used in phylogenetic analyses of mammals show higher rates of evolution, but not reduced independence. PeerJ 8:e8744. https://doi.org/10.7717/peerj.8744

Bronnert C, Métais G (2023) Early Eocene hippomorph perissodactyls (Mammalia) from the Paris Basin. Geodiversitas 45:277–326. https://doi.org/10.5252/geodiversitas2023v45a9

Carneiro LM, Oliveira ÉV (2023) Paleogene metatherians from the Itaboraí Basin: diversity and

affinities. In: Cáceres NC, Dickman CR (eds) American and Australasian Marsupials. Springer, Cham, Switzerland, pp 269–324. https://doi.org/10.1007/978-3-030-88800-8_5-1

Carneiro LM, Goin FJ, Bampi H, Silva RC, Rangel CC, Guimarães BMG, Arêas MR (2024) A tiny-sized Herpetotheriidae (Mammalia, Metatheria) from the Itaboraí basin (early Eocene), Brazil: Paleobiogeographic and systematic implications for Herpetotheriidae. J South Am Earth Sci 144. https://doi.org/10.1016/j.jsames.2024.105016

Cifelli RL, Muizon C de (1998) Marsupial mammal from the Upper Cretaceous North Horn Formation, central Utah. J Paleontol 72:532-537. https://doi.org/10.1017/S0022336000024306

Clemens WA (1966) Fossil mammals of the type Lance Formation, Wyoming. Part II, Marsupialia. Univ Calif Publ Geol Sci 62:1–122.

Clemens WA (2006) Early Paleocene (Puercan) peradectid marsupials from northeastern Montana, North American Western Interior. Palaeontogr Abt A 277:19–31. https://doi.org/10.1127/pala/277/2006/19

Coillot T, Smith R, Gigase P, Smith T (2013) Tarsal diversity in the earliest Eocene mammal fauna of Dormaal, Belgium. Geol Belg 16:274-283.

Cojan I, Moreau MG, Stott LE (2000) Stable carbon isotope stratigraphy of the Paleogene pedogenic series of southern France as a basis for continental-marine correlation. Geology 28:259–262.

Crespo VD, Goin FJ (2021) Taxonomy and affinities of African cenozoic metatherians. Span J Palaeontol 36:133–148. https://doi.org/10.7203/sjp.36.2.20974

Crochet JY (1977a) Les Didelphidae (Marsupicarnivora, Marsupialia) holarctiques tertiaires. C R Acad Sci Paris 284:357–360.

Crochet JY (1977b) Les didelphidés paléogènes holarctiques : historique et tendances évolutives. Geobios Mem Spec 1:127–134

Crochet JY (1979) Diversité systématique des Didelphidae (Marsupialia) européens tertiaires. Geobios 12:365–378.

Crochet JY (1980a) L'occlusion dentaire chez *Peradectes*, *Amphiperatherium* et *Peratherium*, marsupiaux du Tertiaire d'Europe. Palaeovertebrata 9:79–89.

Crochet JY (1980b) Les marsupiaux du Tertiaire d'Europe. Edtions Foundation Singer-Polignac, Paris.

Crochet JY (1986) *Kasserinotherium tunisiense* nov. gen., nov. sp., troisième marsupial découvert en Afrique (Eocène inférieur de Tunisie). C R Acad Sci Paris 302:923–926.

Crompton AW, Hiiemae K (1970) Molar occlusion and mandibular movements during occlusion in the American opossum, *Didelphis marsupialis* L. Zool J Linn Soc 49:21-47. https://doi.org/10.1111/j.1096-3642.1970.tb00728.x

Danilo L, Remy J, Vianey-Liaud M, Marandat B, Sudre J, Lihoreau F (2013) A new Eocene locality in southern France sheds light on the basal radiation of Palaeotheriidae (Mammalia, Perissodactyla, Equoidea). J Vertebr Paleontol 33:195–215. https://doi.org/10.1080/02724634.2012.711404

Davis BM (2011) Evolution of the tribosphenic molar pattern in early mammals, with comments on the "dual-origin" hypothesis. J Mamm Evol 18:227–244. https://doi.org/10.1007/s10914-011-9168-8

Ducrocq S, Buffetaut E, Buffetaut-Tong H, Jaeger JJ, Jongkanjanasoontorn Y, Suteethorn V (1992) First fossil marsupial from South Asia. J Vertebr Paleontol 12:395–399.

Duprat M (1997) Les faciès à mammifères (MP 6 à MP 16) dans le Nord-Est du Bassin de Paris (France): argumentation du modèle tectono-sédimentaire des dépôts paléogènes. In: Aguilar JP, Legendre S, Michaux J (eds) Actes du Congrès BiochroM'97, Mémoires et travaux de l'EPHE 21. Ecole Pratique des Hautes Etudes, Institut de Montpellier, Montpellier, pp 315–336.

Eberle J, Storer JE (1995) *Herpetotherium valens* (Lambe), a didelphid marsupial from the Calf Creek Local Fauna (Chadronian), Saskatchewan. J Vertebr Paleontol 15:785–794.

Escarguel G (1999) Les rongeurs de l'Eocène inférieur et moyen d'Europe occidentale. Systématique, phylogénie, biochronologie et paléobiogéographie des niveaux repères MP 7 à MP 14. Palaeovertebrata 28:89–351.

Estravís C (2000) Nuevos mamíferos del Eoceno Inferior de Silveirinha (Baixo Mondego, Portugal). Coloquios Paleontol 51:281–311.

Farris JS (1989a) The retention index and homoplasy excess. Syst Biol 38:406-407. https://doi.org/10.2307/2992406

Farris JS (1989b) The retention index and the rescaled consistency index. Cladistics 5:417-419. https://doi.org/10.1111/j.1096-0031.1989.tb00573.x

Flores DA, Abdala F (2001) Diferencias morfológicas de cráneo y dentición en *Didelphis albiventris* y *D. marsupialis* (Didelphimorphia: Didelphidae) de Argentina y Bolivia. Comun Mus Ciênc Tecnol PUCRS, Sér Zool 14:101–110.

Fox RC (1983) Notes on the North American Tertiary marsupials *Herpetotherium* and *Peradectes*. Can J Earth Sci 20:1565–1578.

Gazin CL (1956) Paleocene mammalian faunas of the Bison Basin in South-Central Wyoming. Smithson Misc Collect 131:1–57.

Gheerbrant E (1991) *Bustylus* (Eutheria, Adapisoriculidae) and the absence of ascertained marsupials in the Palaeocene of Europe. Terra Nov 3:586–592.

Gheerbrant E (1992) Les mammifères paléocènes du bassin d'Ouarzazate (Maroc). I. Introduction générale et Palaeoryctidae. Palaeontogr Abt A 224:67–132.

Gingerich PD, Smith T (2006) Paleocene-Eocene land mammals from three new latest Clarkforkian and earliest Wasatchian Wash sites at Polecat Bench in the Northern Bighorn Basin. Contrib Mus Paleontol Univ Mich 31:245–303.

Godinot M (1981) Les mammifères de Rians (Eocène inférieur, Provence). Palaeovertebrata 10:43–126.

Godinot M (1984) Un noveau genre de Paromomyidae (Primates) de l'Eocène Inférieur d'Europe [A new genus of Paromomyidae (Primates) from the early Eocene of Europe]. Folia Primatol 43:84–96.

Godinot M (1992) Apport à la systématique de quatre genres d'Adapiformes (Primates, Eocène). C R Acad Sci Paris 314:237–242.

Godinot M, Crochet JY, Hartenberger JL, Lange-Badré B, Russell DE, Sigé B (1987) Nouvelles données sur les mammifères de Palette (Eocène inférieur, Provence). Münch Geowiss Abh (A) 10:273-288.

Goin FJ, Woodburne MO, Zimicz AN, Martin GM, Chornogubsky L (2016) A Brief History of South American Metatherians: Evolutionary Contexts and Intercontinental Dispersals. Springer, Dordrecht, Netherlands.

Goin FJ, Candela AM, Muizon C de (2003) The affinities of *Roberthoffstetteria nationalgeographica* (Marsupialia) and the origin of the polydolopine molar pattern. J Vertebr Paleontol 23:869–876. https://doi.org/10.1671/2383-11

Goloboff PA (1993) Estimating character weights during tree search. Cladistics 9:83–91.

Gordon CL (2003) A first look at estimating body size in dentally conservative marsupials. J Mamm Evol 10:1-21. https://doi.org/10.1023/A:1025545023221

Green M, Martin JE (1976) *Peratherium* (Marsupialia: Didelphidae) from the Oligocene and Miocene of South Dakota. In: Churcher CS (ed) Athlon: Essays on Palaeontology in Honour of Loris Shano Russell. Roy Ontario Mus Misc Publ, Toronto, pp 155–168.

Gunnell GF (2010) Marsupialia. In: Werdelin L, Sanders WJ (eds) Cenozoic Mammals of Africa. University of California Press, Berkeley, pp 77-79.

Hand SJ, Sigé B (2017) A new archaic bat (Chiroptera: Archaeonycteridae) from an Early Eocene forest in the Paris Basin. Hist Biol 30:227–236. https://doi.org/10.1080/08912963.2017.1297435

Hayes FG (2005) Arikareean (Oligocene-Miocene) *Herpetotherium* (Marsupialia, Didelphidae) from Nebraska and Florida. Bull Fla Mus Nat Hist 45:335–353.

Hershkovitz P (1997) Composition of the family Didelphidae Gray, 1821 (Didelphoidea: Marsupialia), with a review of the morphology and behavior of the included four-eyed pouched opossums of the genus *Philander* Tiedemann, 1808. Fieldiana Zool 86:1–103.

Hooker JJ (1996) Mammalian biostratigraphy across the Paleocene-Eocene boundary in the Paris, London and Belgian basins. In: Knox RWOB, Corfield RM, Dunay RE (eds) Correlation of the Early Paleogene in Northwest Europe. Geol Soc Lond, Spec Publ 101, pp 205–218. https://doi.org/10.1144/gsl.sp.1996.101.01.13

Hooker JJ (1998) Mammalian faunal change across the Paleocene-Eocene transition in Europe. In: Aubry MP, Berggren WA, Lucas SG (eds) Late Paleocene-Early Eocene Climatic and Biotic Events in the Marine and Terrestrial Records. Columbia University Press, New York, pp 419–441.

Hooker JJ (2010) The mammal fauna of the early Eocene Blackheath formation of Abbey Wood, London. Monogr Palaeontogr Soc 164:1–153. https://doi.org/10.1080/25761900.2022.12131814

Hooker JJ (2015) A two-phase mammalian dispersal event across the Paleocene–Eocene transition. Newsl Stratigr 48:201–220 https://doi.org/10.1127/nos/2015/0060

Hooker JJ (2020) A mammal fauna from the Paleocene-Eocene Thermal Maximum of Croydon, London, UK. Proc Geol Assoc 131:458–473. https://doi.org/10.1016/j.pgeola.2018.01.001

Hooker JJ, Russell DE (2012) Early Palaeogene Louisinidae (Macroscelidea, Mammalia), their relationships and north European diversity. Zool J Linn Soc 164:856–936. https://doi.org/10.1111/j.1096-3642.2011.00787.x

Hooker JJ, Sánchez-Villagra MR, Goin FJ, Simons EL, Attia Y, Seiffert ER (2008) The origin of Afro-Arabian 'didelphimorph' marsupials. Palaeontology 51:635-648. https://doi.org/10.1111/j.1475-4983.2008.00779.x

Horovitz I, Martin T, Bloch J, Ladevèze S, Kurz C, Sánchez-Villagra MR (2009) Cranial anatomy of the earliest marsupials and the origin of opossums. PLoS One 4:1–9. https://doi.org/10.1371/journal.pone.0008278

Hough JR (1961) Review of Oligocene didelphid marsupials. J Paleontol 35:218–228.

International Commission of Zoological Nomenclature (ICZN) (1999) International Code of Zoological Nomenclature. The International Trust for Zoological Nomenclature, London. http://www.nhm.ac.uk/hosted-sites/iczn/code/

Jernvall J, Jung HS (2000) Genotype, phenotype, and developmental biology of molar tooth characters. Am J Phys Anthropol 113:171–190.

Johanson Z (1994) New information concerning the Late Cretaceous marsupial *Albertatherium* Fox, 1971. J Vertebr Paleontol 14:595–602.

Johanson Z (1996) New marsupial from the Fort Union Formation, Swain Quarry, Wyoming. J Paleontol 70:1023–1031.

Kaboth-Bahr S, Schmitt C, Bauersachs T, Zeeden C, Wonik T, Schandl J, Lenz O, Wedmann S, Vasiliev I, Mulch A, Lourens L, Pross J, Bahr A (2024) Improved chronostratigraphy for the Messel Formation (Hesse, Germany) provides insight into early to middle Eocene climate variability. Newsletters on Stratigraphy. https://doi.org/10.1127/nos/2024/0799

Kihm AJ, Schumaker KK (2015) Marsupials from the Chadronian (latest Eocene) Medicine Pole Hills local fauna, North Dakota. Paludicola 10: 93-112.

Koenigswald W von (1970) *Peratherium* (Marsupialia) im Ober-Oligozän und Miozän von Europa. Bayer Akad Wiss Math-Natur Kl Abh (NF) 144:1–79.

Korth WW (1994) Middle Tertiary marsupials (Mammalia) from North America. J Paleontol 68:376–397.

Korth WW (2008) Marsupialia. In: Janis CM, Gunnell GF, Uhen MD (eds) Evolution of Tertiary Mammals of North America: Volume 2, Small Mammals, Xenarthrans, and Marine Mammals. Cambridge University Press, Cambridge, pp 39–47.

Korth WW (2018) Review of the marsupials (Mammalia: Metatheria) from the late Paleogene (Chadronian–Arikareean: late Eocene–late Oligocene) of North America. PalZ 92:499-523. https://doi.org/10.1007/s12542-017-0396-y

Krishtalka L, Stucky RK (1983a) Revision of the Wind River faunas, early Eocene of Central Wyoming. Part 3. Marsupialia. Ann Carnegie Mus 52:205–227.

Krishtalka L, Stucky RK (1983b) Paleocene and Eocene marsupials of North America. Ann Carnegie Mus 52:229–263.

Krishtalka L, Stucky RK (1984) Middle Eocene marsupials (Mammalia) from northeastern Utah and the mammalian fauna from Powder Wash. Ann Carnegie Mus 53:31–45.

Kurz C (2005) Ecomorphology of opossum-like marsupials from the Tertiary of Europe and a comparison with selected taxa. Kaupia 14:21–26.

Kurz C (2007) The opossum-like marsupials (Didelphimorphia and Peradectia, Marsupialia, Mammalia) from the Eocene of Messel and Geiseltal – Ecomorphology, diversity and palaeogeography.

Kaupia 15:3–65.

Kurz C, Habersetzer J (2004) Untersuchungen der zahnmorphologie von beutelratten aus Messel mit der mikroröntgenmethode CORR. Cour Forsch-Inst Senckenberg 252:13–21.

Ladevèze S, Muizon C de, Beck RMD, Germain D, Cespedes-Paz R (2011) Earliest evidence of mammalian social behaviour in the basal Tertiary of Bolivia. Nature 474:83–86. https://doi.org/10.1038/nature09987

Ladevèze S, Selva C, Muizon C de (2020) What are "opossum-like" fossils? The phylogeny of herpetotheriid and peradectid metatherians, based on new features from the petrosal anatomy. J Syst Palaeontol 18:1463–1479. https://doi.org/10.1080/14772019.2020.1772387

Ladevèze S, Smith R, Smith T (2012) Reassessment of the morphology and taxonomic status of the earliest herpetotheriid marsupials of Europe. J Mamm Evol 19:249–261. https://doi.org/10.1007/s10914-012-9195-0

Laurent Y, Adnet S, Bourdon E, Corbalan D, Danilo L, Duffaud S, Fleury G, Garcia G, Godinot M, Le Roux G, Maisonnave C, Métais G, Mourer-Chauviré C, Presseq B, Sigé B, Solé F (2010) La Borie (Saint-Papoul, Aude): un gisement exceptionnel dans l'Éocène basal du Sud de la France. Bull Soc Hist Nat Toulouse 146:89-103.

Lebrun R (2018) MorphoDig, an open-source 3D freeware dedicated to biology. 5th International Paleontological Congress (IPC5) – *The Fossil Week*, July 9–13th, 2018 (Paris, France).

Lebrun R, Orliac MJ (2016) MorphoMuseuM: an online platform for publication and storage of virtual specimens. Paleontol Soc Pap 22:183-195. https://doi.org/10.1017/scs.2017.14

Lecomte G (1994) Étude paléontologique et sédimentologique de l'Yprésien de l'est du bassin de Paris. Dissertation, University Paris VI, France.

Legendre S, Marandat B, Sigé B, Crochet JY, Godinot M, Hartenberger JL, Sudre J, Vianey-Liaud M, Muratet B, Astruc JG (1992) La faune de mammifères de Vielase (phosphorites du Quercy, Sud de la France): Preuve paléontologique d'une karstification du Quercy dès l'Eocène inférieur. Neues Jahrb Geol Paläontol 7:414–428.

Lillegraven J (1969) Latest Cretaceous mammals from the upper part of the Edmonton Formation of Alberta, Canada, and review of marsupial placental dichotomy in mammalian evolution. Univ Kans Paleontol Contrib 50:1–122.

Lillegraven J (1976) Didelphids (Marsupialia) and *Uintasorex* (?Primates) from later Eocene sediments of San Diego County, California. Trans San Diego Soc Nat Hist 18:85–112.

López-Martínez N, Smith R, Peláez-Campomanes P, Smith T (2006). The acme of the micromammal *Paschatherium* across the Paleocene-Eocene boundary in continental Europe. Micropaleontology 52:267-280.

López-Torres S, Silcox MT (2018) The European Paromomyidae (Primates, Mammalia): Taxonomy, phylogeny, and biogeographic implications. J Paleontol 92:920–937. https://doi.org/10.1017/jpa.2018.10

Louis P (1970) Note préliminaire sur un gisement de mammifères de l'Eocène inférieur situé Route de Broyes à Sézanne (Marne). Ann Univ A.R.E.R.S. Reims 8:48–62.

Louis P (1996) Recherches de mammifères paléogènes dans les départements de l'Aisne et de la Marne pendant la deuxième moitié du vingtième siècle. Palaeovertebrata 25:83–113.

Louis P, Laurain M (1983) Nouveau gisement de vertébrés dans le Cuisien supérieur de Saint-Agnan (Aisne). Ses relations stratigraphiques avec les autres gisements yprésiens du Bassin parisien. Bull Inf Géol Bass Paris 20:3–20.

Maddison WP, Maddison DR (2019) Mesquite, a modular system for evolutionary analysis. Version 3.61. http://mesquiteproject.org

Maga AM, Beck RMD (2017) Skeleton of an unusual, cat-sized marsupial relative (Metatheria: Marsupialiformes) from the middle Eocene (Lutetian: 44-43 million years ago) of Turkey. PLoS One 12:e0181712. https://doi.org/10.1371/journal.pone.0181712

Manz CL, Bloch JI (2015) Systematics and phylogeny of Paleocene-Eocene Nyctitheriidae (Mammalia, Eulipotyphla?) with description of a new species from the late Paleocene of the Clarks Fork Basin, Wyoming, USA. J Mamm Evol 22:307–342. https://doi.org/10.1007/s10914-014-9284-3

Marandat B (1986) Decouverte d'une faune de micromammiferes d'âge cuisien superieur dans les marno-calcaires d'Agel à Azillanet (Minervois, Hérault). Geol Fr 2:197–204.

Marandat B (1991) Mammifères de l'Ilerdien Moyen (Eocène Inférieur) des Corbières et du Minervois. Palaeovertebrata 20:55–144.

Marandat B (1997) La disparité des faunes mammaliennes du niveau MP 7 (Eocène inférieur) des domaines péri-mésogéens et nordiques. Investigation d'un provincialisme intra-européen. Newsl Stratigr 35:63–82.

Marandat B, Adnet S, Marivaux L, Martinez A, Vianey-Liaud M, Tabuce R (2012) A new mammalian fauna from the earliest Eocene (Ilerdian) of the Corbières (Southern France): Palaeobiogeographical implications. Swiss J Geosci 105:417–434. https://doi.org/10.1007/s00015-012-0113-5

Marshall LG, Case JA, Woodburne MO (1990) Phylogenetic relationships of the families of marsupials. In: Genoways HH (ed) Current Mammalogy, Volume 2. Plenum Press, New York, pp 433-505.

Marshall LG, Muizon C de (1988) The dawn of the age of mammals in South America. Natl Geogr Res 4:23–55.

Marshall LG, Muizon C de (1995) Part II: The skull. In: Muizon C de (ed) *Pucadelphys andinus* (Marsupialia, Mammalia) from the early Paleocene of Bolivia. Mém Mus Hist Nat 195:21-90.

Martin GM (2005) Intraspecific variation in *Lestodelphys halli* (Marsupialia: Didelphimorphia). J Mammal 86:793–802. https://doi.org/10.1644/1545-1542(2005)086[0793:IVILHM]2.0.CO;2

Martin T, Averianov AO, Schultz JA, Schwermann AH (2023) A stem therian mammal from the Lower Cretaceous of Germany. J Vertebr Paleontol 42:e2224848. https://doi.org/10.1080/02724634.2023.2224848

Matthew W, Granger W (1921) New genera of Paleocene mammals. Am Mus Novit 13:1–7.

McGrew PO (1937) New marsupials from the Tertiary of Nebraska. J Geol 45:448-455.

McGrew PO (1939) *Nanodelphys*, an Oligocene didelphine. Field Mus Nat Hist Geol Ser 6:393–400. https://doi.org/10.5962/bhl.title.5208

McKenna M (1960) Fossil Mammalia from the early Wasatchian Four Mile fauna, Eocene of northwest Colorado. Univ Calif Publ Geol Sci 37:1–130.

Mein P, Ginsburg L (1997) Les mammifères du gisement miocène inférieur de Li Mae Long, Thaïlande: systématique, biostratigraphie et paléoenvironnement. Geodiversitas 19:783-844.

Missiaen P, Quesnel F, Dupuis C, Storme JY, Smith T (2013) The earliest Eocene mammal fauna of the Erquelinnes Sand Member near the French-Belgian border. Geol Belg 16:262–273.

Muizon C de (1991) La fauna de mamíferos de Tiupampa (Paleoceno Inferior, Formacion Santa Lucia), Bolivia. In: Suarez-Soruco R (ed) Fósiles y Facies de Bolivia, Vol. 1. Vertebrados. Yacimientos Petrolíferos Fiscales Bolivianos, Santa Cruz, Bolivia, pp 575–624.

Muizon C de, Ladevèze S (2020) Cranial anatomy of *Andinodelphys cochabambensis*, a stem metatherian from the early Paleocene of Bolivia. Geodiversitas 42:597-739. https://doi.org/10.5252/geodiversitas2020v42a30

Muizon C de, Ladevèze S (2022) New material of *Incadelphys antiquus* (Pucadelphyda, Metatheria, Mammalia) from the early Palaeocene of Bolivia reveals phylogenetic affinities with enigmatic North and South American metatherians. Geodiversitas 44:609–643. https://doi.org/10.5252/geodiversitas2022v44a22

Muizon C, Lange-Badré B (1997) Carnivorous dental adaptations in tribosphenic mammals and phylogenetic reconstruction. Lethaia 30:353-366. https://doi.org/10.1111/j.1502-3931.1997.tb00481.x

Muizon C de, Ladevèze S, Selva C, Vignaud R., Goussard F. (2018) *Allqokirus australis* (Sparassodonta, Metatheria) from the early Palaeocene of Tiupampa (Bolivia) and the rise of the metatherian carnivorous radiation in South America. Geodiversitas 40:363-459. https://doi.org/10.5252/geodiversitas2018v40a16

Murphey PC, Kelly TS, Chamberlain KR, Tsukui K, Clyde WC (2018) Mammals from the earliest Uintan (middle Eocene) Turtle Bluff Member, Bridger Formation, southwestern Wyoming, USA, Part 3: Marsupialia and a reevaluation of the Bridgerian-Uintan North American Land Mammal Age transition. Palaeontol Electron 21(2):25A:1–52. https://doi.org/10.26879/804

Neal JE (1996) Summary of Paleogene sequence stratigraphy in northwest European and the North Sea. In: Knox RWOB, Corfield RM, Dunay RE (eds) Correlation of the Early Paleogene in Northwest Europe. Geol Soc London Spec Publ 101, pp 15–42. https://doi.org/10.1144/GSL.SP.1996.101.01.02

Nel A, de Plöeg G, Dejax J, Dutheil D, de Franceschi D, Gheerbrant E, Godinot M, Hervet S, Menier JJ, Augé M, Bignot G, Cavagnetto C, Duffaud S, Gaudant J, Stéphane H, Jossang A, de Lapparent de Broin F, Pozzi JP, Paicheler JC, Beuchet F, Rage JC (1999) Un gisement sparnacien exceptionnel à plantes, arthropodes et vertébrés (Eocène basal, MP7): Le Quesnoy (Oise, France). C R Acad Sci Paris 329:65–72. https://doi.org/10.1016/S1251-8050(99)80229-8

Ni X, Meng J, Wu W, Ye J (2007) A new Early Oligocene peradectine marsupial (Mammalia) from the Burqin region of Xinjiang, China. Naturwissenschaften 94:237–241. https://doi.org/10.1007/s00114-006-0182-2

Noiret C, Steurbaut E, Tabuce R, Marandat B, Schnyder J, Storme JY, Yans J (2016) New bio-chemostratigraphic dating of a unique early sequence from southern results in precise mammalian

biochronological tie-points. Newsl Stratigr 49:469–480. https://doi.org/10.1127/nos/2016/0336

O'Leary MA, Bloch JI, Flynn JJ, Gaudin TJ, Giallombardo A, Giannini NP, Goldberg SL, Kraatz BP, Luo ZX, Meng J, Ni X, Novacek MJ, Perini FA, Randall ZS, Rougier GW, Sargis EJ, Silcox MT, Simmons NB, Spaulding M, Velazco PM, Weksler M, Wible JR, Cirranello AL (2013) The placental mammal ancestor and the Post-K-Pg radiation of placentals. Science 339:662–667. https://doi.org/10.1126/science.1229237

Oliveira ÉV, Goin FJ (2011) A reassessment of bunodont metatherians from the Paleogene of Itaboraí (Brazil): systematics and age of the Itaboraian SALMA. Rev Bras Paleontol 14:105-136. https://doi.org/10.4072/rbp.2011.2.01

Orliac MJ, Boivin M, Tabuce R (2018) A mandible of *Diacodexis* cf. *gigasei* (Artiodactyla, Diacodexeidae) from the Early Eocene locality of Palette (Bouches-du-Rhône, France). MorphoMuseuM 4:1–4. https://doi.org/10.18563/journal.m3.60

Philip J, Vianey-Liaud M, Martin-Closas C, Tabuce R, Léonide P, Margerel JP, Noël J (2017) Stratigraphy of the Haut Var Paleogene continental series (Northeastern Provence, France): New insight on the age of the 'Sables bleutés du Haut Var' Formation. Geobios 50:319–339. https://doi.org/10.1016/j.geobios.2017.06.002

R Core Team (2020) R: A language and environment for statistical computing. R Foundation for Statistical Computing, Vienna, Austria. https://www.R-project.org

Ramdarshan A, Godinot M, Bédécarrats S, Tabuce R (2015) Holotype specimen of *Donrussellia magna*, an adapiform primate from the early Eocene (MP7) of Southern France. MorphoMuseuM 1:1–3. https://doi.org/10.18563/m3.1.2.e2

Rat P (1965). La succession stratigraphique des Mammifères dans l'Eocène du bassin de Paris. Bull Soc Géol Fr 7:248-256.

Reig OA, Kirsch JAW, Marshall LG (1985) New conclusions on the relationships of the opossum-like marsupials, whith an annotated classifícation of the Didelphimorphia. Ameghiniana 21:335–343.

Reig OA, Kirsch JAW, Marshall LG (1987) Systematic relationships of the living and Neocenozoic American "opossum-like" marsupials (suborder Didelphimorphia), with comments on the classification of these and the Cretaceous and Paleogene New World and European metatherians. In: Archer M (ed) Possums and Opossums: Studies in Evolution. Surrey Bea, Sydney, pp 1–89.

Rose KD (1981) The Clarkforkian Land-Mammal Age and mammalian faunal composition across the Paleocene-Eocene boundary. Univ Mich Pap Paleontol 26:1–197.

Rose KD (2010) New marsupial from the Early Eocene of Virginia. J Paleontol 84:561–565. https://doi.org/10.1666/09-140.1

Rose KD (2012) The importance of Messel for interpreting Eocene Holarctic mammalian faunas. Palaeobiodivers Palaeoenviron 92:631–647. https://doi.org/10.1007/s12549-012-0090-8

Rose KD, Chew AE, Dunn RH, Kraus MJ, Fricke HC, Zack SP (2012) Earliest Eocene mammalian fauna from the Paleocene-Eocene Thermal Maximum at Sand Creek Divide, Southern Bighorn Basin, Wyoming. Univ Mich Pap Paleontol 36:1–122.

Rose KD, Godinot M, Bown TM (1994) The early radiation of euprimates and the initial diversification of Omomyidae. In: Fleagle J, Kay R (eds) Anthropoid Origins. Plenum Press, New York, pp 1–

28.

Rothecker J, Storer JE (1996) The marsupials of the Lac Pelletier Lower Fauna, Middle Eocene (Duchesnean) of Saskatchewan. J Vertebr Paleontol 16:770–774.

Russell DE, Galoyer A, Louis P, Gingerich PD (1988) Nouveaux vertébrés sparnaciens du Conglomérat de Meudon à Meudon, France. C R Acad Sci Paris 307:429–433.

Russell DE, Godinot M (1988) The Paroxyclaenidae (Mammalia) and a new form from the Early Eocene of Palette, France. Paläontol Z 62:319–331.

Ruxton GD (2006) The unequal variance *t*-test is an underused alternative to Student's *t*-test and the Mann–Whitney *U* test. Behav Ecol 17:688-690. https://doi.org/10.1093/beheco/ark016

Sánchez-Villagra M, Ladevèze S, Horovitz I, Argot C, Hooker JJ, Macrini TE, Martin T, Moore-Fay S, Muizon C de, Schmelzle T, Asher RJ (2007) Exceptionally preserved North American Paleogene metatherians: Adaptations and discovery of a major gap in the opossum fossil record. Biol Lett 3:318–322. https://doi.org/10.1098/rsbl.2007.0090

Sansom RS, Wills MA, Williams T (2017) Dental data perform relatively poorly in reconstructing mammal phylogenies: Morphological partitions evaluated with molecular benchmarks. Syst Biol 66:813-822. https://doi.org/10.1093/sysbio/syw116

Schmidt-Kittler N, Godinot M, Franzen JL, Hooker JJ, Legendre S, Brunet M, Vianey-Liaud M (1987) European reference levels and correlation tables. Münch Geowiss Abh (A) 10:13–31.

Selva C, Ladevèze S (2017) Computed microtomography investigation of the skull of Cuvier's famous ‘opossum’ (Marsupialiformes, Herpetotheriidae) from the Eocene of Montmartre. Zool J Linn Soc 180:672-693. https://doi.org/10.1111/zoj.12495

Sigé B (1971) Les Didelphoidea de Laguna Umayo (formation Vilquechico, Crétacé supérieur, Pérou), et le peuplement marsupial d’Amérique du Sud. C R Acad Sci Paris 273:2479–2481.

Sigé B (1972) La faunule de mammifères du Crétacé supérieur de Laguna Umayo (Andes péruviennes). Bull Mus Natl Hist Nat 99:375–405.

Simpson GG (1928) American Eocene didelphids. Am Mus Novit 307:1–7.

Simpson GG (1935) The Tiffany Fauna, upper Paleocene: I. Multituberculata, Marsupialia, Insectivora, and ?Chiroptera. Am Mus Novit 795:1–20.

Smith T (2000) Mammals from the Paleocene-Eocene transition in Belgium (Tienen formation, MP7): palaeobiogeographical and biostratigraphical implications. GFF 122:148–149.

Smith T, Dupuis C, Folie A, Quesnel F, Storme JY, Iacumin P, Riveline J, Missiaen P, Ladevèze S, Yans J (2011) Un nouveau site à vertébrés terrestres juste après la limite Paléocène-Eocène, dans la Formation de Mortemer en Haute-Normandie, France. C R Palevol 10:11–20. https://doi.org/10.1016/j.crpv.2010.11.004

Smith T, Smith R (2013) A land micro-mammal fauna from the Early Eocene marine Egem deposits (NP12, Belgium) and the first occurrence of the peradectid marsupial *Armintodelphys* outside North America. Geol Belgica 16:302–310.

Solé F (2014) New carnivoraforms from the early Eocene of Europe and their bearing on the evolution

of the Carnivoraformes. Palaeontology 57:963–978. https://doi.org/10.1111/pala.12097

Solé F, Fournier M, Ladevèze S, Le Verger K, Godinot M, Laurent Y, Smith T (2023) New postcranial elements of mesonychid mammals from the Ypresian of France: New hypotheses for the radiation and evolution of the mesonychids in Europe. J Mamm Evol 30:371–401. https://doi.org/10.1007/s10914-023-09651-x

Solé F, Gheerbrant E, Godinot M (2011) New data on the Oxyaenidae from the Early Eocene of Europe; biostratigraphic, paleobiogeographic and paleoecologic implications. Palaeontol Electron 14(2):13A:1-41. palaeo-electronica.org/2011_2/258/index.html

Solé F, Gheerbrant E, Godinot M (2013) Sinopaninae and Arfianinae (Hyaenodontida, Mammalia) from the Early Eocene of Europe and Asia; evidence for dispersal in Laurasia around the Paleocene/Eocene boundary and for an unnoticed faunal turnover in Europe. Geobios 46:313-327. https://doi.org/10.1016/j.geobios.2013.02.003

Solé F, Godinot M, Laurent Y, Galoyer A, Smith T (2018) The European mesonychid mammals: Phylogeny, ecology, biogeography, and biochronology. J Mamm Evol 25:339–379. https://doi.org/10.1007/s10914-016-9371-8

Solé F, Smith T, Tabuce R, Marandat B (2015) New dental elements of the oldest proviverrine mammal from the early Eocene of Southern France support possible African origin of the subfamily. Acta Palaeontol Pol 60:527–538. https://doi.org/10.4202/app.00146.2014

Speijer RP, Pälike H, Hollis CJ, Hooker JJ, Ogg JG (2020) The Paleogene Period. In: Gradstein FM, Ogg JG, Schmitz MD, Ogg GM (eds) Geologic Time Scale 2020. Elsevier, Amsterdam, pp 1087–1140. https://doi.org/10.1016/B978-0-12-824360-2.00028-0

Stehlin HG (1940) Über die säugetierfauna der teredinasande von Epernay und umgebung. Eclogae Geol Helv 33:291-298.

Steurbaut E, Magioncalda R, Dupuis C, Van Simaeys S, Roche E, Roche M (2003) Palynology, paleoenvironments, and organic carbon isotope evolution in lagoonal Paleocene-Eocene boundary settings in North Belgium. Spec Pap Geol Soc Am 369:291–317. https://doi.org/10.1130/0-8137-2369-8.291

Stock C (1936) Sespe Eocene didelphids. Proc Natl Acad Sci USA 22:122–124.

Storch G, Qiu Z (2002) First Neogene marsupial from China. J Vertebr Paleontol 22:179–181. https://doi.org/10.1671/0272-4634(2002)022[0179:FNMFC]2.0.CO;2

Storer JE (1991) The mammals of the Gryde local fauna, Frenchman Formation (Maastrichtian: Lancian), Saskatchewan. J Vertebr Paleontol 11:350–369.

Swofford DL (2002) PAUP* Phylogenetic analysis using parsimony (* and other methods). Version 4. Sinauer Associates, Sunderland.

Szalay FS (1994) Evolutionary History of the Marsupials and an Analysis of Osteological Characters. Cambridge University Press, Cambridge.

Tejedor MF, Goin FJ, Gelfo JN, López G, Bond M, Carlini AA, Scillato-Yane GJ, Woodburne MO, Chornogubsky L, Aragón E, Reguero MA, Czaplewski NJ, Vincon S, Martin GM, Ciancio MR (2009) New early Eocene mammalian fauna from western Patagonia, Argentina. Am Mus Novit 3638:1–43. https://doi.org/10.1206/577.1

Van Valen L (1966) Deltatheridia, a new order of mammals. Bull Am Mus Nat H 132:1-126.

Vautrin Q, Tabuce R, Lihoreau F, Bronnert C, Gheerbrant E, Godinot M, Metais G, Yans J, Dutour Y, Vialle N, Philip J, Billet G (2020) New remains of *Lophiaspis maurettei* (Mammalia, Perissodactyla) from the early Eocene of France and the implications for the origin of the Lophiodontidae. J Vertebr Paleontol 40:1–20. https://doi.org/10.1080/02724634.2020.1878200

Vianey-Liaud M, Lihoreau F, Solé F, Gernelle K, Vautrin Q, Bronnert C, Bourget H, Vidalenc D, Tabuce R (2024). A revision of the late early Eocene mammal faunas from Mas de Gimel and Naples (Montpellier, Southern France) and the description of a new theridomorph rodent. Geodiversitas 46:387-422. https://doi.org/10.5252/geodiversitas2024v46a10

Vianey-Liaud M, Marivaux L (2021) The beginning of the adaptive radiation of Theridomorpha (Rodentia) in Western Europe: morphological and phylogenetic analyses of early and middle Eocene taxa; implications for systematics. Palaeovertebrata 44:1–105. https://doi.org/10.18563/pv.44.2.e2

Vullo R, Gheerbrant E, Muizon C de, Néraudeau D (2009) The oldest modern therian mammal from Europe and its bearing on stem marsupial paleobiogeography. Proc Natl Acad Sci USA 106:19910–19915. https://doi.org/10.1073/pnas.0902940106

Wessels W, van de Weerd AA, Marković Z (2024) Marsupials (herpetotheriids) from the late Palaeogene of south-east Serbia. Palaeobio Palaeoenv. https://doi.org/10.1007/s12549-024-00600-x

West RM (1973) Geology and mammalian paleontology of the New Fork-Big Sandy area, Sublette County, Wyoming. Fieldiana Zool 29:1–193.

Wickham H (2016) ggplot2: Elegant graphics for data analysis. Use R!, Springer. https://doi.org/10.1007/978-3-319-24277-4

Williamson TE, Lofgren DL (2014) Late Paleocene (Tiffanian) metatherians from the Goler Formation, California. J Vertebr Paleontol 34:477–482. https://doi.org/10.1080/02724634.2013.804413

Williamson TE, Taylor LH (2011) New species of *Peradectes* and *Swaindelphys* (Mammalia: Metatheria) from the Early Paleocene (Torrejonian) Nacimiento Formation, San Juan Basin, New Mexico, USA. Palaeontol Electron 14(3):23A:1–16. https://palaeo-electronica.org/2011_3/21_williamson/index.html

Williamson TE, Brusatte SL, Carr TD, Weil A, Standhardt BR (2012) The phylogeny and evolution of Cretaceous-Palaeogene metatherians: Cladistic analysis and description of new early Palaeocene specimens from the Nacimiento Formation, New Mexico. J Syst Palaeontol 10:625–651. https://doi.org/10.1080/14772019.2011.631592

Williamson TE, Brusatte SL, Wilson GP (2014) The origin and early evolution of metatherian mammals: The Cretaceous record. Zookeys 465:1–76. https://doi.org/10.3897/zookeys.465.8178

Yans J, Marandat B, Masure E, Serra-Kiel J, Schnyder J, Storme JY, Marivaux L, Adnet S, Vianey-Liaud M, Tabuce R (2014) Refined bio-(benthic foraminifera, dinoflagellate cysts) and hemostratigraphy (δ13Corg) of the earliest Eocene at Albas-Le Clot (Corbières, France): Implications for mammalian biochronology in Southern Europe. Newsl Stratigr 47:331–353. https://doi.org/10.1127/nos/2014/0050

Supplementary material

Online resource 1 Additional measurement tables

Online resource 2 Taxa used in phylogenetic analyses, with references and stratigraphic extensions

Online resource 3 List of characters included in the phylogenetic analyses

Online resource 4 Taxon-character matrix of the first phylogenetic analysis

Online resource 5 Results and modifications made in the second and third phylogenetic analyses

Online resource 6 Lingual (medial) view of the surface model of the right hemi-mandible fragment MHN.AIX.PV.2017.6.8

Online Resource 1 Additional tables

Table S1. Measurements of molars of *Peradectes crocheti* sp. nov. Abbreviations: L, length (mm); W, width (mm); L/W, length to width ratio.

Specimen	Locality	Locus	L (mm)	W (mm)	L/W
MHN.AIX.PV.2018.26.14	Palette	M1	1,55	1,59	0,97
MHN.AIX.PV.2018.26.20	Palette	M1	1,51	1,4	1,08
UM-FDN-1	Fordones	M1	1,64	1,57	1,04
UM-FNR2-1	Fournes	M1	1,71	1,41	1,21
MNHN.F.Me16079	Meudon	M1		1,41	
MNHN.F.SN76	Soissons	M1	1,58	1,57	1,01
MHN.AIX.PV.2018.26.14	Palette	M2	1,5	1,7	0,88
NHMUK.PV.M44991	Abbey Wood	M2	1,57		
NHMUK.PV.M66046	Croydon	M2	1,81	1,85	0,98
UM-FDN-21	Fordones	M2	1,5		
UM-FDN-285	Fordones	M2	1,45		
UM-FDN-287	Fordones	M2		1,66	
UM-FNR2-2	Fournes	M2	1,58		
MNHN.F.Me15975	Meudon	M2	1,56		
MHN.AIX.PV.2017.6.7	Palette	M3	1,53	1,98	0,77
MHN.AIX.PV.2018.26.14	Palette	M3	1,4	1,77	0,79
UM-FDN-21	Fordones	M3		1,79	
UM-FDN-23	Fordones	M3	1,53		
MNHN.F.SN18	Soissons	M3	1,6	1,83	0,87
MNHN.F.SN78	Soissons	M3		1,79	
Fig. 5.18 Smith et al. 2011	Sotteville-sur-Mer	M3	1,58	1,91	0,83
UM-FDN-286	Fordones	M4	1,12		
MNHN.F.Me16084	Meudon	M4	1,26	1,79	0,70
MHN.AIX.PV.2017.6.9	Palette	m1	1,57	0,93	1,69
MNHN.F.Ri516	Rians	m1		0,94	
MNHN.F.SN121	Soissons	m1	1,47	0,86	1,71
MHN.AIX.PV.2017.6.8	Palette	m2	1,65	1,04	1,59
MHN.AIX.PV.2017.6.9	Palette	m2	1,64	1,03	1,59
MNHN.F.Me16101	Meudon	m2	1,69	0,99	1,71
MNHN.F.Ri221	Rians	m2	1,69		
MHN.AIX.PV.2017.6.8	Palette	m3	1,66	1,04	1,60
MHN.AIX.PV.2017.6.9	Palette	m3	1,68	1,06	1,58
MHN.AIX.PV.2017.6.10	Palette	m3	1,54	0,87	1,77
UM-PAT-103	Palette	m3	1,53	0,94	1,63
MNHN.F.SN2508	Soissons	m3	1,61	0,95	1,69
MHN.AIX.PV.2017.6.9	Palette	m4	1,55	0,92	1,68

Table S2. Detailed measurements of molars of *Peradectes louisi*. Abbreviations: L, length (mm); W, width (mm); L/W, length to width ratio; *, *Peradectes* cf. *louisi*.

Specimen	Locality	Locus	L (mm)	W (mm)	L/W
MNHN.F.Mu18005	Mutigny	dP3/	1,54	1,26	1,22
MNHN.F.Mu18006	Mutigny	M1	1,57	1,56	1,01
MNHN.F.Av16023	Avenay	M1	1,56	1,66	0,94
MNHN.F.Av16036	Avenay	M1	1,57	1,51	1,04
MNHN.F.Av16057	Avenay	M1	1,65	1,61	1,02
UM-AV-1-SK	Avenay	M1	1,49	1,55	0,96
UM-AV-2-SK	Avenay	M1	1,62	1,52	1,07
UM-AV-3-SK	Avenay	M1	1,62	1,6	1,01
MNHN.F.GL1	Sables de Brasles	M1	1,47	1,46	1,01
MNHN.F.GL296	Sables de Brasles	M1	1,53	1,45	1,06
MNHN.F.Mu6511	Mutigny	M2	1,62	1,86	0,87
MNHN.F.Av18003	Avenay	M2		1,78	
MNHN.F.Av18004	Avenay	M2		1,87	
MNHN.F.GL154	Sables de Brasles	M2		1,71	
MNHN.F.GL272	Sables de Brasles	M2	1,56		
MNHN.F.CB1486	Condé-en-Brie	M2		1,71	
MNHN.F.CB3213	Condé-en-Brie	M2	1,52	1,77	0,86
MNHN.F.CB3228	Condé-en-Brie	M2	1,71	1,74	0,98
MNHN.F.CB3637	Condé-en-Brie	M2	1,65		
MNHN.F.CB3707	Condé-en-Brie	M2	1,58	1,69	0,93
MNHN.F.CB4183	Condé-en-Brie	M2		1,83	
MNHN.F.CB4182	Condé-en-Brie	M3	1,51	1,92	0,79
MNHN.F.GL197	Sables de Brasles	M3	1,63	1,85	0,88
MNHN.F.SZ18000	Sézanne-Broyes	M3	1,41	1,83	0,77
MNHN.F.SZ18005	Sézanne-Broyes	M3	1,47	1,72	0,85
MNHN.F.SZ18004	Sézanne-Broyes	M4	1,33	1,88	0,71
MNHN.F.Av16028	Avenay	m1	1,56	0,77	2,03
MNHN.F.Av7229	Avenay	m1	1,51	0,85	1,78
UM-AV-7-SK	Avenay	m1	1,45	0,76	1,91
UM-AV-12-SK	Avenay	m1	1,55	0,85	1,82
MNHN.F.CB962	Condé-en-Brie	m1	1,56	0,85	1,84
MNHN.F.CB4391	Condé-en-Brie	m1	1,52	0,83	1,83
MNHN.F.GL136	Sables de Brasles	m1	1,4	0,8	1,75
MNHN.F.SZ18003	Sézanne-Broyes	m1	1,43	0,78	1,83
MNHN.F.Av16016	Avenay	m2	1,54	0,9	1,71
MNHN.F.Av16027	Avenay	m2	1,64	0,94	1,74

MNHN.F.Av16044	Avenay	m2	1,62	0,89	1,82
MNHN.F.Av18001	Avenay	m2	1,58	0,98	1,61
MNHN.F.Av6830	Avenay	m2	1,69	1	1,69
UM-AV-10-SK	Avenay	m2		0,87	
UM-AV-11-SK	Avenay	m2	1,56	0,9	1,73
MNHN.F.CB5090	Condé-en-Brie	m2	1,7	0,93	1,83
MNHN.F.CB5092	Condé-en-Brie	m2	1,73	0,99	1,75
MNHN.F.CB5097	Condé-en-Brie	m2	1,67	0,98	1,70
MNHN.F.CB828	Condé-en-Brie	m2	1,66	0,97	1,71
MNHN.F.CB872	Condé-en-Brie	m2	1,69	0,95	1,78
MNHN.F.CB878	Condé-en-Brie	m2	1,72	1	1,72
MNHN.F.SZ18001	Sézanne-Broyes	m2	1,66	0,92	1,80
MNHN.F.Av18000	Avenay	m3	1,63	0,94	1,73
MNHN.F.Av18002	Avenay	m3	1,6	0,95	1,68
MNHN.F.Av4642	Avenay	m3	1,47		
MNHN.F.AV16149	Avenay	m3	1,58	0,85	1,86
MNHN.F.AV16158	Avenay	m3	1,61	0,91	1,77
UM-AV-4-SK	Avenay	m3	1,51	0,86	1,76
UM-AV-5-SK	Avenay	m3	1,51	0,84	1,80
UM-AV-6-SK	Avenay	m3	1,54	0,95	1,62
UM-AV-8-SK	Avenay	m3	1,56	0,92	1,70
UM-AV-9-SK	Avenay	m3	1,59	0,88	1,81
MNHN.F.CB226	Condé-en-Brie	m3	1,61		
MNHN.F.CB5104	Condé-en-Brie	m3	1,6	0,89	1,80
MNHN.F.CB959	Condé-en-Brie	m3	1,62	0,91	1,78
MNHN.F.CB4213	Condé-en-Brie	m3	1,6	0,92	1,74
MNHN.F.GL261	Sables de Brasles	m3	1,54	0,86	1,79
MNHN.F.GL263	Sables de Brasles	m3	1,52	0,86	1,77
MNHN.F.GL383	Sables de Brasles	m3	1,66	0,89	1,87
MNHN.F.SZ18006	Sézanne-Broyes	m3	1,54	0,87	1,77
MNHN.F.Av16032	Avenay	m4	1,53	0,85	1,80
MNHN.F.Av16037	Avenay	m4	1,48	0,85	1,74
MNHN.F.GL301	Sables de Brasles	m4	1,44	0,78	1,85
*MNHN.F.STA296	Saint-Agnan	m4	1,5	0,84	1,79

Table S3. Detailed measurements of molars of *Peradectes russelli*, with the original attribution of the specimens in Crochet (1980). Dash denote unpublished specimens. Abbreviations: L, length (mm); W, width (mm); L/W, length to width ratio.

Specimen	Original attribution	Locality	Locus	L (mm)	W (mm)	L/W
MNHN.F.Mu18004	*Peradectes mutigniensis*	Mutigny	M1	1,88	1,82	1,03
MNHN.F.Mu5532	-	Mutigny	M1	1,85	1,9	0,97
MNHN.F.Av16024	*Peradectes mutigniensis*	Avenay	M1	1,75	1,9	0,92
UM-AV-13-SK	-	Avenay	M1	1,73	1,78	0,97
MNHN.F.CB2501	*Peradectes russelli*	Condé-en-Brie	M1	1,97	2,09	0,94
MNHN.F.CB3007	*Peradectes mutigniensis*	Condé-en-Brie	M1	1,62	1,85	0,88
MNHN.F.CB3275	*Peradectes russelli*	Condé-en-Brie	M1	1,87	1,91	0,98
MNHN.F.Mu18002	*Peradectes mutigniensis*	Mutigny	M2	1,82	2,14	0,85
MNHN.F.CB5103	*Peradectes russelli*	Condé-en-Brie	M2	1,91	2,07	0,92
MNHN.F.CB840	-	Condé-en-Brie	M2	2,02	2,26	0,89
MNHN.F.CB850	-	Condé-en-Brie	M2	1,97	2,27	0,87
MNHN.F.CB2753	*Peradectes russelli*	Condé-en-Brie	M2	2,11		
MNHN.F.Mu5521	*Peradectes mutigniensis*	Mutigny	M3	1,78	2,27	0,78
MNHN.F.Av4813	*Peradectes russelli*	Avenay	M3	1,95	2,27	0,86
MNHN.F.Av6837	*Peradectes mutigniensis*	Avenay	M3	1,82	2,29	0,79
MNHN.F.CB742	*Peradectes mutigniensis*	Condé-en-Brie	M3	1,95	2,4	0,81
MNHN.F.CB924	*Peradectes russelli*	Condé-en-Brie	M3	1,99	2,52	0,79
MNHN.F.CB2502	*Peradectes russelli*	Condé-en-Brie	M3	2,02	2,43	0,83
MNHN.F.CB924	*Peradectes russelli*	Condé-en-Brie	M4	1,35	2,36	0,57
MNHN.F.CB3021	*Peradectes* sp.	Condé-en-Brie	m1	1,71	0,89	1,92
MNHN.F.SZ18002	-	Sézanne-Broyes	m1	1,65	0,92	1,79
MNHN.F.Mu18000	*Peradectes mutigniensis*	Mutigny	m2	1,75	1,06	1,65
MNHN.F.Av7235	*Peradectes russelli*	Avenay	m2	1,98	1,17	1,69
UM-AV-14-SK	-	Avenay	m2	1,77	1,08	1,64
UM-AV-15-SK	-	Avenay	m2	1,97	1,19	1,66
MNHN.F.CB5098	*Peradectes mutigniensis*	Condé-en-Brie	m2	1,8	1,04	1,73
MNHN.F.CB5100	*Peradectes mutigniensis*	Condé-en-Brie	m2	1,94	1,13	1,72
MNHN.F.CB925	*Peradectes russelli*	Condé-en-Brie	m2	2,03	1,25	1,62
MNHN.F.CB928	-	Condé-en-Brie	m2	2,05	1,22	1,68
MNHN.F.GL92	*Peradectes mutigniensis*	Sables de Brasles	m2	1,97	1,1	1,79
MNHN.F.Mu6451	*Peradectes mutigniensis*	Mutigny	m3	1,74	1,05	1,66
MNHN.F.GL410	-	Sables de Brasles	m3	1,85	1,11	1,67
MNHN.F.Mu18003	-	Mutigny	m4	1,75	1	1,75

Table S4. Absolute basal heights of stylar cusps C and D in *Peradectes crocheti* sp. nov., *Pd. louisi* and *Pd. russelli* (attributions from this study). Abbreviations: HC, absolute basal height of stylar cusp C (mm); HD, absolute basal height of stylar cusp D (mm); HC/HD, absolute basal height of stylar cusp C to absolute basal height of stylar cusp D ratio.

Specimen	Species	Locality	Locus	HC (mm)	HD (mm)	HC/HD
MHN.AIX.PV.2018.26.14	*Peradectes crocheti*	Palette	M1	0,03	0,039	0,769
MHN.AIX.PV.2018.26.20	*Peradectes crocheti*	Palette	M1	0,047	0,061	0,77
UM-FDN-1	*Peradectes crocheti*	Fordones	M1	0,083	0,107	0,776
UM-FNR2-1	*Peradectes crocheti*	Fournes	M1	0,057	0,09	0,633
MNHN.F.SN76	*Peradectes crocheti*	Soissons	M1	0,059	0,146	0,404
MHN.AIX.PV.2018.26.14	*Peradectes crocheti*	Palette	M2	0,036	0,074	0,486
NHMUK.PV.M44991	*Peradectes crocheti*	Abbey Wood	M2	0,058	0,064	0,906
NHMUK.PV.M66046	*Peradectes crocheti*	Croydon	M2	0,109	0,122	0,893
MNHN.F.Me15975	*Peradectes crocheti*	Meudon	M2	0,049	0,096	0,51
UM-FDN-285	*Peradectes crocheti*	Fordones	M2	0,046	0,06	0,767
UM-FDN-21	*Peradectes crocheti*	Fordones	M2	0,03	0,065	0,462
MHN.AIX.PV.2017.6.7	*Peradectes crocheti*	Palette	M3	0,086	0,063	1,365
MHN.AIX.PV.2018.26.14	*Peradectes crocheti*	Palette	M3	0,05	0,055	0,909
UM-FDN-21	*Peradectes crocheti*	Fordones	M3	0,073	0,055	1,327
UM-FDN-23	*Peradectes crocheti*	Fordones	M3	0,095	0,049	1,939
MNHN.F.SN18	*Peradectes crocheti*	Soissons	M3	0,103	0,111	0,928
MNHN.F.SN78	*Peradectes crocheti*	Soissons	M3	0,069	0,075	0,92
Fig. 5.18 Smith et al. 2011	*Peradectes crocheti*	Sotteville-sur-Mer	M3	0,131	0,104	1,26
MNHN.F.Mu18006	*Peradectes louisi*	Mutigny	M1	0,018	0,067	0,269
UM-AV-1-SK	*Peradectes louisi*	Avenay	M1	0,024	0,057	0,421
UM-AV-2-SK	*Peradectes louisi*	Avenay	M1	0,068	0,107	0,636
UM-AV-3-SK	*Peradectes louisi*	Avenay	M1	0,062	0,083	0,747
MNHN.F.Av16023	*Peradectes louisi*	Avenay	M1	0,033	0,063	0,524
MNHN.F.Av16036	*Peradectes louisi*	Avenay	M1	0,047	0,062	0,758
MNHN.F.Av16057	*Peradectes louisi*	Avenay	M1	0,03	0,082	0,366
MNHN.F.GL1	*Peradectes louisi*	Sables de Brasles	M1	0,039	0,062	0,629
MNHN.F.GL296	*Peradectes louisi*	Sables de Brasles	M1	0,053	0,1	0,53
MNHN.F.Mu6511	*Peradectes louisi*	Mutigny	M2	0,053	0,127	0,417
MNHN.F.Av18003	*Peradectes louisi*	Avenay	M2	0,04	0,074	0,541
MNHN.F.Av18004	*Peradectes louisi*	Avenay	M2	0,029	0,053	0,547
MNHN.F.CB3213	*Peradectes louisi*	Condé-en-Brie	M2	0,038	0,041	0,927
MNHN.F.CB3228	*Peradectes louisi*	Condé-en-Brie	M2	0,048	0,042	1,143

MNHN.F.GL154	*Peradectes louisi*	Sables de Brasles	M2	0,045	0,07	0,643
MNHN.F.GL272	*Peradectes louisi*	Sables de Brasles	M2	0,041	0,032	1,281
MNHN.F.Mu18001	*Peradectes louisi*	Mutigny	M3	0,019	0,051	0,373
MNHN.F.SZ18005	*Peradectes louisi*	Sézanne-Broyes	M3	0,044	0,04	1,1
MNHN.F.Mu18004	*Peradectes russelli*	Mutigny	M1	0,037	0,127	0,291
MNHN.F.Mu5532	*Peradectes russelli*	Mutigny	M1	0,061	0,114	0,535
MNHN.F.Av16024	*Peradectes russelli*	Avenay	M1	0,068	0,082	0,829
UM-AV-13-SK	*Peradectes russelli*	Avenay	M1	0,069	0,125	0,552
MNHN.F.CB2501	*Peradectes russelli*	Condé-en-Brie	M1	0,047	0,187	0,251
MNHN.F.CB3007	*Peradectes russelli*	Condé-en-Brie	M1	0,023	0,107	0,215
MNHN.F.CB3275	*Peradectes russelli*	Condé-en-Brie	M1	0,064	0,14	0,457
MNHN.F.Mu18002	*Peradectes russelli*	Mutigny	M2	0,097	0,12	0,808
MNHN.F.CB5103	*Peradectes russelli*	Condé-en-Brie	M2	0,067	0,12	0,558
MNHN.F.CB850	*Peradectes russelli*	Condé-en-Brie	M2	0,096	0,167	0,575
MNHN.F.CB2753	*Peradectes russelli*	Condé-en-Brie	M2	0,123	0,199	0,618
MNHN.F.Mu5521	*Peradectes russelli*	Mutigny	M3	0,044	0,087	0,506
MNHN.F.Av4813	*Peradectes russelli*	Avenay	M3	0,057	0,121	0,471
MNHN.F.Av6837	*Peradectes russelli*	Avenay	M3	0,073	0,182	0,401
MNHN.F.CB924	*Peradectes russelli*	Condé-en-Brie	M3	0,069	0,143	0,483
MNHN.F.CB2502	*Peradectes russelli*	Condé-en-Brie	M3	0,075	0,14	0,536
MNHN.F.CB742	*Peradectes russelli*	Condé-en-Brie	M3	0,033	0,141	0,234

Table S5. Measurements (in mm) of dentary height under m2 or m3 and results of dentary height to molar length ratios for *Peradectes crocheti* sp. nov., *Pd. louisi* and *Pd. russelli*. Abbreviations: Hm2, mandibular height below m2; Hm3, mandibular height below m3; Lm2, length of m2; Lm3, length of m3.

Specimen	Species	Hm2 (mm)	Hm3 (mm)	Hm2/Lm2	Hm3/Lm3
MHN.AIX.PV.2017.6.8	*Peradectes crocheti*	2.71	2.73	1.64	1.64
MNHN.F.CB226	*Peradectes louisi*	2.99	3.01	-	1.87
MNHN.F.CB925	*Peradectes russelli*	3.53	-	1.74	-

Supplementary reference for Table S3.

Crochet JY (1980) Les marsupiaux du Tertiare d'Europe. Editions Foundation Singer-Polinac, Paris, France.

Online Resource 2 List of taxa included in the phylogenetic analyses (with authorship and year), their systematic position, the specimens used for coding and references, and the stratigraphic extension of the species.

Deltatheriidae Gregory and Simpson 1926

Deltatheridium pretrituberculare Gregory and Simpson 1926. Casts of ZPAL MGM-I/91 and ZPAL MGM-I/102 (University of Montpellier, France). Descriptions and illustrations from Kielan-Jaworowska (1975).

Marsupialiformes Vullo et al. 2009; family *incertae sedis*

Asiatherium reshetovi Trofimov and Szalay 1994. Descriptions and illustrations from Szalay and Trofimov (1996).

Peradectidae Crochet 1979

Armintodelphys blacki Krishtalka and Stucky, 1983a. Cast of CM 41159 (holotype) consulted (Royal Belgian Institute of Natural Sciences [RBINS], Brussels). Descriptions and illustrations from Krishtalka & Stucky (1983a, 1983b) and Smith and Smith (2013). From latest Wasatchian (Wa-7) to earliest Bridgerian (Br-0) (Krishtalka and Stucky 1983a; Korth 2008).

Armintodelphys dawsoni Krishtalka and Stucky, 1983a. Cast of CM 55569 (holotype) consulted (Royal Belgian Institute of Natural Sciences [RBINS], Brussels). Descriptions and illustrations from Krishtalka & Stucky (1983a, 1983b, 1984) and Smith and Smith (2013). Early Bridgerian (Br-0-Br-1) (Krishtalka and Stucky 1983a; Korth 2008).

Armintodelphys dufraingi Smith and Smith, 2013. Original specimens IRSNB M2152 (holotype) and IRSNB M2153 consulted (Royal Belgian Institute of Natural Sciences [RBINS], Brussels). Descriptions and illustrations from Smith and Smith (2013). Known from ~51-52 Ma (Egemkapel Clay Member; Smith and Smith 2013) to possibly MP10 reference level (this study).

Mimoperadectes labrus Bown and Rose 1979. Casts of UM 66144 (holotype, dental rows illustrated in pl. 1 and pl. 2, fig. 1 in Bown and Rose [1979]) and UM 113418 consulted (RBINS). Descriptions and illustrations from Bown and Rose (1979), Gingerich (1989), Strait (2001), Gingerich and Smith (2006) and Rose et al. (2012). Definitive *M. labrus* specimens are recorded in Wa-M and Wa-0 faunas (Bown and Rose 1979; Strait 2001; Gingerich and Smith 2006; Rose et al. 2012). The species maybe extends back to the latest Paleocene (Rose 1981: 36) and further into the early-middle Wasatchian, *Cantius trigonodus* zone (biochrons Wa-4-Wa-5) (Bown and Rose 1979: 96; Korth 2008: 716; Rose et al. 2012: 22).

Peradectes californicus (Stock 1936). Descriptions and illustrations from Stock (1936), Setoguchi (1975), Lillegraven (1976), Rothecker and Storer (1996) (fig. 1P interpreted as M2

instead of M3) and Murphey et al. (2018). From early Uintan (biochron Ui-1a, ~47 Ma) to late Duchesnean (biochron Du) (Murphey et al. 2018).

Peradectes chesteri (Gazin, 1952). Descriptions and illustrations from Gazin (1952), West (1973), Krishtalka and Stucky (1983a, 1983b, 1984) and Murphey et al. (2018). From late Wasatchian (biochron Wa-7) to early Uintan (biochron Ui-1b) (Murphey et al. 2018).

Peradectes crocheti sp. nov. All original material included in this study. Cast of the M3 from Sotteville-sur-Mer. Additional illustrations from Hooker (2010, 2020) for each Abbey Wood and Croydon specimen. Restricted to the [MP7-MP8+9 reference level] interval, with first occurrence just after the PETM (Smith et al. 2011) and last occurrences after the Eocene Thermal Maximum 2 (~biochron Wa5; Noiret et al. 2016).

Peradectes elegans Matthew and Granger, 1921. Casts of AMNH 17376 (holotype), 17383 and USNM 20879 (University of Montpellier, France). Descriptions and illustrations from Simpson (1928, 1935), Gazin (1956), Mckenna (1960), Fox (1983) and Krishtalka and Stucky (1983b). We followed Williamson et al. (2012) in considering *Pd. pauli* as a junior synonym of *Pd. elegans*. Thus, specimens allocated to *Pd. pauli* (Krishtalka and Stucky 1983b), including USNM 20879, have been used for the coding of *Pd. elegans*. From early Tiffanian (biochron Ti-2 according to Korth 2008, biochron Ti-3 according to Secord 2008) to early Wasatchian (between biochrons Wa1-Wa3; McKenna 1960; Korth 2008).

Peradectes gulottai Rose 2010. Descriptions and illustrations from Rose (2010). Wasatchian in age (Rose 2010).

Peradectes louisi Crochet 1979. All original material included in the revision of *Pd. louisi* (this study). From (~)MP8+9 reference level (Mutigny; ~52-54 Ma; Neal 1996; Duprat 1997), to possibly [MP8+9-MP10] interval (this study).

Peradectes protinnominatus McKenna 1960. Casts of UCMP 44077 (holotype) and UCMP 45950 (University of Montpellier, France). Casts of UM 71663, UM 113305, UM 113391 and UM 113378 consulted at the Royal Belgian Institute of Natural Sciences (Brussels, Belgium). Descriptions and illustrations from McKenna (1960), Bown (1979), Rose (1981), Krishtalka and Stucky (1983b) and Gingerich and Smith (2006). Isolated molars of *Pd. protinnominatus* described by Strait (2001) are not included, because the only available illustration for this species is a herpetotheriid M3 (with a V-shaped centrocrista). From Clarkforkian (biochron Cf-2; Rose 1981) to early Wasatchian (biochron Wa-M to between biochrons Wa-1-Wa-3) (McKenna 1960; Gingerich and Smith 2006; Korth 2008).

Peradectes russelli Crochet 1979. All original material included in the revision of *Pd. russelli* (this study). From (~)MP8+9 reference level (Mutigny; ~52-54 Ma; Neal 1996; Duprat 1997), to possibly ~MP10 reference level (this study).

Supplementary references for Online Resource 2

Bown TM (1979) Geology and mammalian paleontology of the Sand Creek Facies, lower Willwood Formation (lower Eocene), Washakie County, Wyoming. Geological Survey of Wyoming Memoir 2: 1–151.

Bown TM, Rose KD (1979) *Mimoperadectes*, a new marsupial, and *Worlandia*, a new dermopteran, from the lower part of the Willwood Formation (early Eocene), Bighorn Basin, Wyoming. Contributions from the Museum of Paleontology, The University of Michigan 25: 89–104.

Crochet JY (1979) Diversité systématique des Didelphidae (Marsupialia) européens tertiaires. Géobios 12: 365–378.

Duprat M (1997) Les faciès à mammifères (MP 6 à MP 16) dans le Nord-Est du Bassin de Paris (France): argumentation du modèle tectono-sédimentaire des dépôts paléogènes. In: Aguilar JP, Legendre S, Michaux J (eds) Actes du Congrès BiochroM'97, Mémoires et travaux de l'EPHE 21. Ecole Pratique des Hautes Etudes, Institut de Montpellier, Montpellier, pp 315–336.

Gazin CL (1952) The lower Eocene knight formation of western Wyoming and its mammalian faunas. Smithsonian Miscellaneous Collections 117: 1–82.

Gazin CL (1956) Paleocene mammalian faunas of the Bison Basin in south-central Wyoming. Smithsonian Miscellaneous Collections 131: 1-57.

Gingerich PD (1989) New earliest Wasatchian mammalian fauna from the Eocene of northwestern Wyoming: composition and diversity in a rarely sampled high-floodplain assemblage. University of Michigan Papers on Paleontology 28: 1–97.

Gingerich PD, Smith T (2006) Paleocene-Eocene land mammals from three new latest Clarkforkian and earliest Wasatchian wash sites at Polecat Bench in the northern Bighorn Basin, Wyoming. Contributions from the Museum of Paleontology, University of Michigan 31: 245–303.

Gregory WK, Simpson GG (1926) Cretaceous Mammal Skulls from Mongolia. Nature 118: 698–699.

Hooker JJ (2010) The mammal fauna of the early Eocene Blackheath formation of Abbey Wood, London. Monographs of the Palaeontographical Society 164: 1–153.

Hooker JJ (2020) A mammal fauna from the Paleocene-Eocene Thermal Maximum of Croydon, London, UK. Proceedings of the Geologists' Association 131: 458–473.

Kielan-Jaworowska Z (1975) Evolution of the therian mammals in the Late Cretaceous of Asia. Part I. Deltatheridiidae. Palaeontologia Polonica 33: 103–132.

Korth WW (2008) Marsupialia. In: Janis CM, Gunnell GF, Uhen MD (eds) Evolution of Tertiary Mammals of North America: Volume 2, Small Mammals, Xenarthrans, and Marine Mammals. Cambridge University Press, Cambridge, pp 39–47.

Krishtalka L, Stucky RK (1983a) Revision of the Wind River faunas, early Eocene of Central Wyoming. Part 3. Marsupialia. Annals of Carnegie Museum 52: 205–227.

Krishtalka L, Stucky RK (1983b) Paleocene and Eocene marsupials of North America. Annals of Carnegie Museum 52: 229–263.

Krishtalka L, Stucky RK (1984) Middle Eocene marsupials (Mammalia) from northeastern Utah and the mammalian fauna from Powder Wash. Annals of Carnegie Museum 53: 31–45.

Lillegraven JA (1976) Didelphids (Marsupialia) and *Uintasorex* (?Primates) from later Eocene sediments of San Diego County, California. Transactions of the San Diego Society of Natural History 18: 85–112.

McKenna MC (1960) Fossil Mammalia from the early Wasatchian Four Mile fauna, Eocene of northwest Colorado. University of California Publications in Geological Sciences 37: 1–130.

Murphey P, Kelly T, Chamberlain K, Tsukui K, Clyde W (2018) Mammals from the earliest Uintan (middle Eocene) Turtle Bluff Member, Bridger Formation, southwestern Wyoming, USA, Part 3: Marsupialia and a reevaluation of the Bridgerian-Uintan North American Land Mammal Age transition. Palaeontologia Electronica 21(2):25A: 1–52.

Neal JE (1996) Summary of Paleogene sequence stratigraphy in northwest European and the North Sea. In: Knox RWOB, Corfield RM, Dunay RE (eds) Correlation of the Early Paleogene in Northwest Europe. Geol Soc London Spec Publ 101, pp 15–42.

Noiret C, Steurbaut E, Tabuce R, Marandat B, Schnyder J, Storme JY, Yans J (2016) New bio-chemostratigraphic dating of a unique early Eocene sequence from southern Europe results in precise mammalian biochronological tie-points. Newsletters on Stratigraphy 49: 469-480.

Rose KD (1981) The Clarkforkian Land-Mammal Age and mammalian faunal composition across the Paleocene-Eocene boundary. University of Michigan Papers on Paleontology 26: 1–197.

Rose KD (2010) New marsupial from the early Eocene of Virginia. Journal of Paleontology 84: 561–565.

Rose KD, Chew AE, Dunn RH, Kraus MJ, Fricke HC, Zack SP (2012) Earliest Eocene mammalian fauna from the Paleocene-Eocene Thermal Maximum at Sand Creek Divide, Southern Bighorn Basin, Wyoming. University of Michigan Papers on Paleontology 36: 1–122.

Rothecker J, Storer JE (1996) The marsupials of the Lac Pelletier lower fauna, Middle Eocene (Duchesnean) of Saskatchewan. Journal of Vertebrate Paleontology 16: 770–774.

Secord R (2008) The Tiffanian Land-Mammal Age (Middle and Late Paleocene) in the Northern Bighorn Basin, Wyoming. University of Michigan Papers on Paleontology 35: 1–192.

Setoguchi T (1975) Paleontology and geology of the Badwater Creek area, central Wyoming. Part 11. Late Eocene marsupials. Annals of Carnegie Museum 45: 263-275.

Simpson GG (1928) American Eocene didelphids. American Museum Novitates 307: 1–7.

Simpson GG (1935) The Tiffany fauna, Upper Paleocene. I.-Multituberculata, Marsupialia, Insectivora, and ?Chiroptera. American Museum Novitates 795: 1–19.

Smith T, Dupuis C, Folie A, Quesnel F, Storme J-Y, Iacumin P, Riveline J, Missiaen P, Ladevèze S, Yans J (2011) A new terrestrial vertebrate site just after the Paleocene–Eocene boundary in the Mortemer Formation of Upper Normandy, France. Comptes Rendus Palevol 10: 11–20.

Smith T, Smith R (2013) A land micro-mammal fauna from the Early Eocene marine Egem deposits (NP12, Belgium) and the first occurrence of the peradectid marsupial *Armintodelphys* outside North America. Geologica Belgica 16: 302–310.

Stock C (1936) Sespe Eocene Didelphids. Proceedings of the National Academy of Sciences 22: 122–124.

Strait SG (2001) New Wa-0 mammalian fauna from Castle Gardens in the southeastern Bighorn Basin. In: Gingerich, PD (ed) Paleocene-Eocene stratigraphy and biotic change in the Bighorn and Clarks Fork basins, Wyoming. University of Michigan Papers on Paleontology 33, pp. 127–143.

Szalay FS, Trofimov BA (1996) The Mongolian Late Cretaceous *Asiatherium* , and the early phylogeny and paleobiogeography of Metatheria. Journal of Vertebrate Paleontology 16: 474–509.

Trofimov BA, Szalay FS (1994) New Cretaceous marsupial from Mongolia and the early radiation of Metatheria. Proceedings of the National Academy of Sciences 91: 12569–12573.

Vullo R, Gheerbrant E, Muizon C de, Néraudeau D (2009) The oldest modern therian mammal from Europe and its bearing on stem marsupial paleobiogeography. Proceedings of the National Academy of Sciences 106: 19910–19915.

West RM (1973) Geology and mammalian paleontology of the New Fork-Big Sandy area, Sublette County, Wyoming. Fieldiana 29: 1–193.

Williamson TE, Brusatte SL, Carr TD, Weil A, Standhardt BR (2012) The phylogeny and evolution of Cretaceous–Palaeogene metatherians: cladistic analysis and description of new early Palaeocene specimens from the Nacimiento Formation, New Mexico. Journal of Systematic Palaeontology 10: 625–651.

Online Resource 3 List of characters included in the cladistic analyses. It is mentioned if a dental character is taken or modified (change in the spelling and / or character states) from Williamson et al. (2014) or Muizon and Ladevèze (2022), or if it is 'new' [i.e. not mentioned in Williamson et al. (2014) or Muizon and Ladevèze (2022)]. For characters taking biometrics into account, the mean of the observed value for a given taxa was used to select the appropriate character state. States of characters newly introduced and informative for resolving relationships of peradectid species are illustrated (not to scale) when needed.

1. Distal heel on lower premolars [new]: at least one cuspid well-developed (0), small to undistinct (1).

Figure S1. States 0 and 1 for the character 1, illustrated on right p3 of *Peradectes crocheti* sp. nov. (0) and *Mimoperadectes labrus* (1). Drawing of *M. labrus* (reversed view) from Bown and Rose (1979).

2. Diastema posterior to p1 [character 17 in Muizon and Ladevèze 2022]: present (0), absent (1).

3. Relative height of p3 [new]: higher than m1 (0), as high as m1 (1), lower than m1 (2).

4. m1 slightly shorter (< 10% shorter) than m2 [new]: absent (0), present (1).

5. Proportions of m2 or m3 [new]: length / width ratio < 1.75 (0), length / width ratio >= 1.75 (1).

6. m4 relative length [new]: shorter than m3 (0), as long as or longer than m3 (1).

7. Trigonid vs talonid width on m3 [modified from character 60 in Williamson et al. 2014; character 56 in Muizon and Ladevèze 2022]: trigonid wider than talonid (0), trigonid as wide as talonid (1).

8. Talonid length on m4 [new]: shorter than trigonid (0), as long as or longer than trigonid (1).

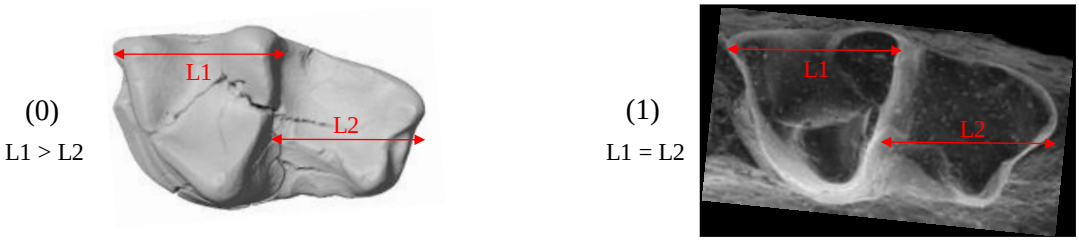

Figure S2. States 0 and 1 for the character 8, illustrated on left m4 of *Peradectes crocheti* sp. nov. (0) and *Armintodelphys blacki* (1). Picture of *Arm. blacki* modified from Smith and Smith (2013).

9. Metaconid position on the anteroposterior axis of m2 or m3 [new]: metaconid almost directly lingual to protoconid (0), metaconid well distolingual to protoconid (1).

(0) 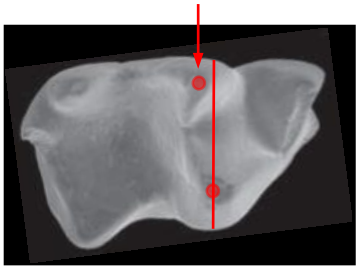 (1) 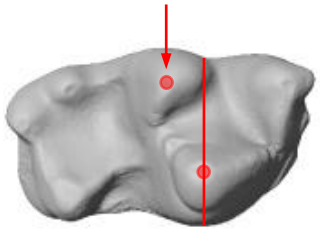

Figure S3. States 0 and 1 for the character 9, illustrated on right m2 and right m3, respectively, of *Peradectes protinnominatus* (0) and *Peradectes louisi* (1). Picture of *Pd. protinnominatus* modified from Gingerich & Smith (2006).

10. Mesial end of cristid obliqua position on m2 or m3 [modified from character 80 in Williamson *et al.*, 2014; character 69 in Muizon & Ladevèze 2022]: ventral or lingual to protocristid notch (0), labial to protocristid notch (1).

11. Mesial end of cristid obliqua on m4 ventral to protocristid notch [modified from character 81 in Williamson et al. 2014]: absent (0), sometimes present (1).

12. Hypoflexid width [character 78 in Muizon & Ladevèze 2022]: deep (ca. 40-50% of talonid width) (0), shallow (less than 40% of talonid width) (1).

13. Emargination of the labial margin of m3 [new]: present (0), absent (1).

(0) 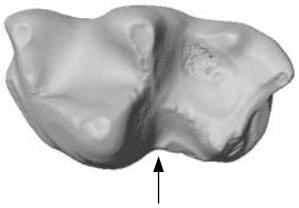 (1) 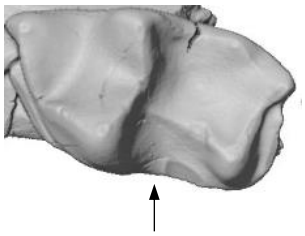

Figure S4. States 0 and 1 for the character 13, illustrated on left m3 of *Peradectes louisi* (0) and *Peradectes crocheti* sp. nov. (1).

14. Angle (in degree of arc) between cristid obliqua and postcristid on m2 or m3 [new]: ca. 70° or more (0), ca. 65° or less (1).

15. Postcristid morphology on m2-m4 [new]: straight at least on one molar locus (0), curved (1).

(0) 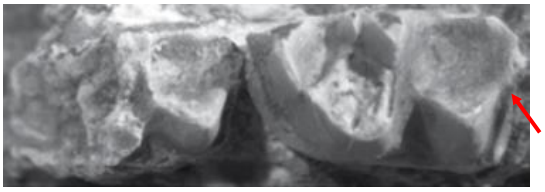 (1) 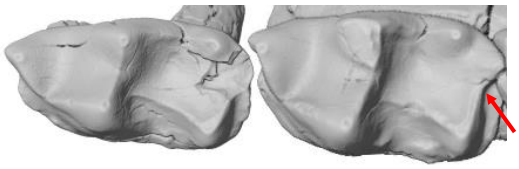

Figure S5. States 0 and 1 for the character 15, illustrated on left m2 of *Mimoperadectes labrus* (0) and *Peradectes crocheti* sp. nov. (1). Picture of *M. labrus* modified from Rose et al. (2012).

16. Postcingulid morphology on m1-m3 [new]: extends lingually towards the hypoconulid tip (0), attenuates labially to the hypoconulid (1).

(0)  (1) 

Figure S6. States 0 and 1 for the character 16, illustrated on left m3 and m2, respectively, of *Armintodelphys dawsoni* (0) and *Peradectes louisi* (1). Picture of *Arm. dawsoni* modified from Krishtalka and Stucky (1984).

17. Postcingulid on m4 [character 74 in Williamson et al. 2014; character 79 in Muizon and Ladevèze 2022]: present (0), absent (1).

18. Notch between entoconid and hypoconulid on m3 [new]: shallower than the metaconid – entoconid notch (0), almost as deep as the metaconid – entoconid notch (1).

(0) 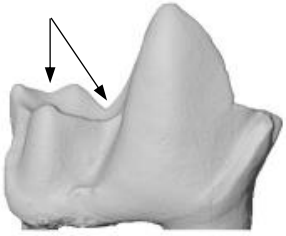 (1) 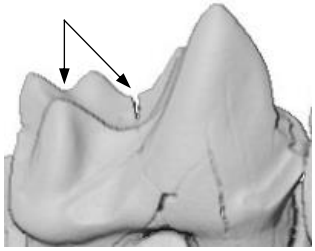

Figure S7. States 0 and 1 for the character 18, illustrated on right m3 of *Peradectes louisi* (0) and *Peradectes crocheti* sp. nov. (1).

19. Relative height of entoconid and hypoconulid [new]: hypoconulid lower than or equal in height to entoconid on all molars, or higher than entoconid only on m4 (0), hypoconulid higher than entoconid on m3 and m4 (1).

(0) 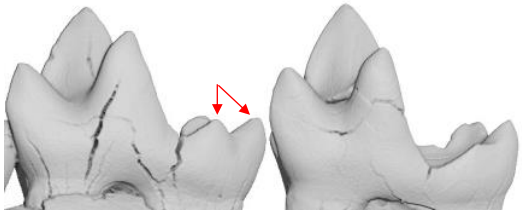 (1) 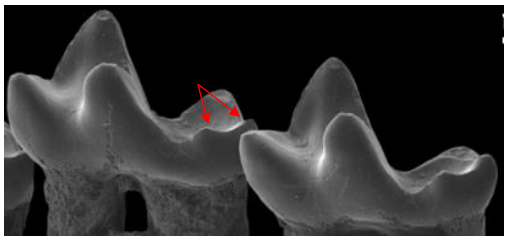

Figure S8. States 0 and 1 for the character 19, illustrated on left (reversed view) and right, respectively, m3 and m4 of *Peradectes crocheti* sp. nov. (0) and '*Armintodelphys*' *dufraingi* (1). Picture of '*Arm.*' *dufraingi* modified from Smith and Smith (2013).

20. Pre-entocristid morphology [character 76 in Muizon and Ladevèze 2022]: absent or weakly developed (0), well-developed and sharp (1).

21. Entoconid apex position relative to trigonid on m2 and m3 [character 75 in Muizon and Ladevèze 2022]: closer to the distolingual corner of the tooth (posterior) (0), intermediate between distal edge of trigonid and distal margin of the tooth (anterior) (1).

22. Disparity of length (L) / width (W) ratio between M2 and M3 [new]: (M2 L/W – M3 L/W) > 0.10 (0), (M2 L/W – M3 L/W) <= 0.10 (1).

23. Talon size [modified from character 46 in Muizon and Ladevèze 2022]: mesiodistally narrow (0), mesiodistally expanded (1).

24. Protocone position [modified from character 51 in Williamson et al. 2014]: lingual to paracone (0), distolingual to paracone (1).

25. Protocone relative height on M1-M3 [modified from character 50 in Williamson et al. 2014]: lower than paracone and metacone (0), subequal or higher than paracone or metacone (1).

26. Conules wing-like (internal and external) cristae on M1-M3 [character 45 in Muizon and Ladevèze 2022]: absent (0), present (1).

27. Largest conule on M1-M3 [new]: paraconule larger or conules subequal in size (0), metaconule larger (1).

28. Relative height of paracone vs metacone on M1-M3 [modified from character 41 in Williamson et al. 2014; character 37 in Muizon and Ladevèze 2022]: sligthly taller (0), sligthly smaller (1).

29. Postmetacrista length on M2 or M3 [character 29 in Muizon and Ladevèze 2022]: subequal to or shorter than preparacrista (0), longer than preparacrista (1).

30. Distal margin morphology on M1-M3 [new]: rectilinear at least on one molar locus, or with a postmetaconular crista extending distolabially to the lingual extremity of the metacone base (0), emarginated between talon and stylar shelf (1).

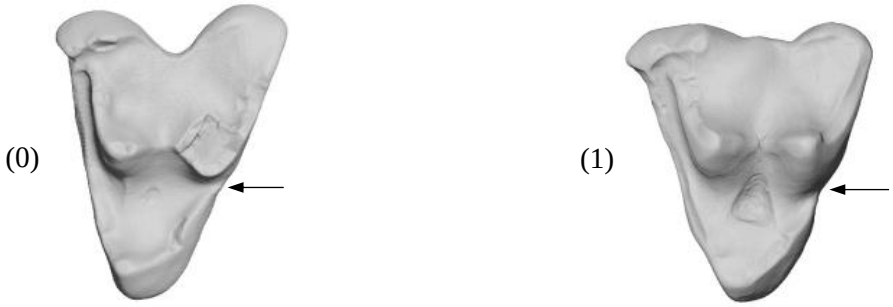

Figure S9. States 0 and 1 for the character 30, illustrated on M3 (reversed view for state 0) of *Peradectes louisi*. The arrow points the distal emargination.

31. Stylar cusp A most frequent position on M2 or M3 [new]: mesial to stylar cusp B (0), mesiolingual to stylar cusp B (1).

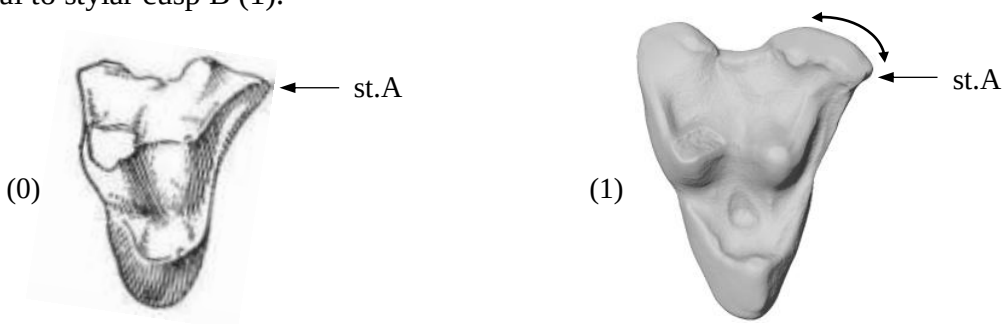

Figure S10. States 0 and 1 for the character 31, illustrated on right M3 of *Peradectes protinnominatus* (0) and *Peradectes russelli* (1). Picture of *Pd. protinnominatus* modified from McKenna (1960).

32. Stylar cusp A relative size (length and width) on M3 [character 22 in Williamson et al. 2014]: subequal to or larger than stylar cusp B (0), distinctly smaller than stylar cusp B (1).

33. Stylar cusp B position on M1-M3 [modified from character 24 in Williamson et al. 2014]: mesiolabial to paracone apex (0), strictly labial to paracone apex at least on M1 and M2 (1).

34. Stylar cusp C on M2-M3 [modified from character 25 in Williamson et al. 2014; character 33 in Muizon and Ladevèze 2022]: absent (0), small (lower than st. B and st. D at least on one molar locus) (1), well-developed (as high as or higher than st. B or st. D) (2).

35. Stylar cusp D position on M1 [modified from character 32 in Williamson et al. 2014]: mesiolabial or strictly labial to metacone apex (0), distolabial to metacone apex (1).

36. M1 ectoflexus [new]: sometimes present (0), absent (1).

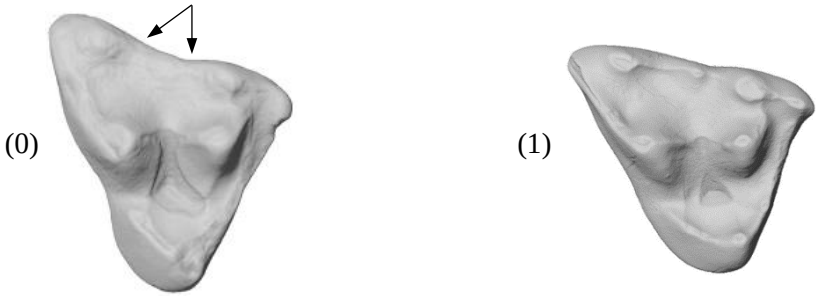

Figure S11. States 0 and 1 for the character 36, illustrated on right M1 of *Peradectes russelli* (0) and *Peradectes crocheti* sp. nov. (1).

37. Ectoflexus symmetry [new]: present on M2 or M3, at least on one specimen (0), absent (1).

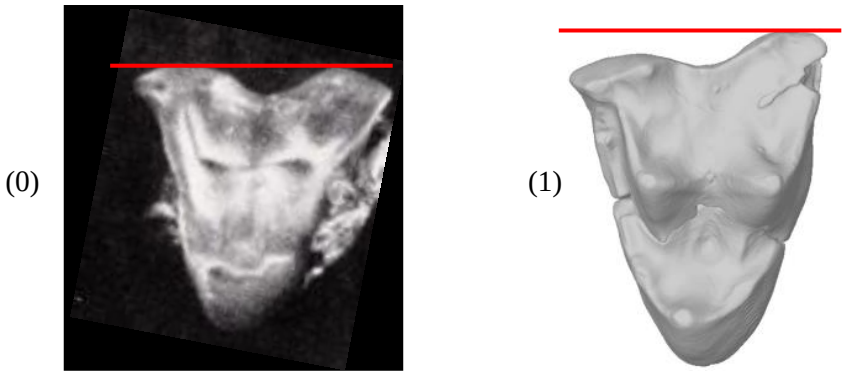

Figure S12. States 0 and 1 for the character 37, illustrated on right M2 of *Peradectes chesteri* (0) and left M3 of *Peradectes crocheti* sp. nov. (1). Picture of *Pd. chesteri* (reversed view) modified from Krishtalka & Stucky (1984).

Supplementary references (not present in Online Resource 2) for Online Resource 3

Muizon C de, Ladevèze S (2022) New material of *Incadelphys antiquus* (Pucadelphyda, Metatheria, Mammalia) from the early Palaeocene of Bolivia reveals phylogenetic affinities with enigmatic North and South American metatherians. Geodiversitas 44:609-643.

Williamson TE, Brusatte SL, Wilson GP (2014) The origin and early evolution of metatherian mammals: the Cretaceous record. ZooKeys 465:1–76.

Online Resource 4 Taxon-character matrix (14 taxa, 37 characters) of the first phylogenetic analysis. A dash denotes inapplicability. Brackets denote morphological polymorphism.

Deltatheridium pretrituberculare	001000001000000-10-000000000010000-00
Asiatherium reshetovi	00100101101001100000011111001010000001
Peradectes elegans	0(01)1001100101(01)0100(01)0100110111100002010
Peradectes protinnominatus	011100000101(01)0110101(01)00001111101(01)2000
Peradectes crocheti sp. nov.	01010010(01)10110110101110(01)01111(01)1112111
Peradectes russelli	???00100110100011001(01)10001111(01)1111101
Peradectes louisi	???11000111100(01)11001110001111(01)1111101
Armintodelphys dufraingi	????1100111100011011??????????????????
Mimoperadectes labrus	11010100111(01)1001(01)01101(01)(01)1111000102100
Armintodelphys blacki	11??011111011011011???????????????
Armintodelphys dawsoni	????011101011000?0110?0000?1000?02??0
Peradectes chesteri	??21(01)000(01)101111100?000000011011101100
Peradectes gulottai	??????????????????????100101111100 1??1
Peradectes californicus	11211100010111111010010011111111001101

Online Resource 5 Modified spelling of characters or character states (modified parts are in bold), subsequent amendments in the scoring and results of the second and third phylogenetic analysis, replacing frequencies of observations by morphological polymorphism.

Changes in the spelling and scoring, and result for the second phylogenetic analysis:

11. Mesial end of cristid obliqua on m4 ventral to protocristid notch [modified from character 81 in Williamson et al. 2014]: absent (0), **present** (1).

31. **Stylar cusp A position** on M2 or M3 [new]: mesial to stylar cusp B (0), mesiolingual to stylar cusp B (1).

36. M1 ectoflexus [new]: **present** (0), absent (1).

Changes in the scoring of character **11**. *Peradectes louisi*, *Mimoperadectes labrus*: 1 -> 0&1

Changes in the scoring of character **31**. *Peradectes protinnominatus*; 0 -> 0&1; *Peradectes crocheti* sp. nov., *Peradectes louisi*, *Peradectes chesteri*, *Peradectes californicus*: 1 -> 0&1

Changes in the scoring of character **36**. *Peradectes louisi*, *Peradectes russelli*: 0 -> 0&1

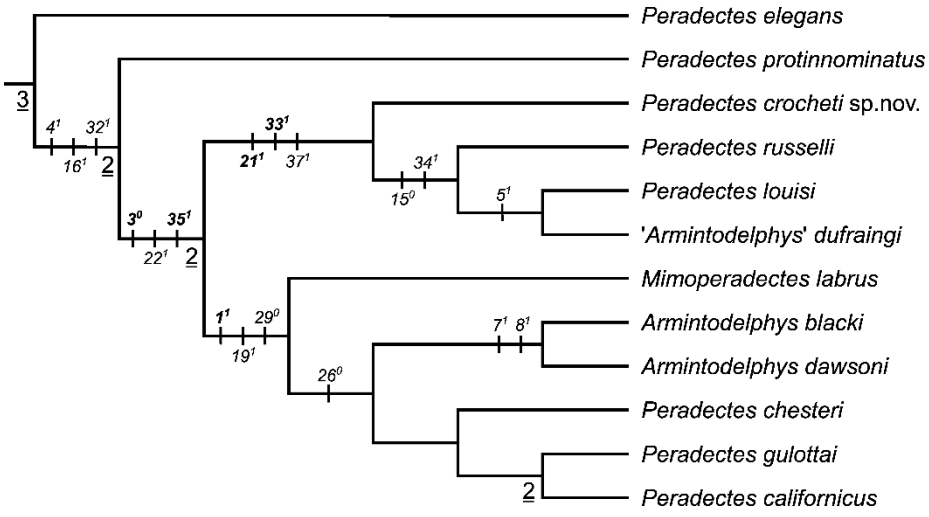

Figure S1 Ingroup from the single most-parsimonious tree obtained in the second analysis (111 steps, same topology as the first analysis; CI = 0.604, RI = 0.517; see main text for described changes in Bremer indices and non-ambiguous synapomorphies).

Additional changes (characters 11, 31 and 36 modified as in the second analysis) in the spelling and scoring, and result for the third phylogenetic analysis:

37. Ectoflexus symmetry [new]: **present on M2 or M3** (0), absent (1).
'present on M2 or M3, **at least on one specimen**' (analysis 1 and 2) > 'present on M2 or M3' (analysis 3).

Change in the scoring of character **37**. *Peradectes chesteri*: 0 -> 0&1

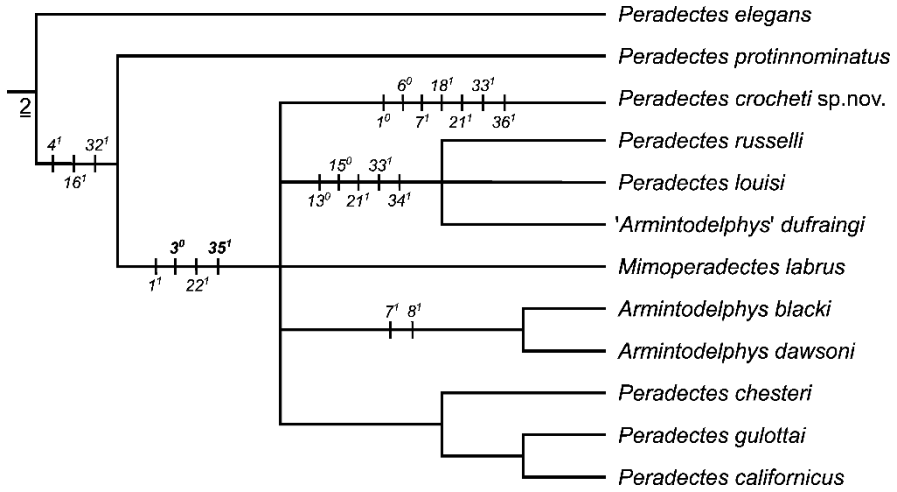

Figure S2 Ingroup from the two most-parsimonious tree obtained in the third analysis, of 112 steps each (CI = 0.607, RI = 0.511). The non-ambiguous synapomorphies for taxa of main interest are figured at node or branch.

Online resource 6 Lingual (medial) view of the surface model of the right hemi-mandible fragment MHN.AIX.PV.2017.6.8, *Peradectes crocheti* sp. nov. from Palette (Provence; MP7-MP8+9 interval).